NASA CONTRACTOR REPORT 166395

Theoretical Evaluation Of A V/STOL Fighter Model Utilizing The Pan Air Code

G.A. Howell
I.C. Bhateley
General Dynamics
Fort Worth Division
Fort Worth, Texas

Prepared for
Ames Research Center
Under Contract NAS2-10649

National Aeronautics and
Space Administration

Ames Research Center
Moffett Field, California 94035

SUMMARY

The PAN AIR computer code has been investigated as a tool for predicting closely coupled aerodynamic and propulsive flowfields of arbitrary configurations. This was the first known application of this code to the solution of a flowfield of this complexity. Several areas of the code were utilized that had not been previously used, hence it was not surprising that a number of problem areas were encountered.

The NASA/Ames V/STOL fighter model, a configuration of complex geometry, was analyzed with the PAN AIR code. A successful solution for this configuration was obtained when the nozzle exit was treated as an impermeable surface and no wakes were included around the nozzle exit. When separated flow was simulated from the end of the nacelle, requiring the use of wake networks emanating from the nozzle exit, a number of problems were encountered. The details of a number of these unresolved problems are discussed in this report. Although the analysis of this model was not satisfactorily completed in this study, considerable progress was made in developing the techniques by which complex configurations can be analyzed with the PAN AIR code.

A circular body nacelle model was used to investigate various techniques for simulating the exhaust plume in PAN AIR. Several approaches were tested and eliminated because they could not correctly simulate the interference effects. Only one plume modeling technique gave good results. This technique represents a plume as a permeable body for which the shape and inflow velocities are computed external to the code. A PAN AIR computation that used a plume shape and inflow velocities obtained from the Navier-Stokes solution for the plume produced results for the effects of power that compared well with experimental data.

TABLE OF CONTENTS

LIST OF FIGURES

LIST OF FIGURES (Cont'd)

LIST OF FIGURES (Cont'd)

LIST OF SYMBOLS

$\vec{i}$	Unit vector in X-direction
M	Mach number
$\hat{n}$	Unit vector normal to panel, outward-pointing from upper surface
s	Sign $(1-M_\infty^2)$
$\vec{U}_o$	Total onset flow
$\vec{U}_\infty$	Uniform onset flow
$\vec{V}$	Total velocity, $\vec{U}_o + \vec{v}$
$\vec{v}$	Perturbation velocity, with components (u, v, w)
$\vec{W}$	Total mass flux, $\vec{U}_o + \vec{w}$
$\vec{w}$	Perturbation mass flux with components $[s(1-M_\infty^2)u, v, w]$
(x,y,x)	Coordinate system

GREEK SYMBOLS

$\mathcal{B}$	Normal component of specified total mass flux in boundary condition equation, i.e. $\vec{W} \cdot \vec{n}$
μ	Doublet strength at a point on a panel
σ	Source strength at a point on a panel
ϕ	Perturbation potential
ψ	$\frac{x}{s(1-M_\infty^2)}, y, z$

SUBSCRIPTS

L	Lower surface value
U	Upper surface value

ACKNOWLEDGEMENTS

A number of persons in several organizations have contributed to the efforts made in this study. The authors wish to acknowledge the major contributors: Susan Braden of the NASA Ames Research Center for monitoring the contract that provided for this study and for coordinating the activities between General Dynamics and NASA; Dr. Larry Erickson of the NASA Ames Reserach Center for his invaluable technical assistance in developing the approaches to problems that had not been previously attempted with the PAN AIR code; persons on the PAN AIR team at Boeing who corrected the identified programming errors; and Chris Reed of the Propulsion Analysis Group at General Dynamics for providing the Navier-Stokes solution to the isolated nacelle model plume.

1 INTRODUCTION

Battle scenarios for the 1990's and beyond place importance on the need for tactical aircraft to have V/STOL and/or STOL capability to counter enemy runway-denial tactics. The interest in incorporating these capabilities in the next generation of fighter aircraft has stimulated an interest in developing the methodology to accurately predict the aerodynamics of these configurations in low-speed flight.

One of the computational methods that offers potential for application in this area is the PAN AIR code, a computer program for predicting subsonic or supersonic potential flowfields about arbitrary configurations (Reference 1). The advantage of this method lies mainly in its ability to model the complex geometric details of realistic aircraft configurations and its flexibility for applying various types of boundary conditions over certain regions of the configuration. These capabilities provide a means by which various methods of modeling the interacting aerodynamic and propulsive flowfields can be investigated without having to resort to development or modification of computational codes.

This report documents progress that has been made in developing techniques for evaluating power effects with the PAN AIR code. Recommendations for approaches to the problem are included, although all of the techniques for obtaining a complete and accurate solution have not yet been determined. During this investigation, several options of the PAN AIR code have been used that had not been previously exercised. Consequently, a number of programming bugs have been encountered. In most cases the errors were isolated and referred to NASA for correction by the PAN AIR maintenance contractor. The powered V/STOL Fighter model evaluated in this study was tested in the 40 by 80-ft wind tunnel at the NASA/Ames Research Center. This model was powered by two turbojet engines and surface pressure instrumentation recorded the aerodynamic effects of the engine exhaust. Results of this test are presented in Reference 2.

This report assumes that the reader has a basic understanding of the PAN AIR code. Therefore, the terminology defined by the User's Manual (Reference 1) is used in this document without re-definition.

2 POWER-OFF FIGHTER MODEL ANALYSIS

The NASA/Ames V/STOL fighter configuration was modeled with three different panelling arrangements in attempts to obtain a successful analytical evaluation with the PAN AIR computer code. The initial panelling arrangement modeled the configuration geometry as closely as possible and consequently, placed considerable demands on the network edge matching logic within the code. After several attempts to resolve problems caused by multiple partial-edge abutments in this panel arrangement, an alternate panelling scheme was developed by modifying certain networks such that exact corner point matching was imposed at a majority of points in the vicinity of the nozzle exit. This arrangement was somewhat less precise in its representation of the actual geometry and imposed fewer demands on the code. When this arrangement still did not resolve all of the problems, a final panel arrangement was devised which imposed exact matching between all network sides and corner points in the vicinity of the nozzle exit. This final arrangement simplified the computer code's task of identifying the abutments.

These arrangements are referred to as the "initial", "improved", and "matching" panelling arrangements in the following discussion. A detailed description of the improved arrangement is presented in Appendix A.

2.1 INITIAL PANELLING ARRANGEMENT

2.1.1 Complete Geometry

The "initial" panelling arrangement for the STOL fighter model (Figure 1) was comprised of 751 panels to define the configuration plus an additional 149 panels to define the wakes. This arrangement was devised to model the configuration as accurately as possible within the guidelines outlined in the PAN AIR User's Manual. (Reference 1). Impermeable mass flux boundary conditions were generally imposed on the non-wake panels by the following equations:

$$\sigma = -\vec{U}_o \cdot \hat{n}$$

$$\phi_- = 0 \qquad (1)$$

Figure 1 Initial Panelling Arrangement for the Fighter Model

which are referred to as Class 1, Subclass UPPER boundary conditions in Reference 1. Several networks were input for convenience such that the unit normal vectors were directed toward the interior of the configuration. In this case the Class 1, Subclass LOWER boundary conditions were used. For simplicity, the following discussion will address all boundary conditions as if the unit normal vectors were directed toward the exterior of the configuration. No attempt was made to model the inlet flow in this study. Hence, impermeable surface boundary conditions were applied to the inlet network. A special set of boundary conditions were applied at the exit to simulate the separated flow of the nacelle in the power-off condition. The governing equations,

$$\mu = -\vec{U}_\infty \cdot \vec{\psi}$$
$$\phi_L = 0 \qquad (2)$$

were specified using Class 4 boundary conditions. As shown in Appendix B of Reference 1, these boundary conditions result in the total potential for mass flux being zero on the downstream side of the nacelle exit plane and hence, should produce zero flow tangential to the exit network. This, combined with the wake networks described below, prevented the flow from turning the corner at the exit since the only flow allowed was normal to the exit network panels. The velocity of this flow was not specified but determined by the aerodynamic solution.

Wake networks that were included in this arrangement are shown in Figure 2. They emanated from the trailing edges of the following components.

- o canard
- o wing
- o flap
- o beaver tail
- o nacelle inboard side
- o nacelle upper side
- o nacelle outer side

The flap and nacelle wakes completely surrounded the nozzle exit and formed a rectangular duct that emanated from the boundaries of the exit network. The wakes, in conjuction with the Equation 2 boundary conditions, prevented the flow from turning in a tangential direction to the exit network.

Figure 2 Wake Networks Attached to the Fighter Model

The wakes were represented by doublet sheet networks whose strengths are obtained by matching the doublet strength at the wake leading edge to the resultant doublet strength at the trailing edge of the configuration networks from which the wake network emanates. The wake doublet strength varies in a spanwise direction but is constant in the streamwise direction. This type of network is referred to as a Class 1, Subclass WAKE 1 network.

There were several unique features in the initial panelling arrangement for the figher model. Some of these features were unavoidable because of the complexity of the configuration. Others resulted because of convenience in developing the panelling arrangement but ultimately placed great demands on the abutment matching procedures in the code. Some of these features were:

- The top and upper sides of the nacelle were panelled with a single inverted U-shaped network.

- The outer side of the nacelle included some very high aspect ratio panels that had short edges abutting the exit network.

- There were high aspect ratio panels forming the outboard closure of the strake and beaver tail.

- The flap upper surface, strake upper closure, and beaver tail upper closure were within the domain enclosed by the nacelle wakes.

- Some abutments contained parts of several networks. For instance, the inboard edge of the flap wake abutted two networks on the closure of the strake and two networks on the closure of the beaver tail.

- Partial edge abutments were often used, for example, where the canard abutted the nacelle (Figure A-15).

- The abutments around the exit network were quite complex. They included the impermeable networks of the nacelle, the doublet networks of the wakes, and the Class 4 network of the exit. Additionally, some of these networks had more panels than others, resulting in either the addition of gap-filling panels, or of doublet matching across gaps.

A PAN AIR evaluation of this panelling arrangement produced inconclusive results. The wing chordwise pressures appeared to be of the correct magnitude, but the variation of the computed values with angle of attack were cause for concern. Detailed examination of the predicted pressure distributions revealed that the pressure coefficients on several panels near the nozzle exit had extremely high negative values. Figure 3 shows the pressure coefficients at the center control points of each panel near the nozzle exit at an angle of attack of zero degrees. The panels with the highest negative pressure coefficients were located near the abutment at the inboard and outboard edges of the flap. For instance, one panel on the strake closure had a pressure coefficient of -51.8, which is the vacuum pressure coefficient for a Mach number of 0.166 (the condition for this run). Other panels in the vicinity of the nozzle exit, while not exhibiting extreme values of C_p, still did not have the values of pressure coefficients that were anticipated. Note that the fuselage, strake, nacelle, and wing all had positive pressure coefficients on the panels shown in Figure 3.

To isolate the reasons for the erroneous results, several simplified models were investigated in a systematic study. Since the abnormally high suction pressures occurred near the complex abutments in the vicinity of the nozzle exit, the study concentrated on this area of the model.

2.1.2 Simplified Aftend Models

Several simplified models were developed during the investigation of the high negative pressure coefficients in the vicinity of the nozzle exit of the fighter model. The objective of using the simplified models was to conserve computer resources used for this study. It was found that most of the salient features of the fighter model could be represented with a fewer number of panels using these simplified models. An angle of attack of zero degrees was used in the investigation of all of the aftend models.

Aftend Model No. 1. The first simplified model developed is shown in Figure 4. It contained the basic components of the fighter model, including the wing, nacelle, flap, and strake. The wakes were included in the same manner as on the fighter model, with the flap upper surface and the upper portion of the strake closure within a domain completely encompassed by the nacelle and flap wakes. This model preserved most of the characteristics of the fighter model, including the boundary conditions of the exit network and the arrangement of the wakes near the nozzle exit. Hence it was anticipated that the

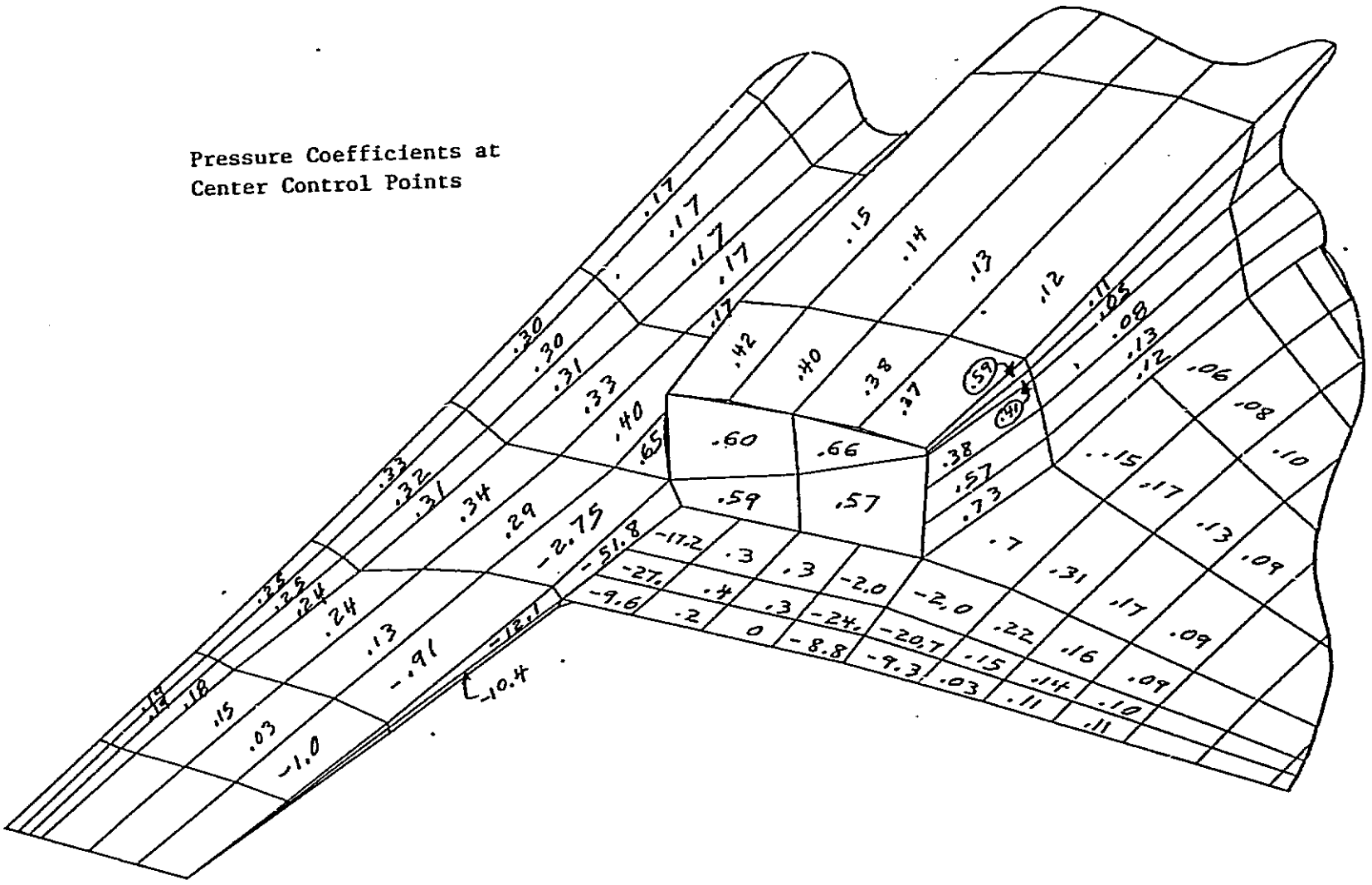

Figure 3 Pressures Near the Exit

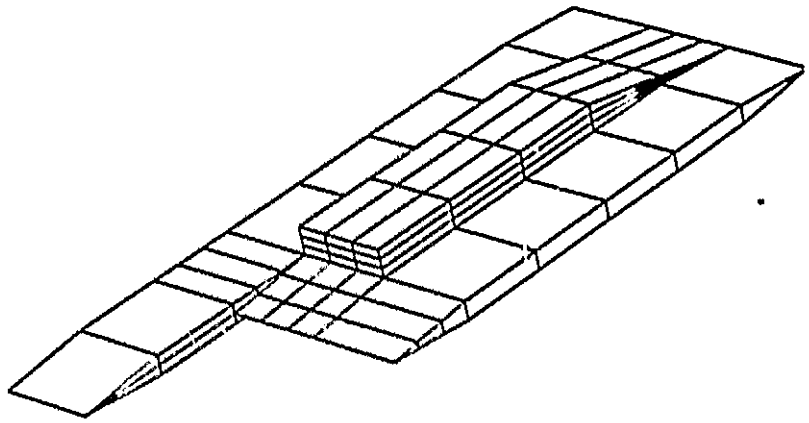

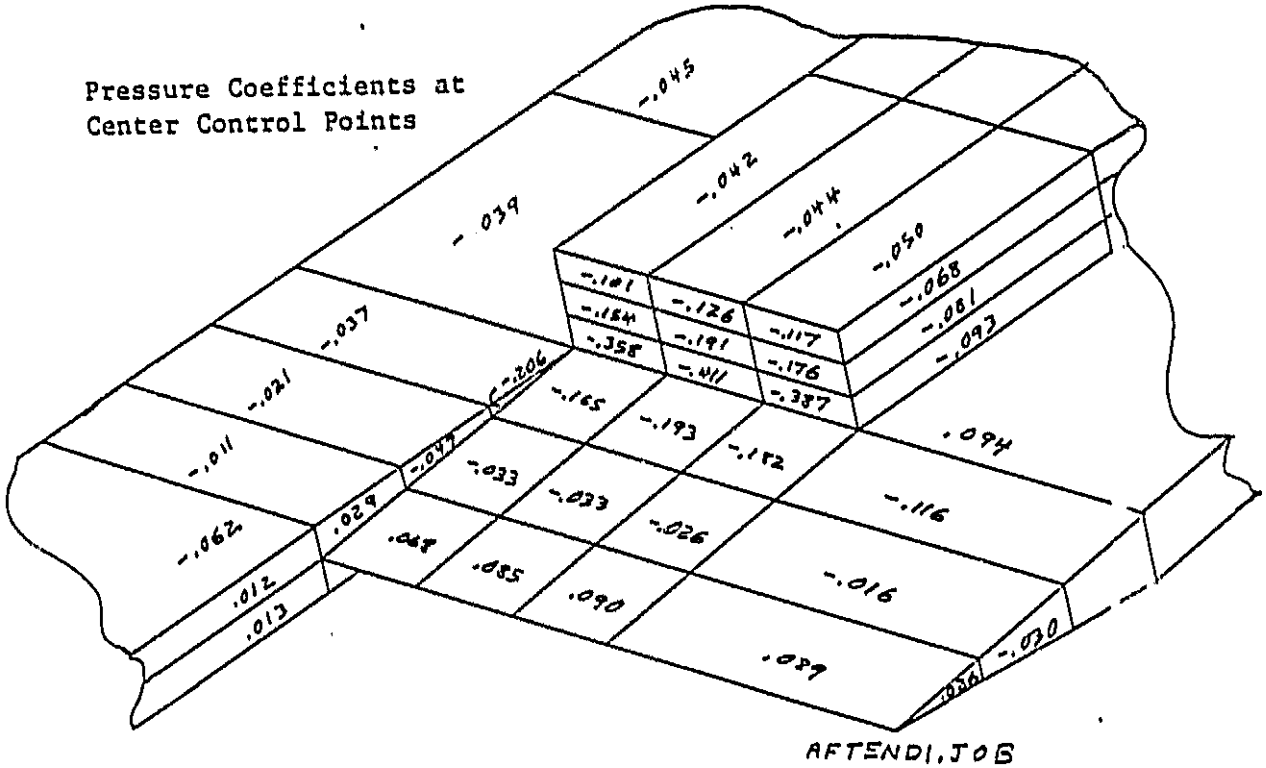

Figure 4 Aftend Model Number 1

pressure coefficients computed for this model would also show high negative pressure coefficients near the nozzle exit. Numerous modifications to the model were planned that would isolate the reason for the abnormal values.

Surprisingly, the high negative pressures were not computed by PAN AIR for this model. As shown in Figure 4, all of the pressure coefficients appear to be within a reasonable range. This model was next modified by panelling the nacelle with a single U-shaped network and then revising the input order of the flap upper-surface to make it even more consistent with the fighter model input. Neither of these modifications caused a significant change in the computed pressure coefficients. Therefore, it was concluded that the modeling characteristic causing the problem with the fighter model was not present in this simplified model. It is noted that this simplified model eliminated the following complexities of the fighter model: high aspect ratio panels, non-matching panel corner points within the abutments at the nozzle exit, gap-filling panels, and curvature in the exit plane abutments. The approach taken next was to progressively remove networks from the fighter model panelling arrangement until the problem could be isolated.

Aftend Model No. 2. This model was developed directly from the fighter model by removing the fuselage, and most of the panels on the canard and wing, as shown in Figure 5. Both the wing and canard were represented by networks that had only one panel width in a spanwise direction, but maintained the 10 chordwise panels. The total number of panels were reduced by approximately 50 percent by the changes noted above. The computed pressure coefficients shown in Figure 5 were not significantly different from those computed for the complete fighter model.

Aftend Model No. 3. This model, shown in Figure 6, was developed to investigate the effects of the wakes. Therefore, the wakes attached to the sides and top of the nacelle were removed and the boundary conditions on the exit network were changed to that of an impermeable surface (Class 1, UPPER). The canard and canard wake were also removed. The computed pressure coefficients for this model appear reasonable at all panels and vary as one would expect. Thus, the conclusion was reached that the problem was being generated by (1) the abutments between the wakes and the solid networks and/or (2) the boundary condition on the exit network that set the total potential equal to zero.

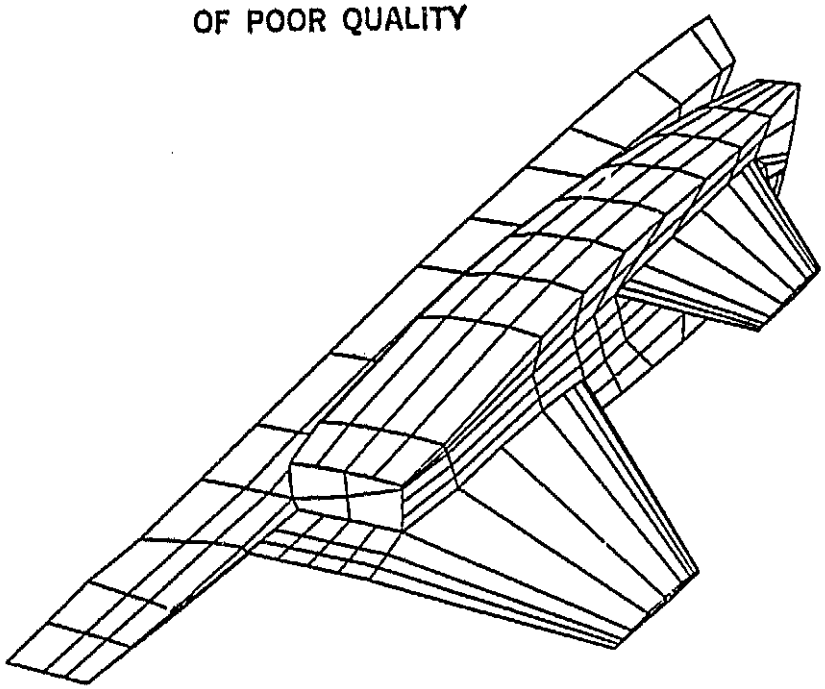

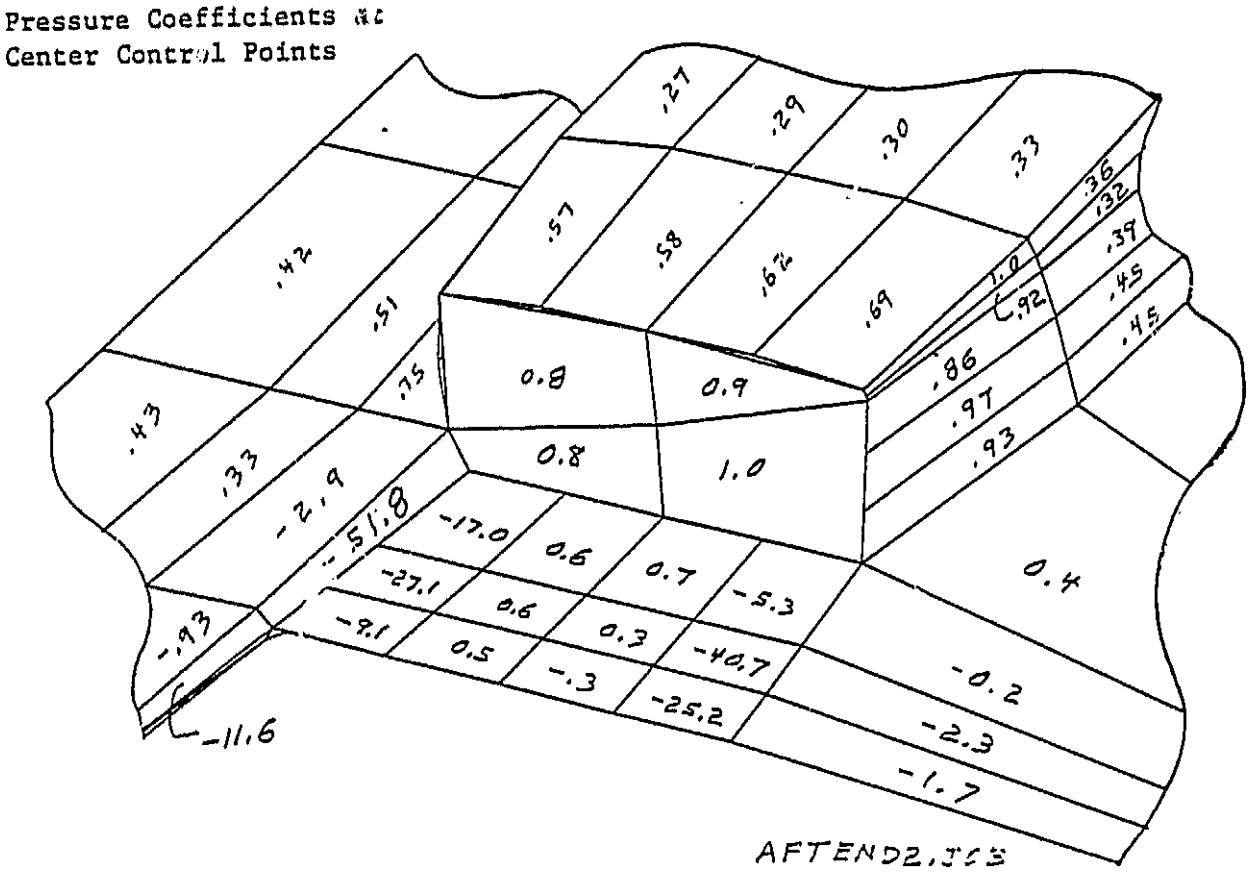

Figure 5 Aftend Model Number 2

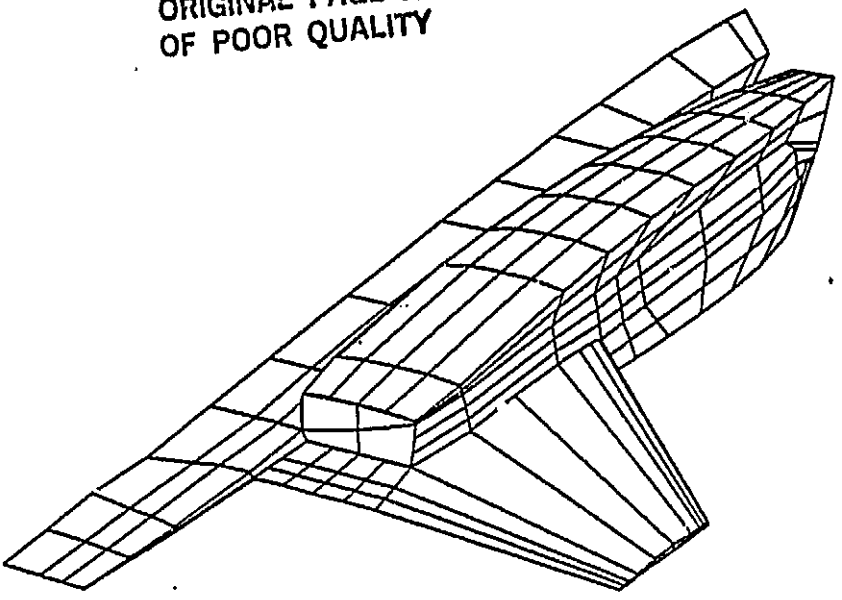

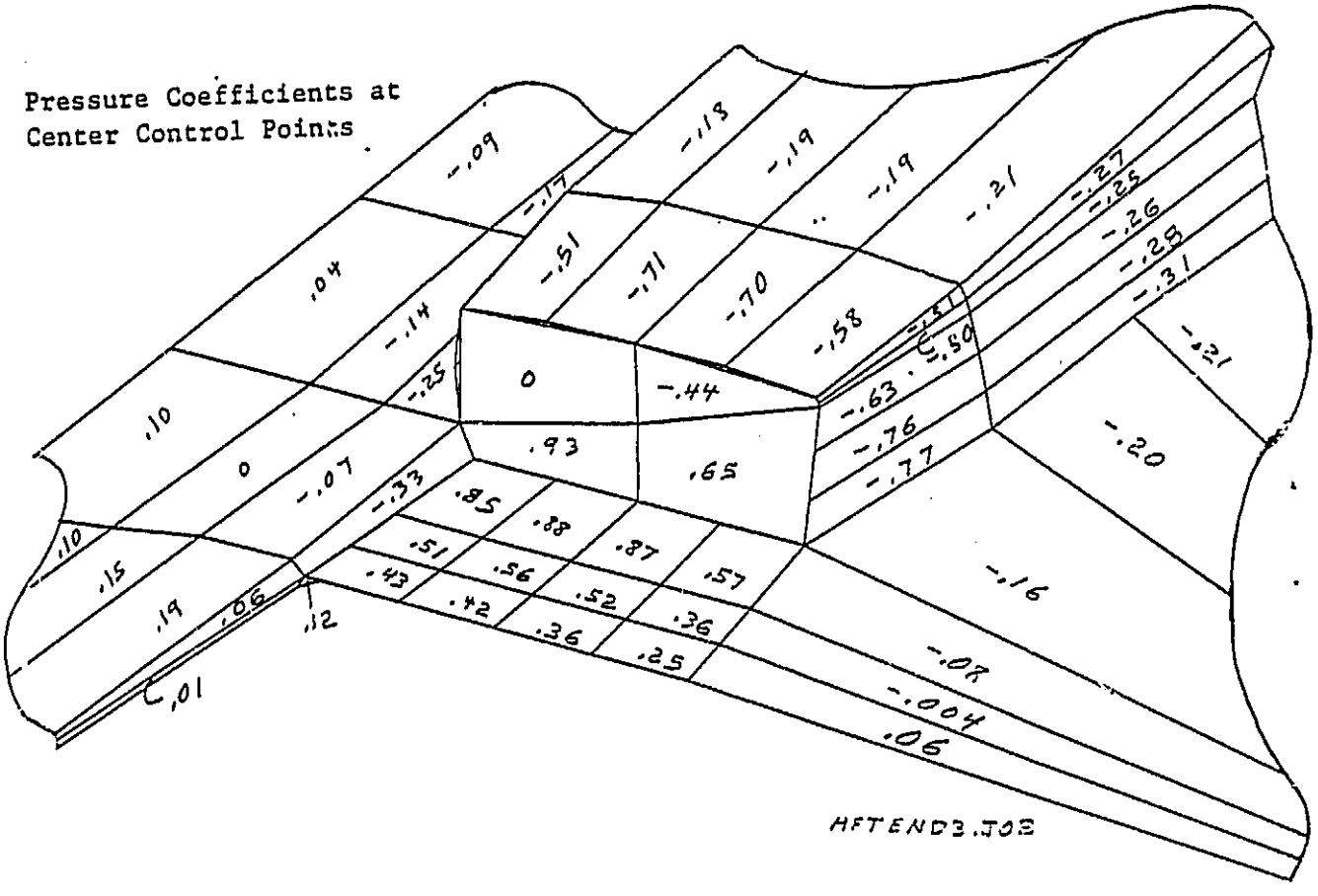

Figure 6 Aftend Model Number 3

Aftend Model No. 6. This model (Figure 7) was developed to simplify the abutments between the wakes and the nacelle. The number of panels on the exit plane was increased such that an exact corner point matching of the panels on the exit network with the panels on the nacelle was achieved. All of the wake leading-edge panel corner points matched the abutting panels, except on the inboard side of the nacelle where two wake panels joined five panels on the exit network. The beaver tail and a large portion of the strake were removed to reduce the number of abutments in this vicinity. These computed pressure coefficients were similar to those of the fighter model (Figure 3) except that additional high negative pressure coefficients appeared on the exit network and on one of the high aspect ratio panels on the nacelle side.

Aftend Model No. 7. This model was similar to Aftend Model No. 6, which had wakes attached to the sides of the nacelle that also joined the flap upper surface. The nacelle side wakes were modified such that a Class 1, WAKE 2 type of network abutted with the flap upper surface, as shown in Figure 8. This was done to remove the constant doublet strength edge of the wakes from direct contact with the flap upper surface. The void between the wake and flap upper surface was filled by a WAKE 2 type network. As shown by a comparison of the results in Figures 7 and 8, this wake modification made no significant difference in the computed values of pressure coefficients.

Aftend Model No. 8. The canard, wing, and strake were removed to create Aftend Model No. 8, as shown in Figure 9. The panels in the nacelle outboard sides were adjusted to close the gap where the wing and canard had previously intersected the nacelle. The upper and lower surfaces of the flap were also collapsed to form a sharp edge.

The computer drawn illustrations shown herein were not available at the time this work was being accomplished, and an oversight was made in the panelling of this model. It is evident in Figure 9 where a gap appears between the bottom of the nacelle and the flap lower surface. This condition would normally be an error, but in this run the abutment between the bottom of the nacelle and the flap lower surface was specified in the input and the gap exceeded the specified TOLERANCE distance. Therefore, the code added gap-filling panels and appropriately handled the abutment.

This model included wake networks that joined the sides and top of the nacelle and the trailing edge of the flap. Abutment specifications were input for each of the abutments in the vicinity of the exit network. This model had only two panels with

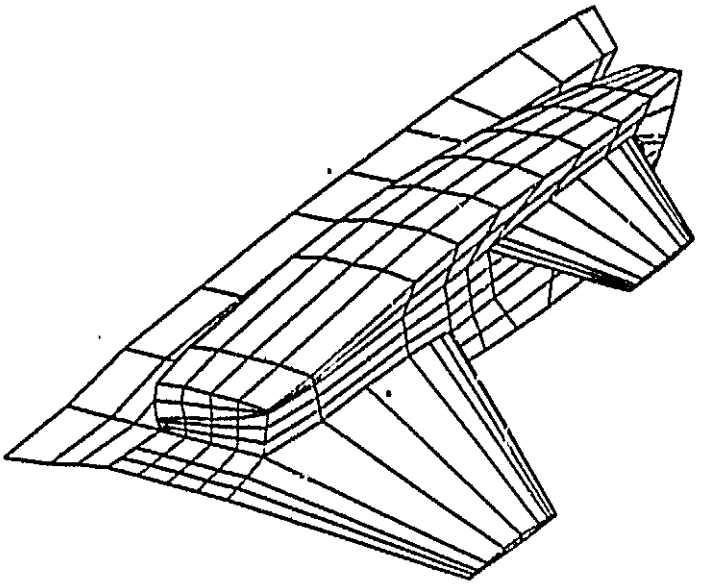

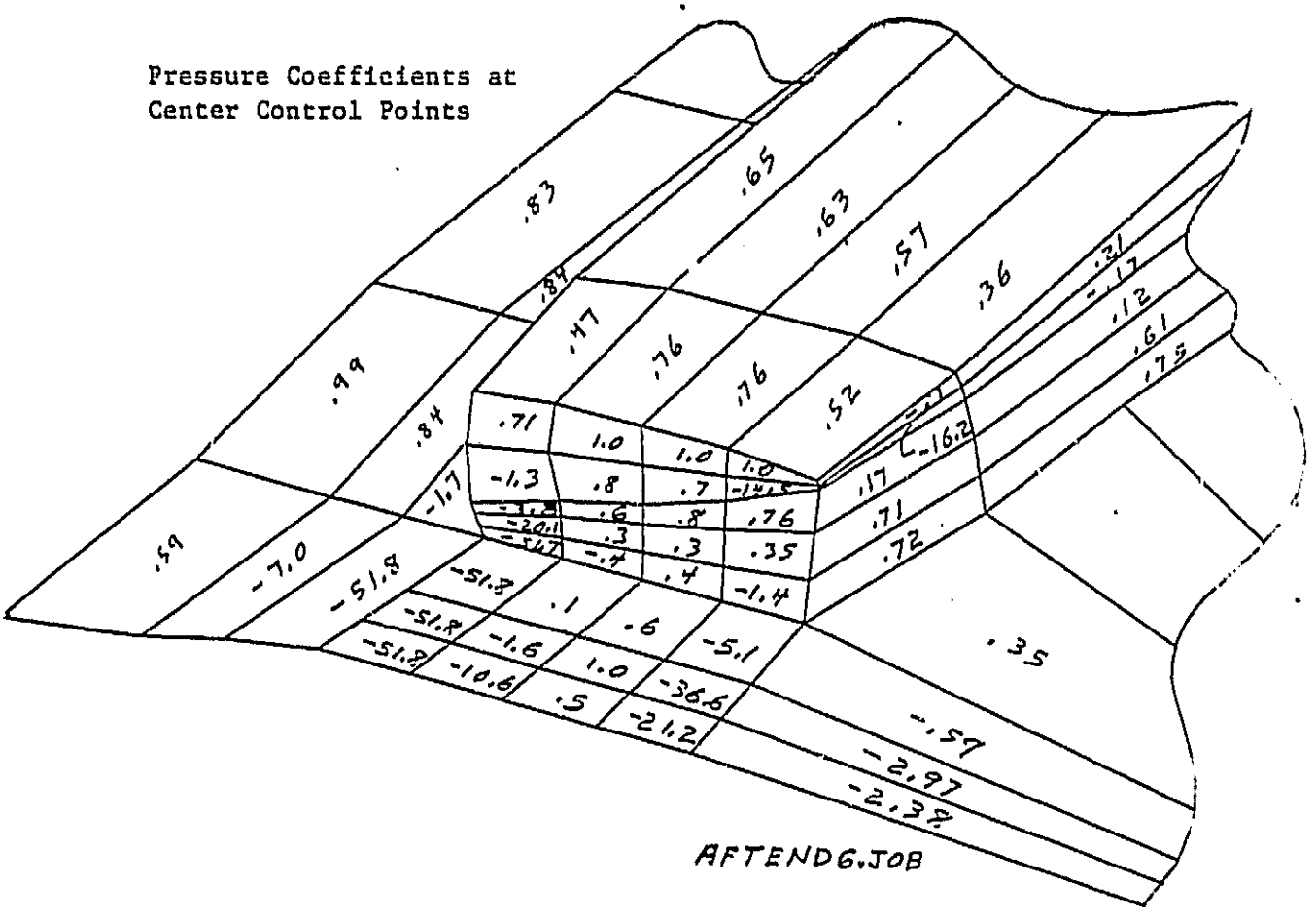

Figure 7 Aftend Model Number 6

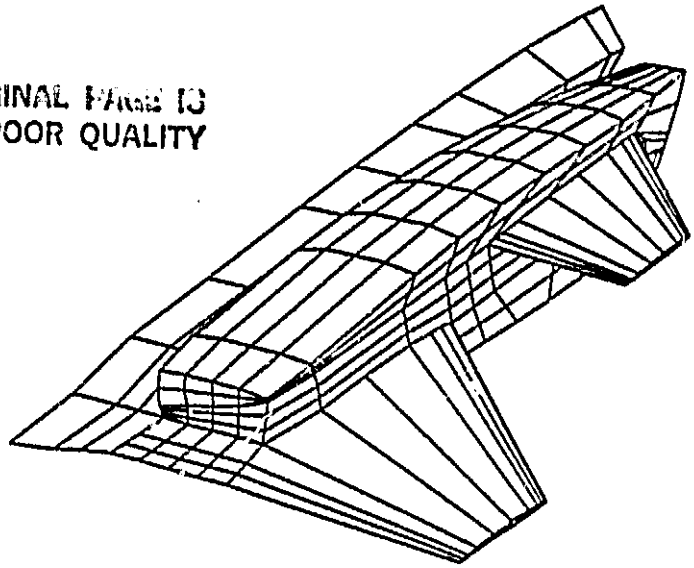

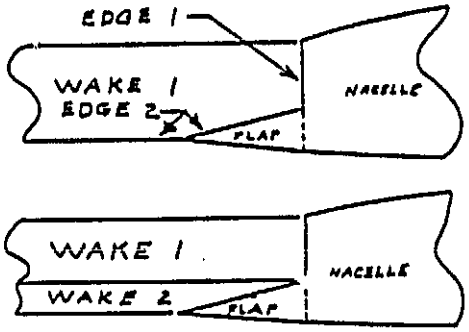

OTHER MODELS

AFTEND MODEL NO. 7

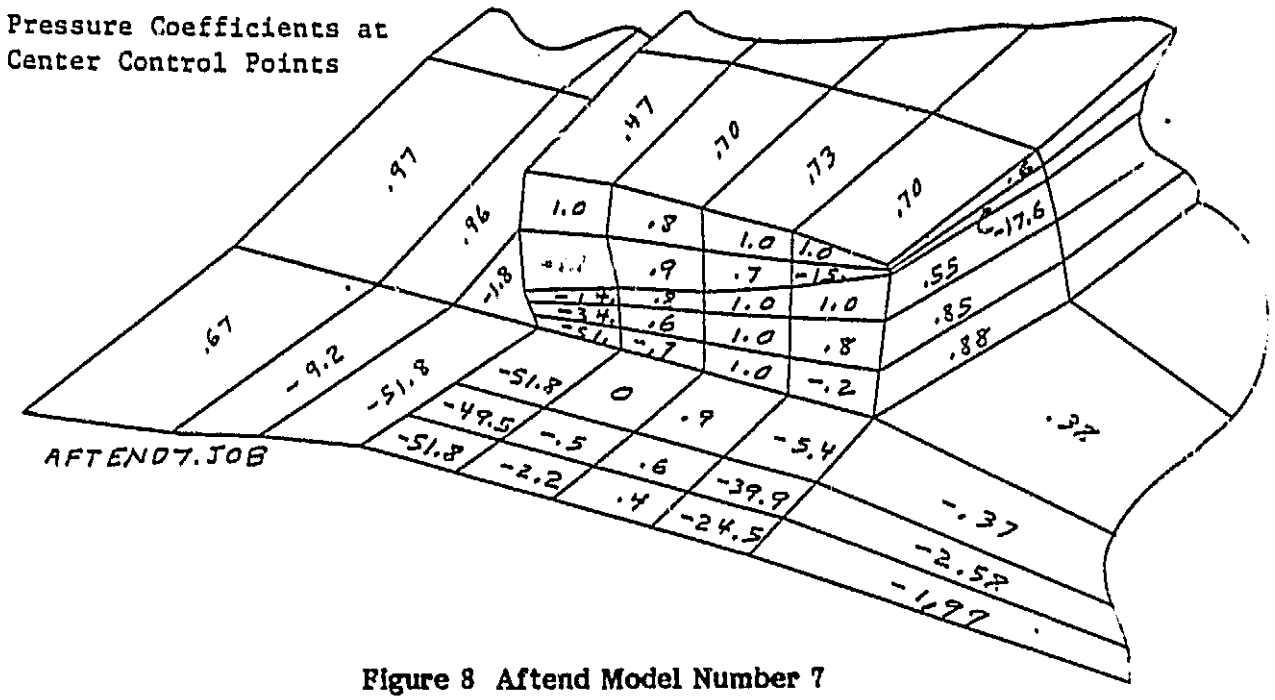

Figure 8 Aftend Model Number 7

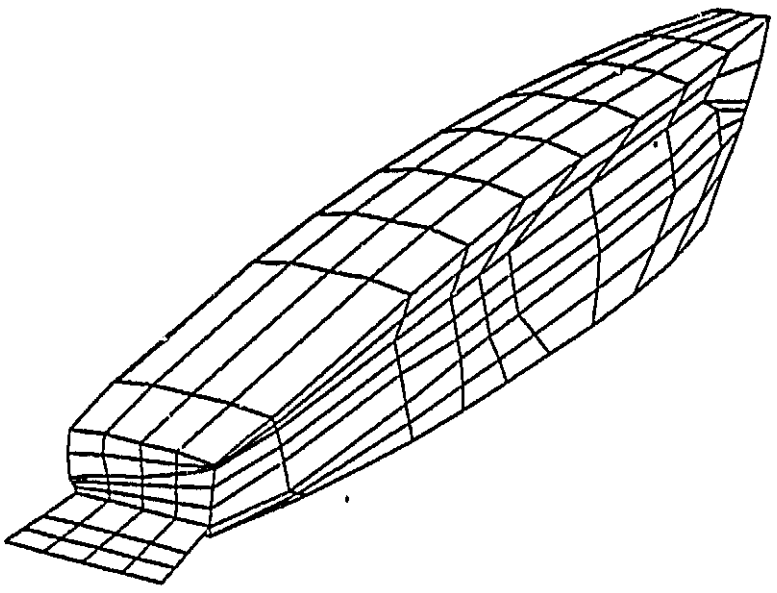

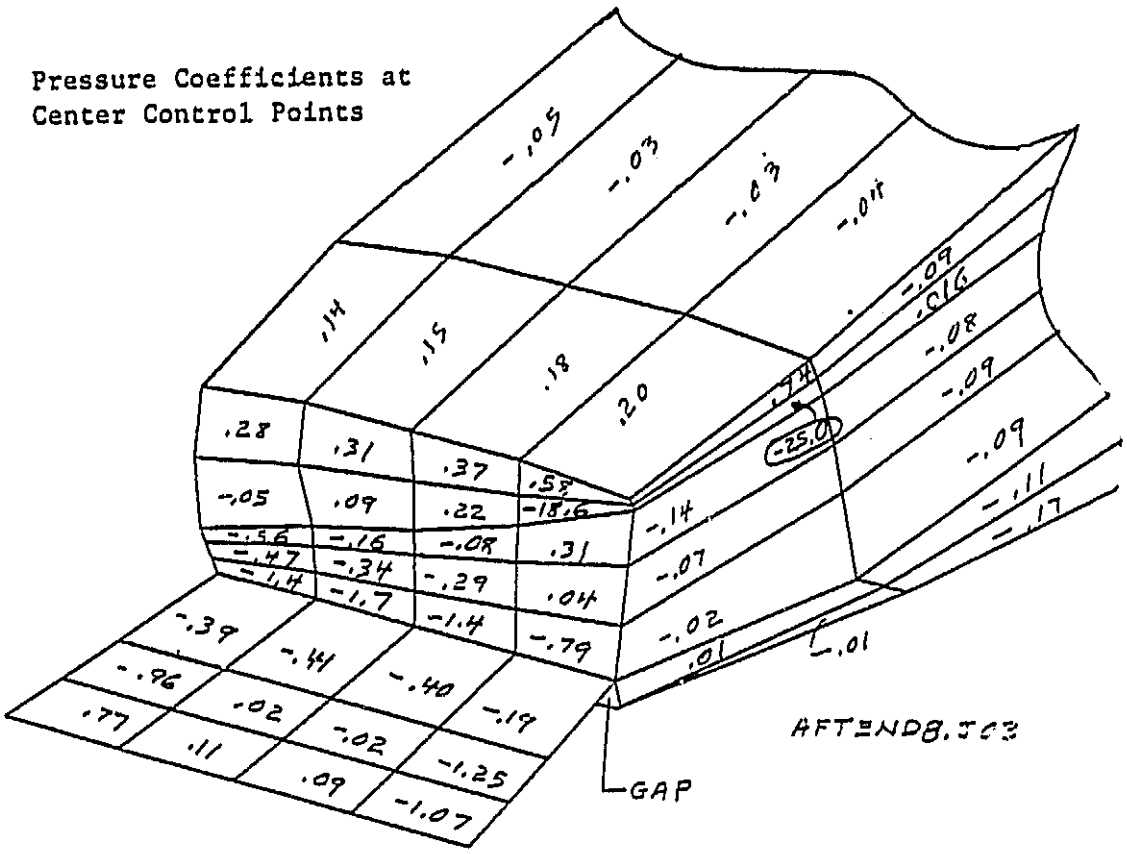

Figure 9 Aftend Model Number 8

extremely high negative values of pressure. One was toward the upper, right-hand corner of the exit, and the other was one of the high aspect ratio panels on the nacelle side. The pressures on the flap upper surface were improved from previous runs, but still the basic cause of the problems could not be identified.

- **Aftend Model No. 10.** The model shown in Figure 10 was developed to specifically investigate the doublet matching across the abutments near the exit. The nacelle in this model was similar to the fighter model nacelle, but the canard, wing, fuselage, and aft portion of the strake were not included in this model. High negative pressure coefficients were computed on the high aspect ratio panels on the outboard side of the nacelle. Therefore, a detailed investigation of the computed values at all of the control points on these panels was made to determine the reason for these abnormally high negative pressure coefficients.

Figure 11 shows shaded panels where the computed pressure coefficients were abnormally high on the nacelle and exit networks. The pressure coefficients and doublet strengths were examined at all the control points on these panels. Figure 12 shows an exploded view of these panels, in addition to the two wake panels that joined the nacelle side panels. The locations of each of the control points are indicated, and two values are shown for most of the pressure coefficients. These were computed by the boundary condition method (B.C.) and the velocity influence coefficient method (V.I.C.). As shown in Figure 12, the pressure coefficients computed by these two methods were not significantly different. It is noteworthy, however, that there were large pressure coefficient differences between the center and edge control points on the nacelle side panels.

The computed doublet strengths, shown in Figure 13, have the same characteristics as the pressure coefficients. For example, on the upper panel of the nacelle side, the doublet strength changes from 3.6 at the center point to -79.1 at the trailing edge. This is consistent behavior since rapidly changing pressures imply rapidly changing values of both the doublet strength and the doublet strength gradient. Thus, the basic doublet distribution, from which the pressures are ultimately computed, appears to be wrong. This suggests that perhaps the doublet matching condition was not being done correctly at the two abutments along the outboard side of the exit (see Figure 11).

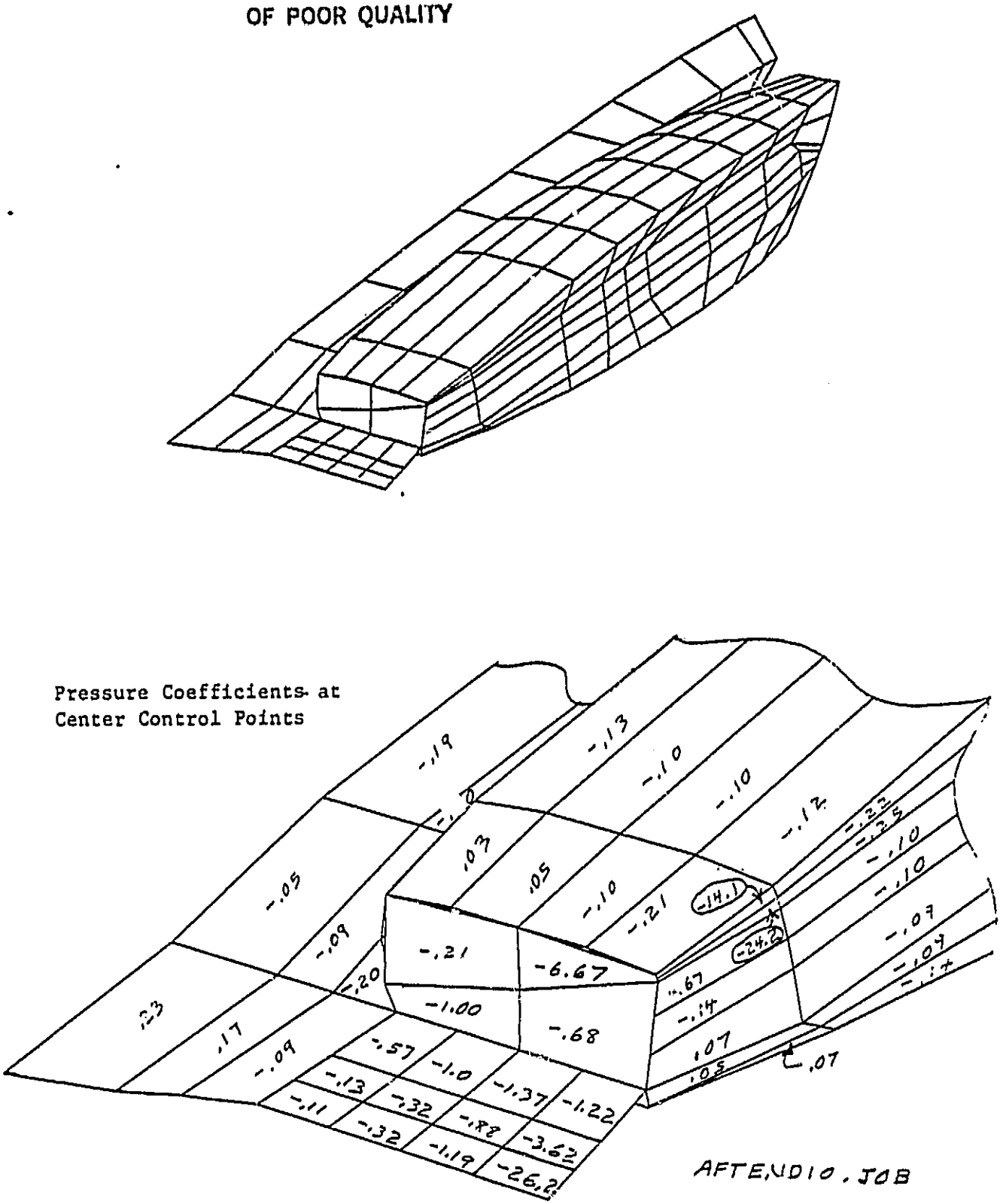

Figure 10 Aftend Model Number 10.

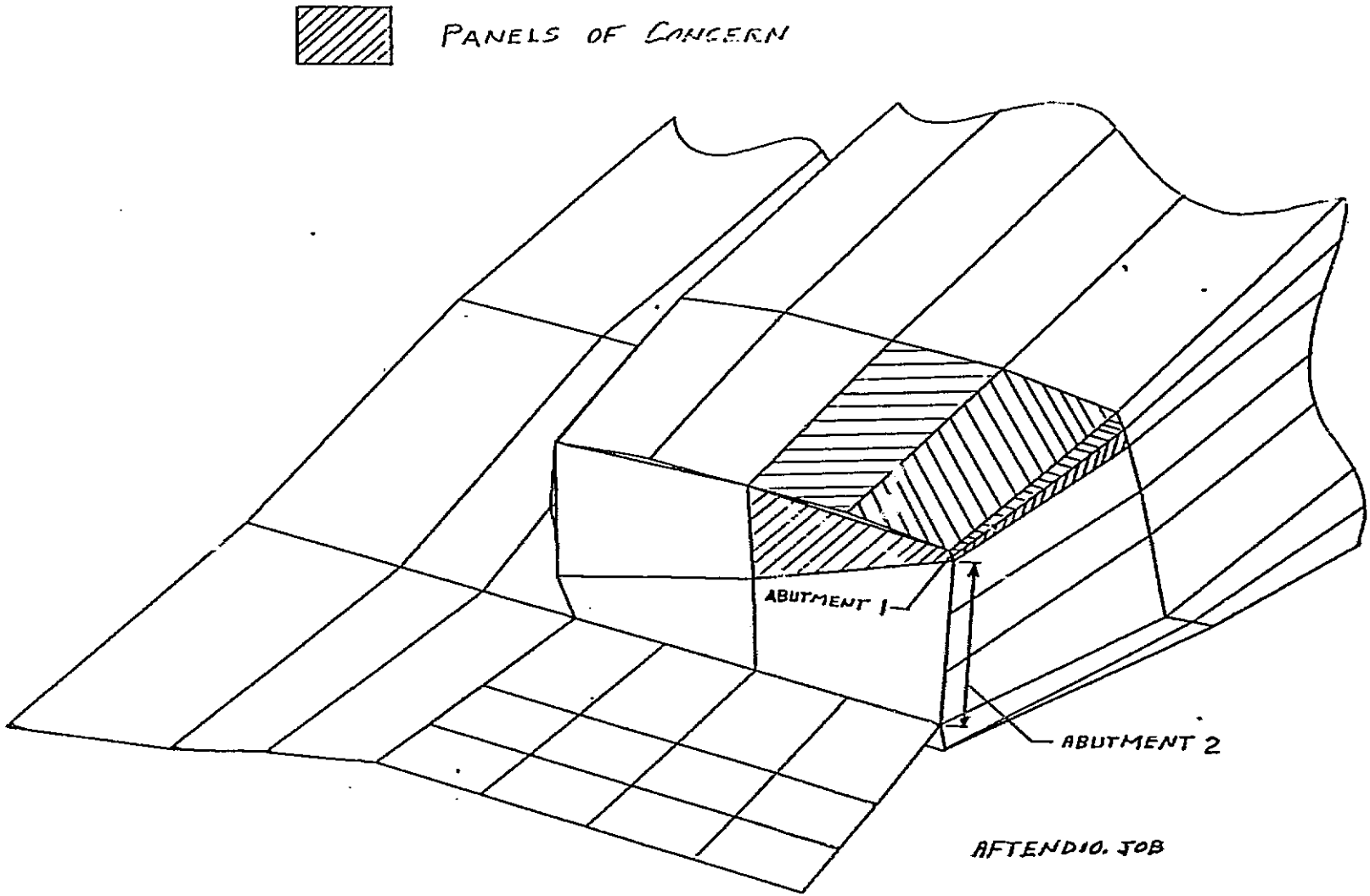

Figure 11 Panels of Concern on Aftend Model Number 10

B.C. = Boundary Condition Method
V.I.C. = Velocity Influence Coefficient Method

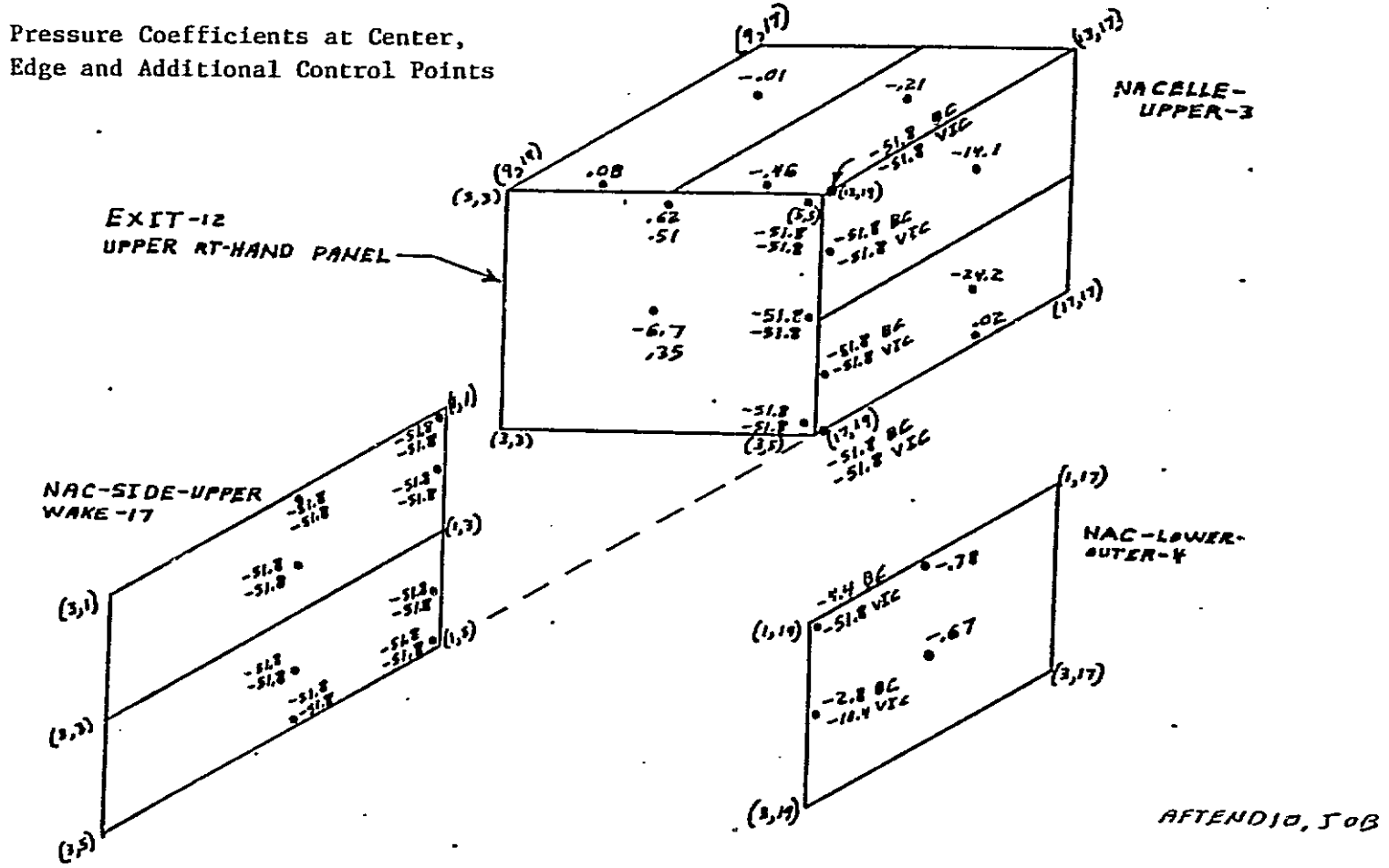

Figure 12 Pressures on Panels of Concern

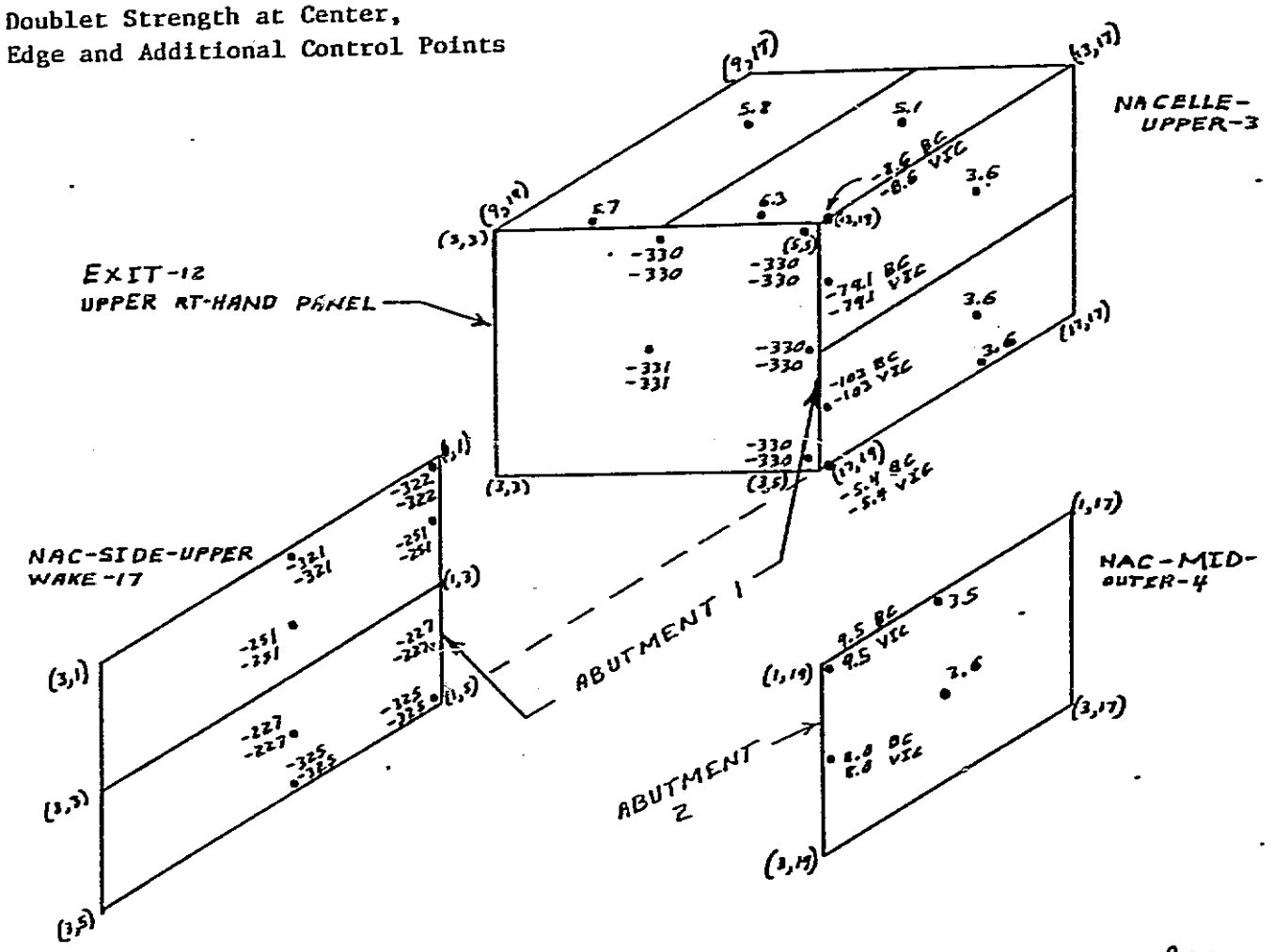

Figure 13 Doublet Strength on Panels of Concern From PDP

ORIGINAL PAGE 13
OF POOR QUALITY

AFTENDIO. JOE

In order to check the accuracy of the doublet matching, the direction of the normal vectors of the two networks forming the outboard nacelle side, the exit plane, and the two abutting wakes were examined. The unit normal vectors of the nacelle outboard side and exit were toward the exterior of the configuration while the unit normal of the wake was toward the interior of the wake domain. Therefore, the doublet strength about this abutment was summed in a clockwise direction as viewed from the top; for example, at one point of abutment 1,

$$\mu_{\substack{\text{NACELLE}\\\text{SIDE}}} + \mu_{\text{WAKE}} - \mu_{\text{EXIT}} = -79 - 251 - (-330) = 0$$

As indicated by the numbers given above, the directed sum of the doublet strength was zero at this particular point in the abutment. The same was true at all other points in the two abutments. Thus, at least to the accuracy of the digits printed, the doublet matching was done correctly. But, for some unknown reason, the doublet strength was not apportioned correctly between the nacelle side network and the side wake network where these networks abut with a portion of the outboard edge of the exit network (abutment 1 of Figures 11 and 13). This can be seen from Figure 13. Along abutment 1, the doublet strength on the exit panel is, from Equation 2.

$$\mu = -\vec{U}_\infty \cdot \vec{\psi} = -330$$

at the top and bottom ends of abutment 1. The wake doublet strengths are -322 and -325, respectively; the corresponding nacelle doublet strengths are -8.6 and -5.4, respectively, values not too different from the upstream values of 3.6. This behavior is qualitatively correct, that is, the doublet strength on the nacelle side varies slowly and the large change in doublet strength introduced by the exit panels is taken up by the wake network. However, at the upper and lower intermediate points of abutment 1, only 76% and 69%, respectively, of the exit panel doublet strength is taken by the wake network; the remaining portion is taken by the nacelle network. The resulting extreme variation in doublet strength on the nacelle is what causes the large negative pressure coefficients there.

In the discussions of this problem, it was suggested that possibly the basic solution for the doublet singularity strengths was being correctly computed by the PAN AIR

matrix solution (in module RHS) and that these results were not correctly passed to the PDP module which computes the pressures and prints the results. To check this, the SINGRID utility program was run to print the doublet strengths after RHS was run, i.e., before the doublet strengths were passed to PDP. SINGRID results for the Aftend Model No. 10 are shown in Figure 14. The values for doublet strength printed by SINGRID are essentially the same as those printed by PDP (Figure 13). This established that the incorrect apportionment of doublet strength between the nacelle side and the wake was due to something in the basic solution procedure.

In an attempt to find a work-around to this problem, two separate modifications were made to Aftend Model No. 10. The first of these dealt with the large doublet strength of the exit network and is described next; the second modification was geometric in nature and corresponds to Aftend Model No. 12.

The large doublet strength of the nacelle exit network ($\mu \approx$ -330 to -332, see Figure 14) is due to the boundary conditions given by Equations 2. These equations are the $\overline{\Phi}_u = 0$ case of the more general equations

$$\mu = \overline{\Phi}_u - \vec{U}_\infty \cdot \vec{\psi}$$

$$\Phi_L = 0 \quad .$$

where $\overline{\Phi}_u$ is the total potential (for mass flux) on the downstream side of the exit network. Selecting $\overline{\Phi}_u = 0$ was done merely for input convenience. Theoretically, any constant value could be selected since it's the gradient of $\overline{\Phi}_u$ that determines the flow field (i.e., adding a constant to $\overline{\Phi}_u$ shouldn't change the flow field solution).

Equation 4 shows that increasing $\overline{\Phi}_u$ on the exit network by a constant amount is the same as increasing μ by the same amount. Therefore, to reduce the doublet strength on the four panels of the exit network to approximately zero, a value $\Delta\mu = 332$ was added to the $\mu = -\vec{U}_\infty \cdot \vec{\psi} = -331$ values used in the original Aftend No. 10 model.

The results of the $\Delta\mu = 332$ run are shown in Figures 15 and 16. The pressure coefficients are now reasonable on the panels that previously had large negative values. Also, the nacelle doublet strengths along abutment 1 are now all of the same order of magnitude. Thus, it appears that a judicious choice for the exit network doublet strength greatly reduces the error in apportionment of doublet strength. (A discussion of the force data in Section 2.4 indicates that this adjustment of the doublet strength only rectifies the local extreme pressures but does not fully correct the results.)

Doublet Strength at
All Control Points

Results of SINGRID Code

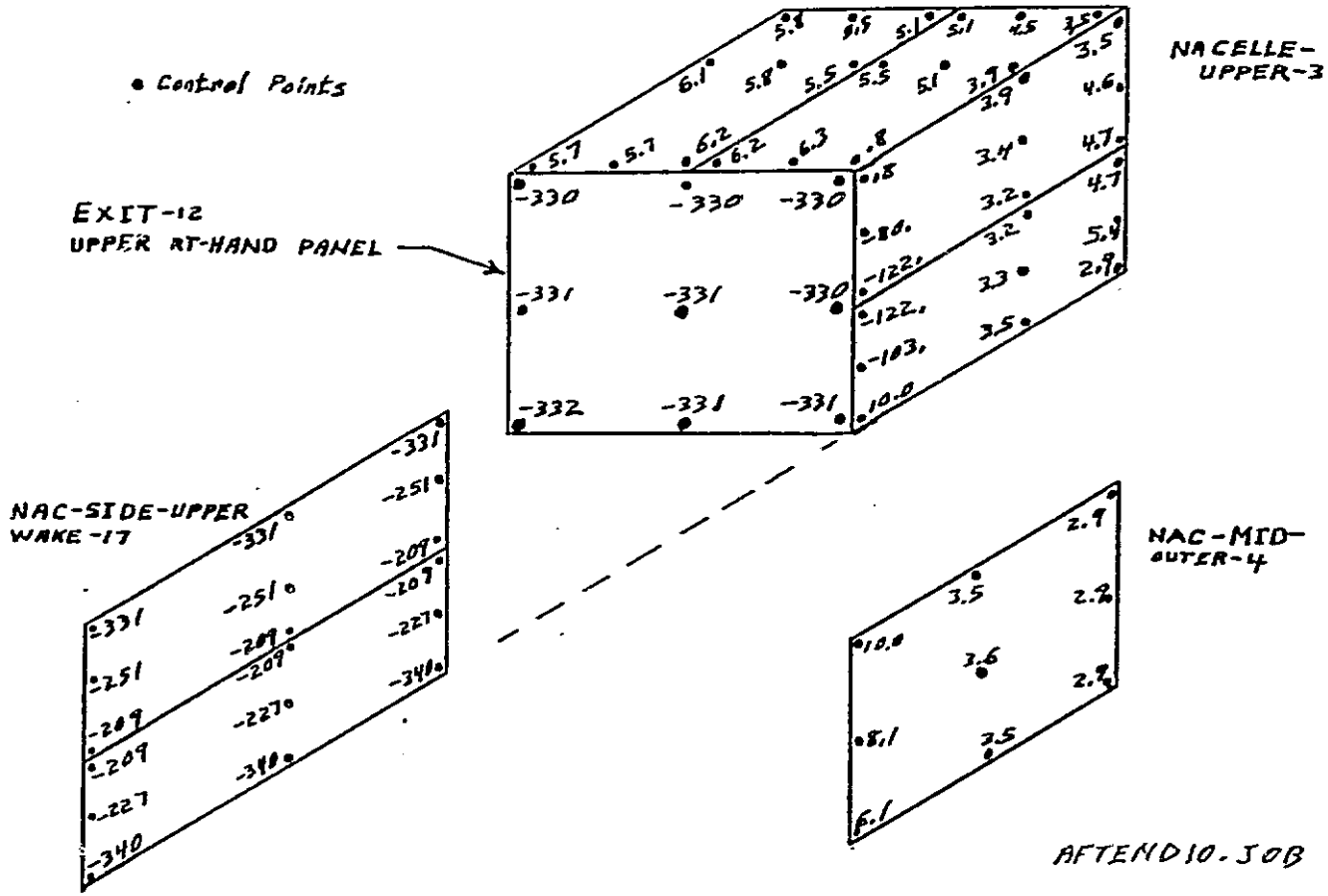

Figure 14 Doublet Strength on Panels of Concern, From SINGRID

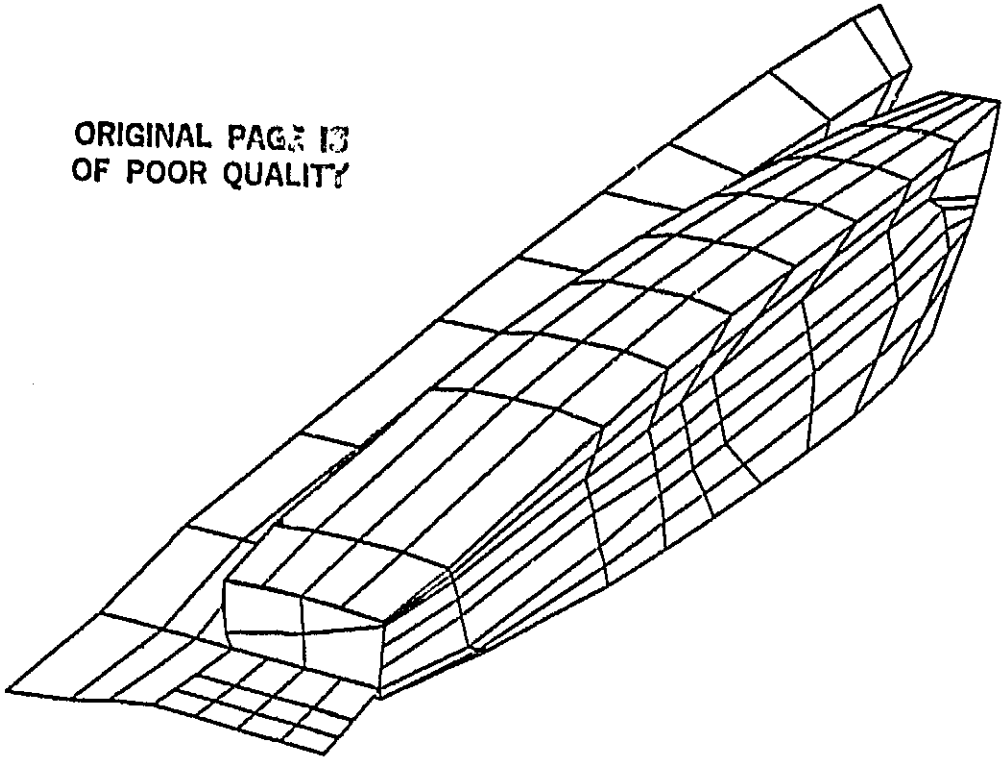

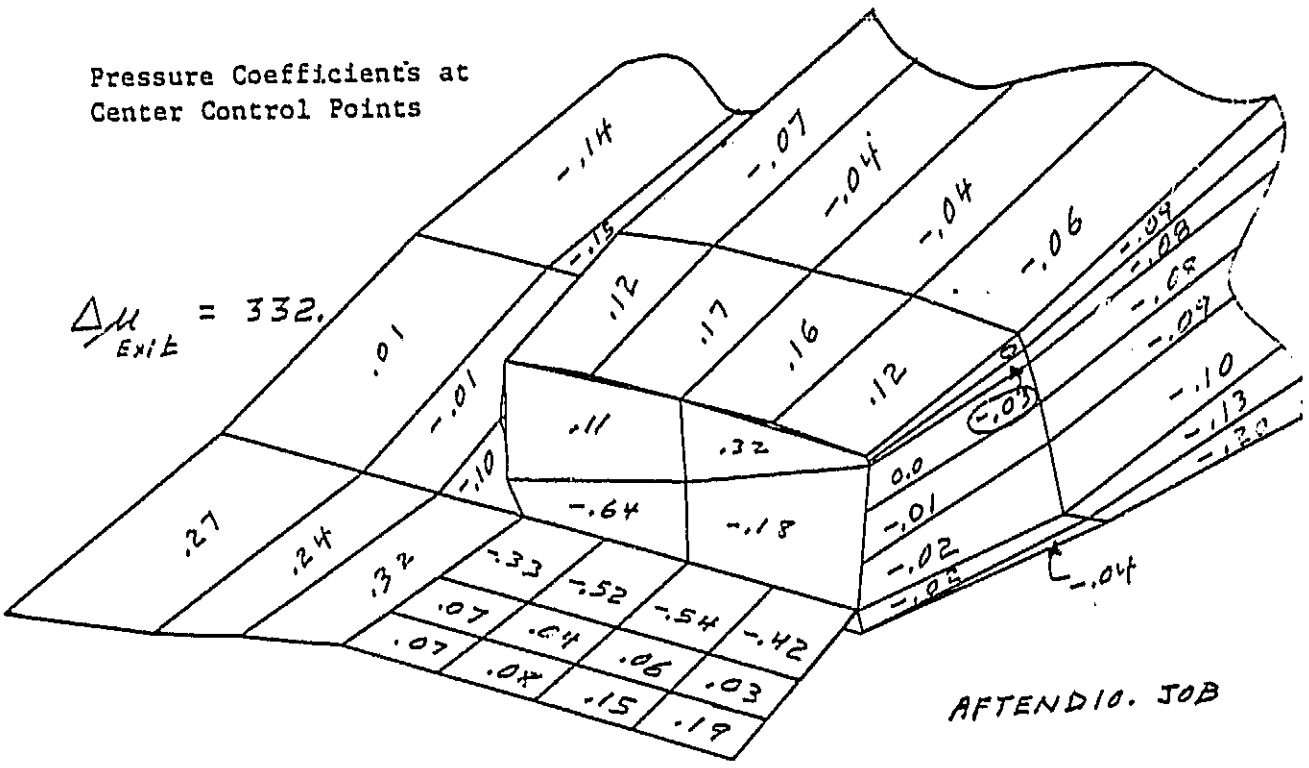

Figure 15 Pressure Coefficients for Aftend Model Number 10 With Adjusted Doublet Strength

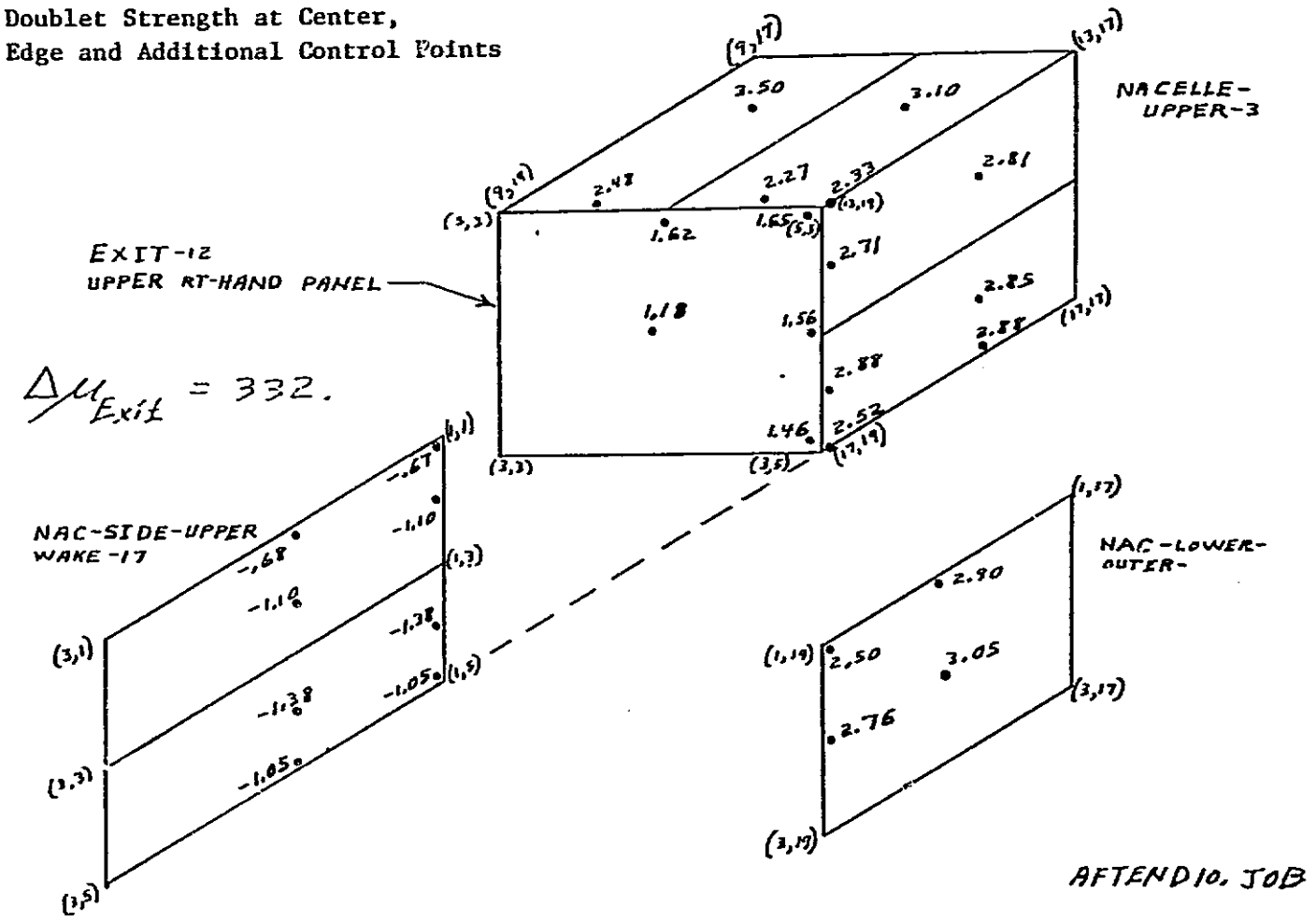

Figure 16 Doublet Strength For Panels of Concern on Aftend Model Number 10 With Adjusted Doublet Strength

Aftend Model No. 12. This model geometry (Figure 17) was similar to Aftend Model No. 10 in all respects, except for the widths of the panels in the last row on the side of the nacelle, which were changed to eliminate the two very high aspect ratio panels. The boundary conditions were also identical, except that the doublet strength on the exit network was not adjusted. The pressures in Figure 17 and the doublet strengths in Figure 18 appear reasonable and also compare favorably with the Aftend Model No. 10 results that included the doublet strength added to the exit network (Figures 15 and 16).

The computed normal force coefficients also compare favorably between Model No. 10 with the adjusted doublet strength and Model No. 12. These results are shown in Table 1. The normal force coefficients for these two models are considerably different from those of Aftend Model No. 10 without the doublet strength adjusted.

Careful consideration of all the results obtained to this point led to the conclusion that the doublet strength was not being handled correctly in complex abutments that included wake networks. Apparent errors were observed in the apportionment of doublet strength to the networks of these abutments when the abutments included high-aspect ratio panels and when there were large differences in doublet strength between the networks.

2.2 IMPROVED PANELLING ARRANGEMENT

The investigation of the simplified aftend models indicated that the high negative pressures near the nozzle exit were the result of doublet apportionment errors at the complex abutments involving the nacelle, exit, and wake networks. The apportionment process is handled by a set of subroutines utilizing a highly complex logical structure. Although the precise cause of the problem was not identified, it was felt that under certain geometrical conditions the logic of these subroutines failed to correctly apportion the doublet strength. One way to avoid this problem was to simplify the geometry such that less demand was placed on the logic of these subroutines. Therefore, the fighter model was repanelled to eliminate as many potential problem areas as possible. The "improved" panelling arrangement, Figure 19, does not appear significantly different from the initial panelling arrangement (Figure 1). However, it incorporates the following changes:

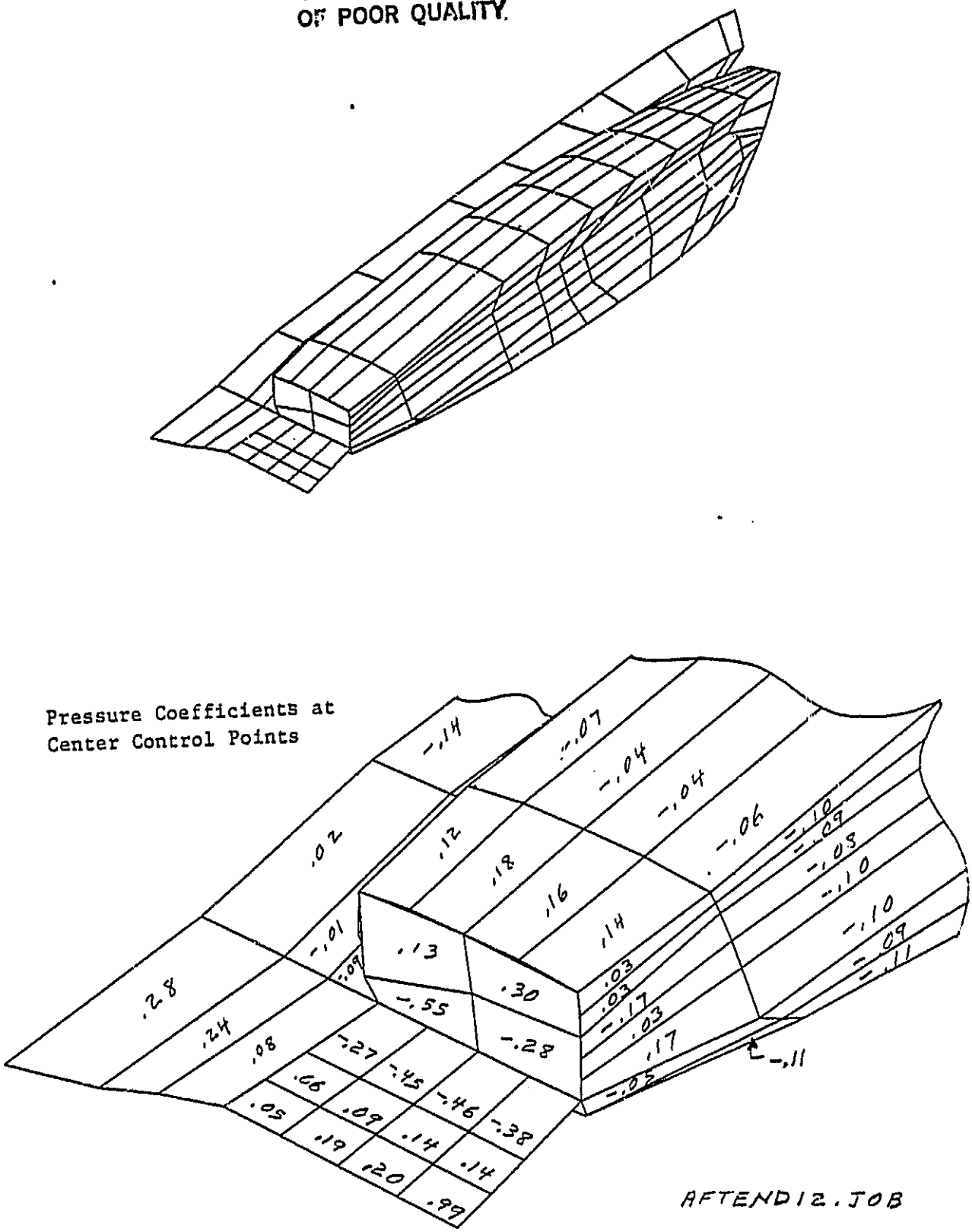

Figure 17 Aftend Model Number 12

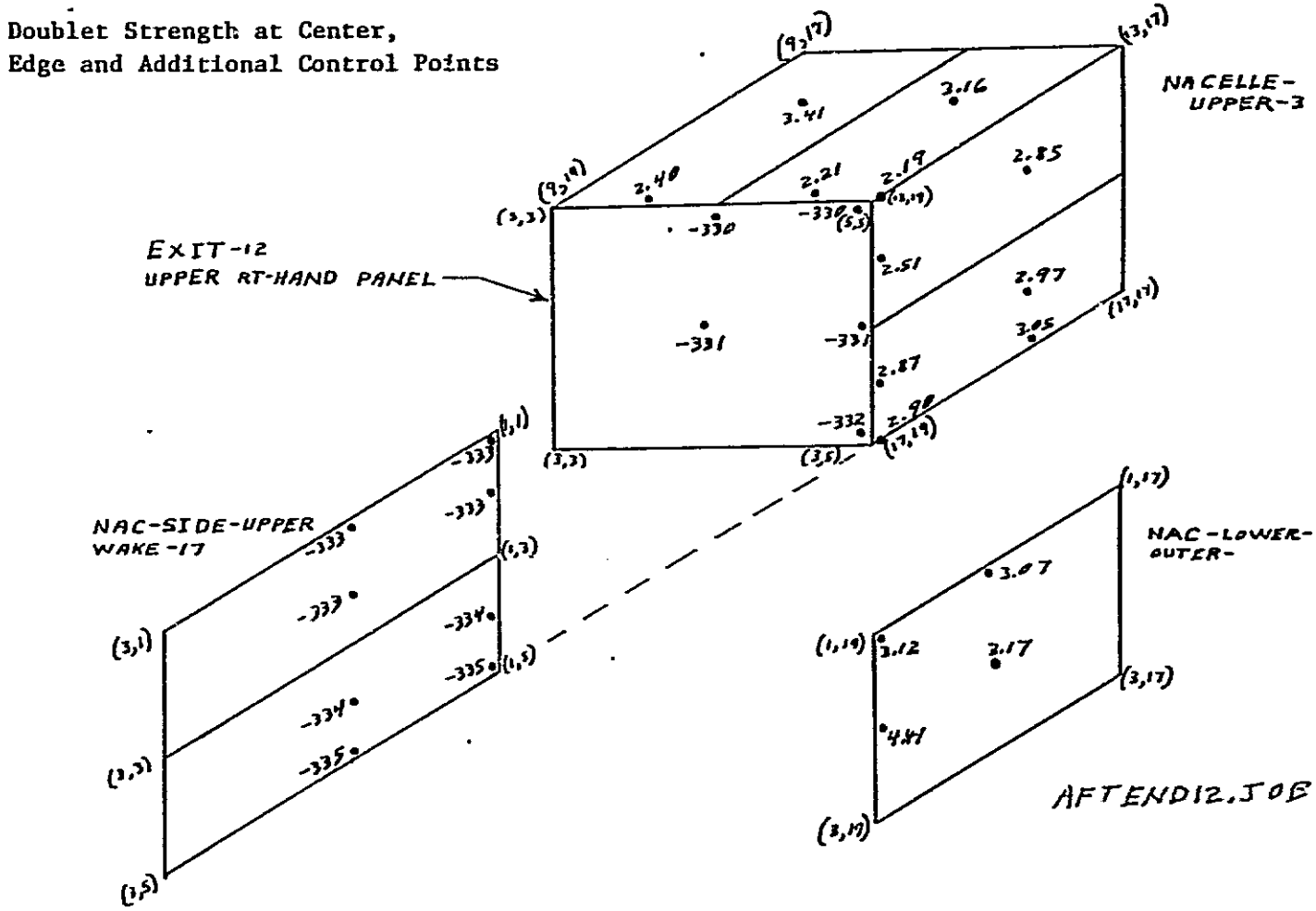

Figure 18 Doublet Strength on Panels of Concern, Aftend Model Number 12

TABLE 1

NORMAL FORCES ON SELECTED MODEL COMPONENTS

MODEL COMPONENTS	MODEL NO. 10* $\Delta\mu = 0$	MODEL NO. 10** $\Delta\mu = +332$	MODEL NO. 12+ $\Delta\mu = 0$
Upper Strake	.034	.024	.024
Lower Strake	-.018	-.025	-.027
Upper Nacelle	.042	.025	.025
Flap Upper	.067	.004	.003
Flap Lower	-.021	.004	-.002
Exit Network	.024	.000	.000
Total (all networks)	.206	-.003	-.023

*Original panelling
**Original panelling with added doublet strength
+Original panelling with lower aspect ratio nacelle panels

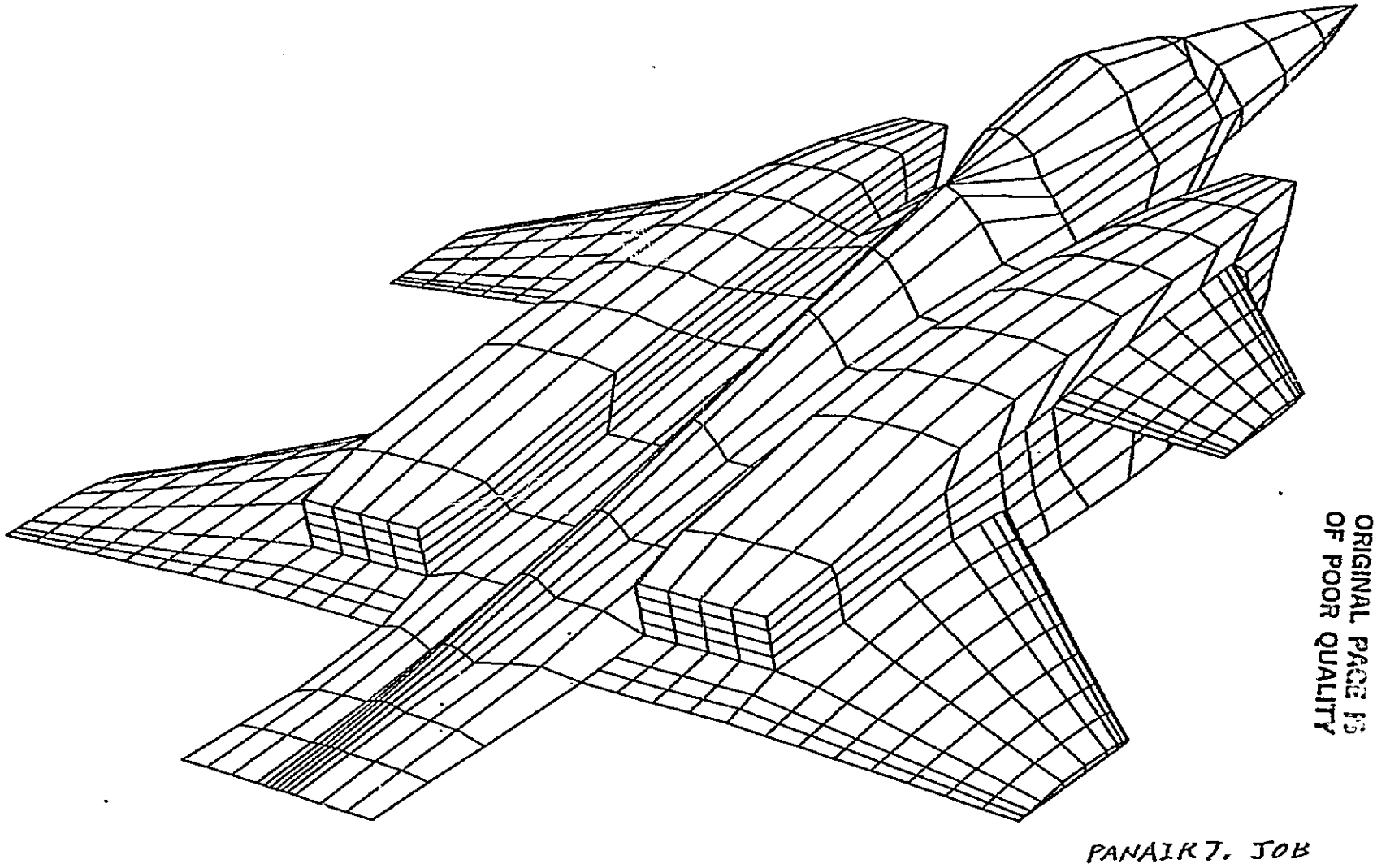

Figure 19 Improved Panelling Arrangement for the Fighter Model

- The number of panels on the nacelle sides was decreased, and the number of panels on the exit was increased to provide for exact panel corner point matching. This eliminated all gaps.

- The exit plane was modified such that the actual contours were approximated by a rectangular, planar network.

- The high aspect ratio panels on the side of the nacelle were eliminated.

- The high aspect ratio panels that formed the closure of the strake and beaver tail were removed, and the upper and lower networks of the strake and beaver tail were collapsed to form the closure as a sharp edge. This reduced the number of networks near the exit and simplified the abutment containing the inboard nacelle wake and the solid components of the configuration.

- The inverted U-shaped network which had previously represented the sides and top of the nacelle was divided into three separate networks.

These modifications required some deviation from the actual geometry of the fighter model. They were minor, however, and should have only a small, localized influence on the computed flowfield.

2.2.1 Nacelle Wakes Removed

The model with the improved panelling arrangement discussed in the previous section was initially evaluated with the nacelle wakes removed. The canard, wing, flap, and beaver tail wakes, however, were retained for this run. Because the wakes were removed from the nacelle, it was necessary to change the boundary conditions on the exit network to those for an impermeable surface (Class 1, UPPER).

The computed pressure coefficients at the center control points, shown in Figure 20, are within a reasonable range for all panels. However, there were numerous "edge" and "additional" control points where the computed pressure coefficients were in an unreasonable range. It has been reported by NASA that the error causing the high negative values at these control points has been identified and will be corrected in a later version of PAN AIR.

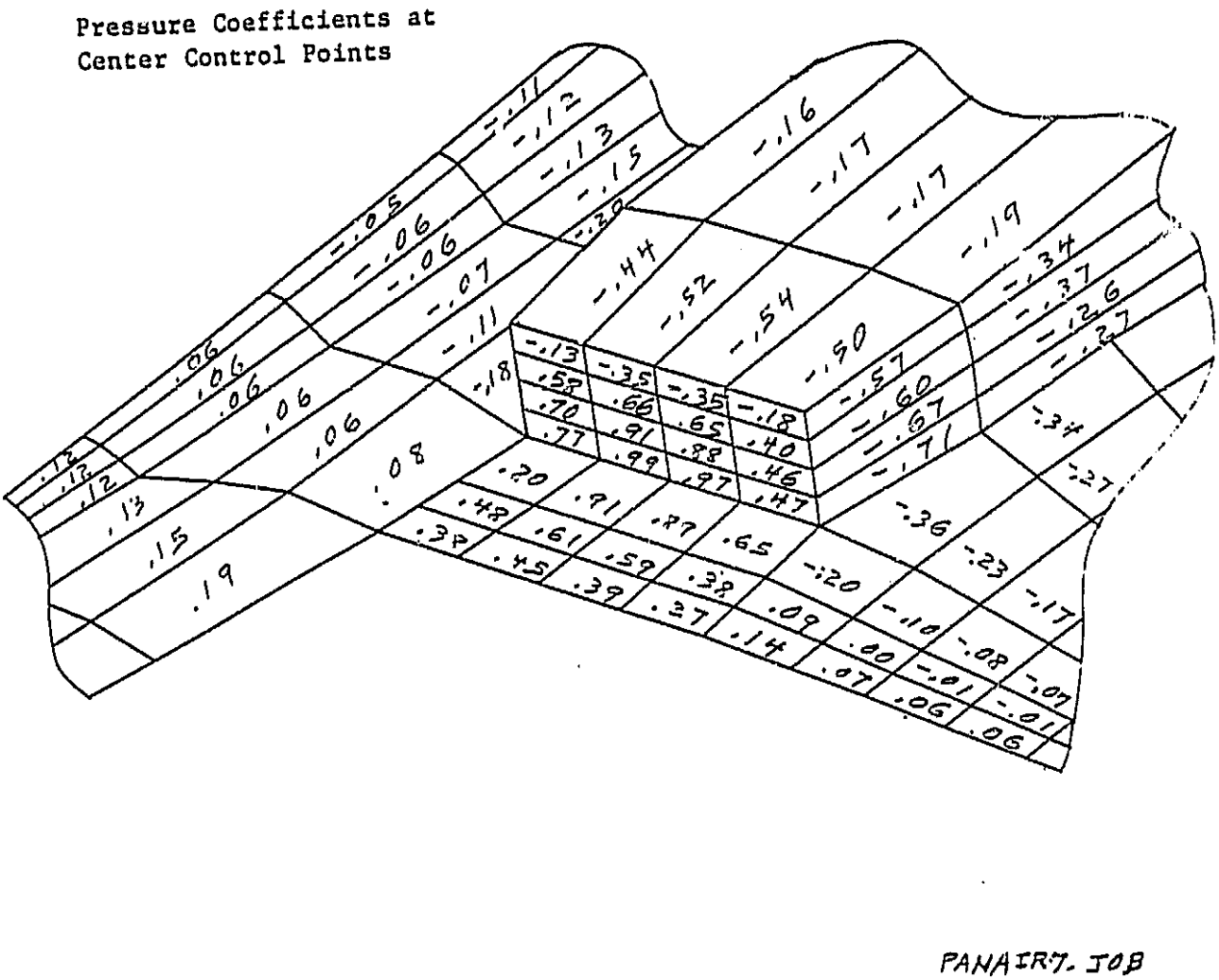

Figure 20 Pressures With Nacelle Wakes Removed, Improved Panelling Arrangement

2.2.2 Nacelle Wakes Included

Encouraged by the results computed for the model with the improved panelling arrangement and with the nacelle wakes off, the analysis of this configuration with all the wakes included was made using the PAN AIR code. The exit network boundary conditions of Equation 2 were also used for this model. The pressure coefficients computed for the first run appeared reasonable on all of the impermeable panels (Figure 21a). However, the inboard nacelle wake had high negative pressures where it abutted the strake and flap upper surface (Figure 21b). This abutment was unique in that the strake had only one panel in this abutment, whereas the flap upper network contributed three panels to the abutment.

The panelling arrangements of the strake and fuselage were modified as shown in Figure 22, so that the surface networks in that abutment would have matching panel corner points. The pressure coefficients computed for this arrangement were reasonable for all configuration panels, as shown in Figure 22a. However, the pressures remained unreasonable at the center control points of the wake in that abutment, as shown in Figure 22b.

At this point, it appeared that the problem was introduced by the abutment of three panels in each of the surface networks with a single panel in the wake network (Figure 22b). Therefore, Aftend Model No. 13 (Figure 23) was developed to investigate this specific feature of the panelling arrangement. The panelling arrangement is shown without any of the wakes and also with the inboard nacelle wake included. When this model was evaluated, wakes were included that emanated from the flap, the sides of the nacelle, and the beaver tail. Table 2 lists five variations of the panelling arrangments that were evaluated with this model. Figure 23 shows the center control point pressure coefficients for Case D. The computed values for this case are reasonable and are typical of all of the variatons that were evaluated. The pressure coefficients also appeared correct at the edge and additional control points. Thus, the problem that developed at a similar abutment on the improved fighter model panelling arrangement could not be simulated by any of the cases with Aftend Model No. 13.

The last run with the improved panelling arrangement model was made after adjusting tne doublet strength of the exit network in the manner discussed in Subsection 2.1.2. The pressure coefficients predicted by this computation (Figure 24) appear

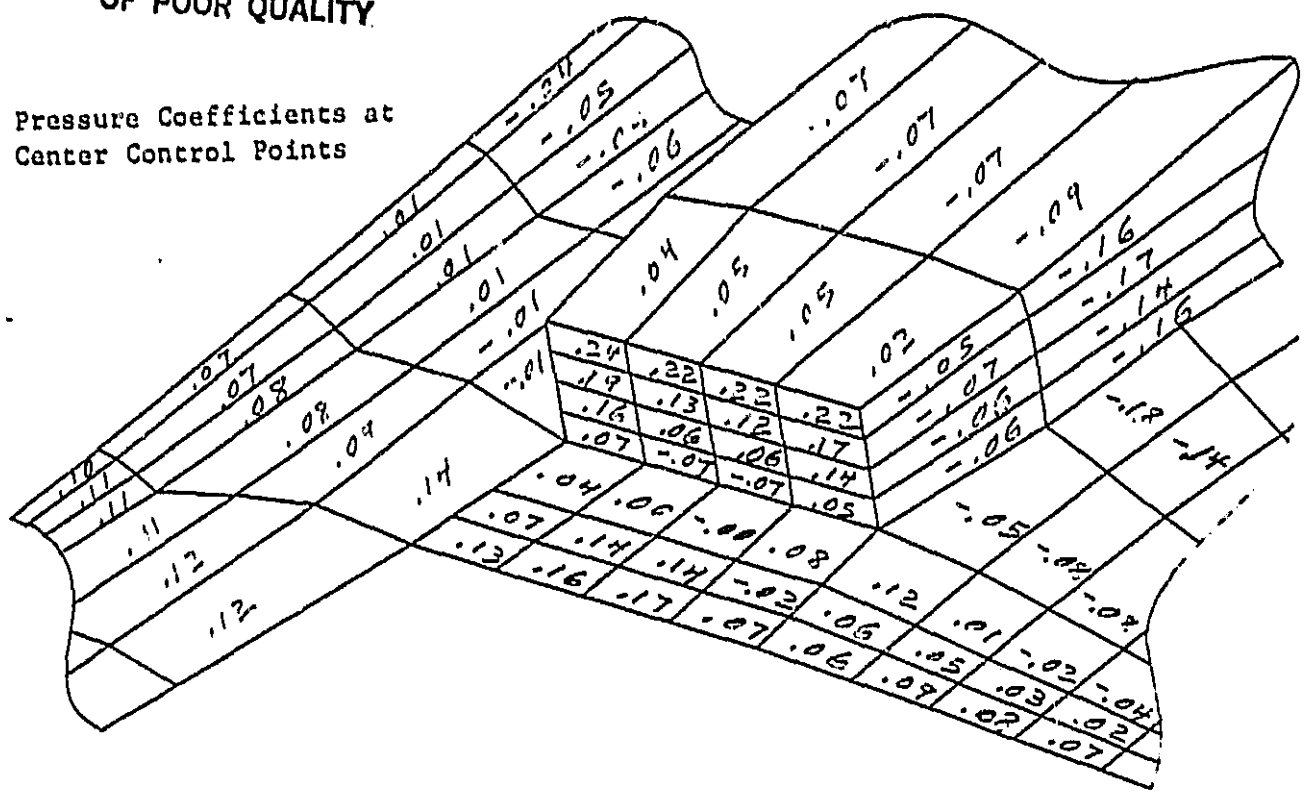

(a) Pressure Coefficients on solid panels

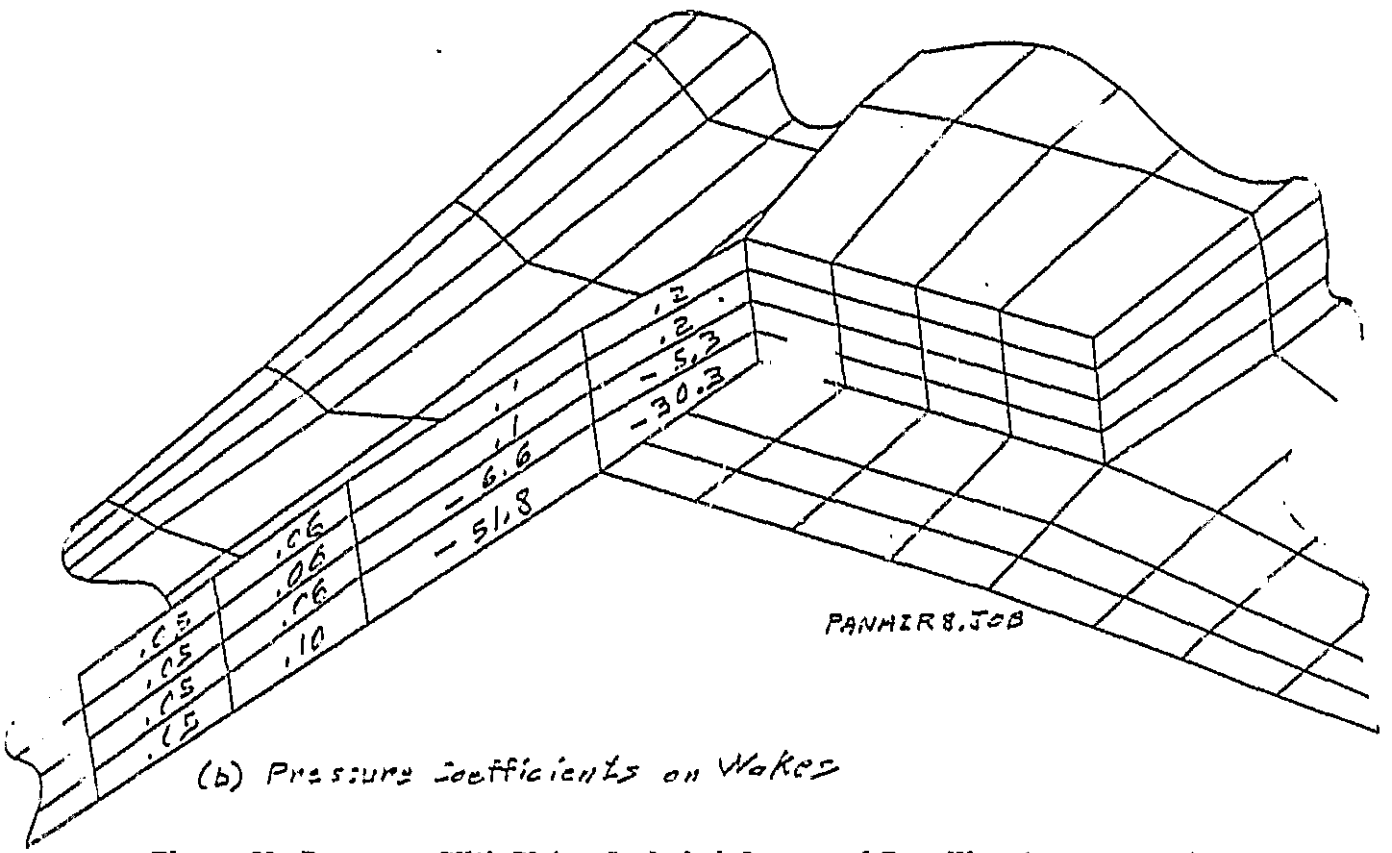

(b) Pressure Coefficients on Wakes

Figure 21 Pressures With Wakes Included, Improved Panelling Arrangement

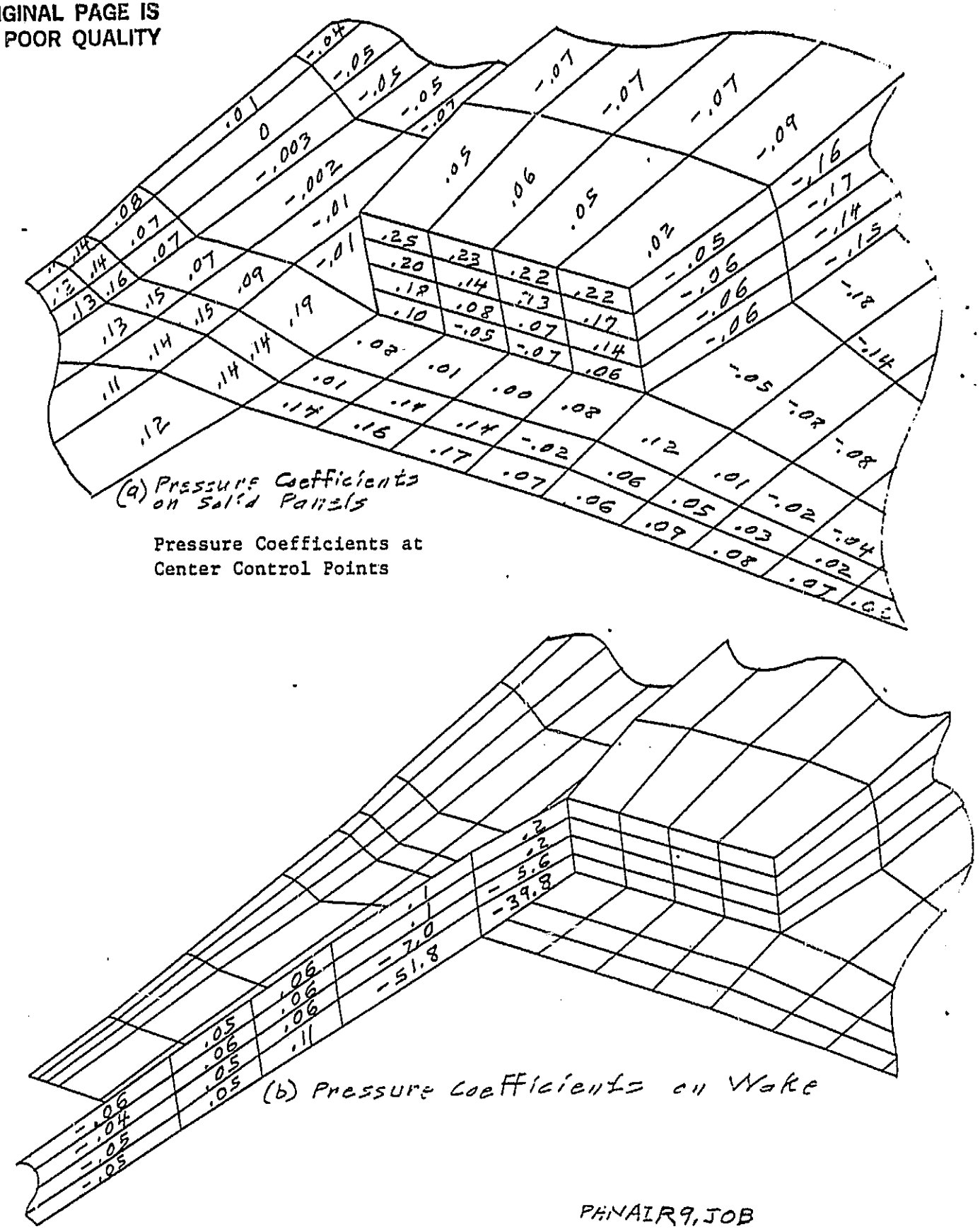

Figure 22 Pressures With Wakes Included and Panels Added on Strake

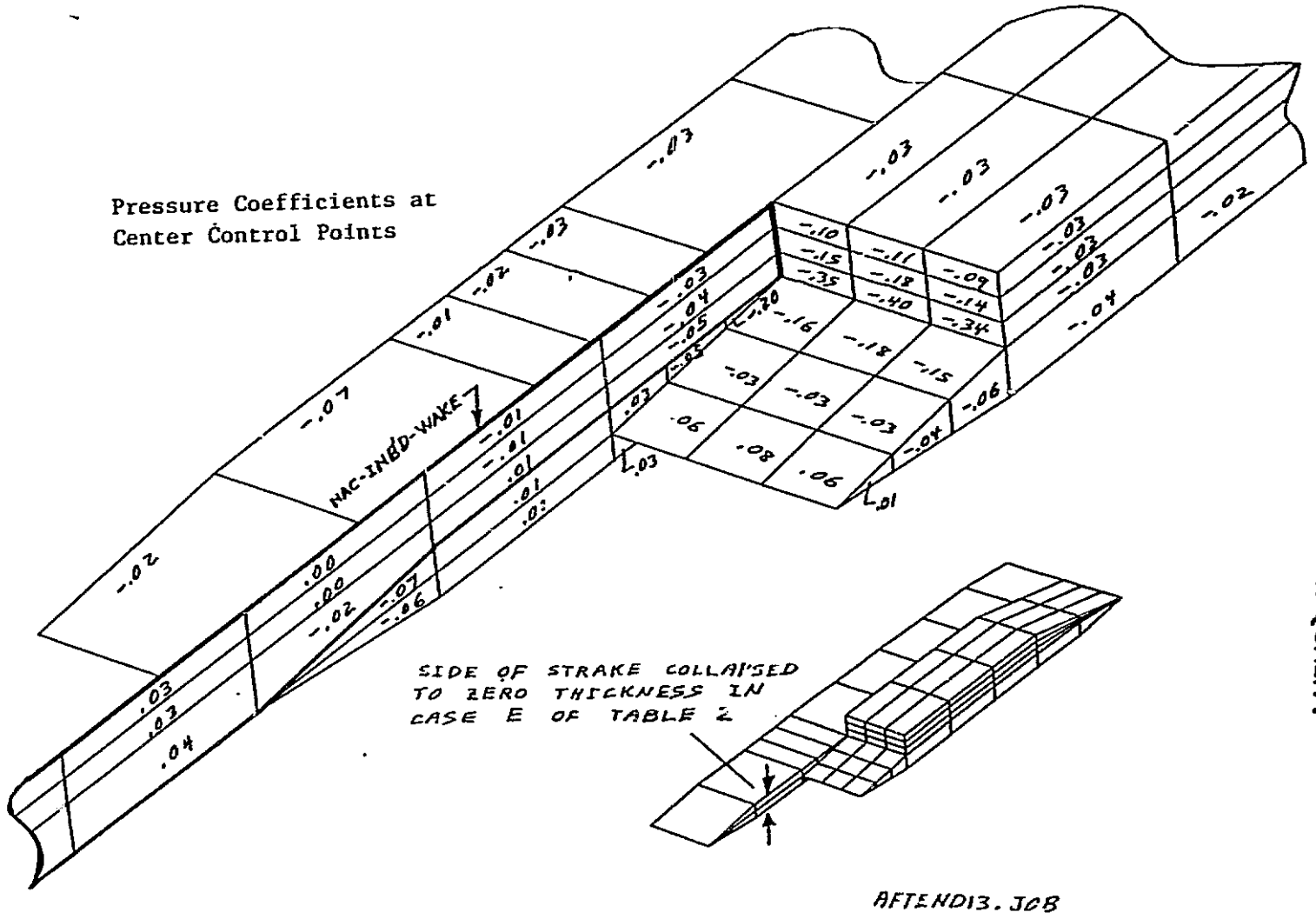

Figure 23 Aftend Model Number 13

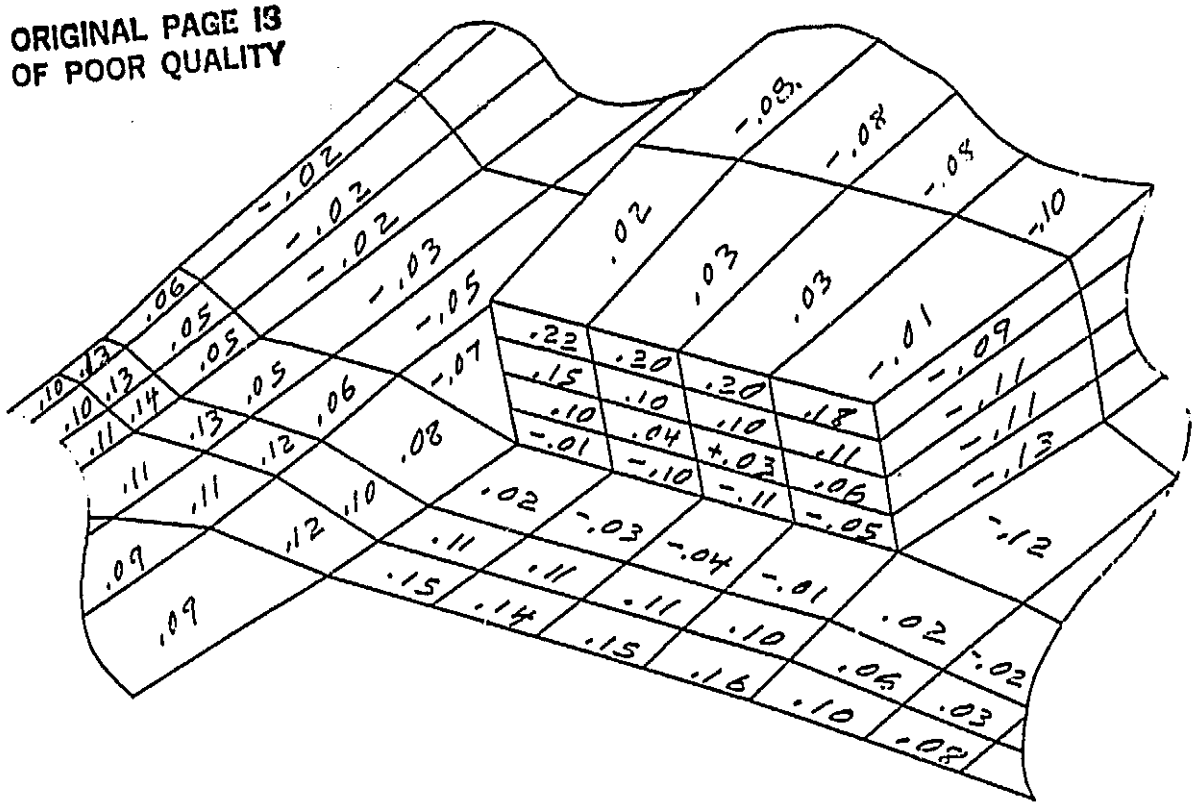

Pressure Coefficients at
Center Control Points

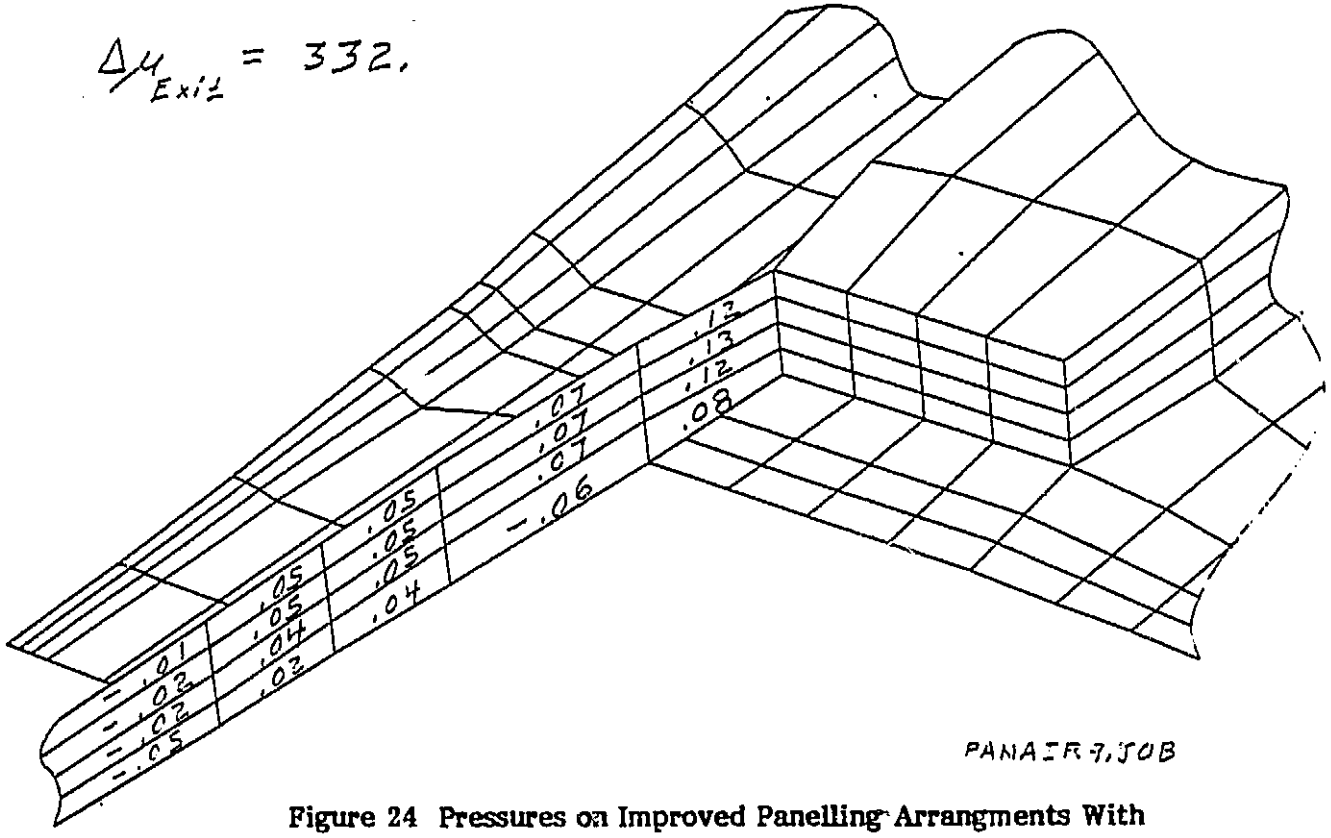

Figure 24 Pressures on Improved Panelling Arrangments With
Adjustment to Doublet Strength

TABLE 2

CONDITIONS AT FLAP INBOARD ABUTMENT
FOR AFTEND MODEL NO. 13

Case	Strake Panels in Abutment	Wake Panels in Abutment	Collapsed Edge of Strake	Abutments Specified
A	3	3	No	No
B	1	3	No	No
C	1	3	No	Yes
D	3	1	No	No
E	1	1	Yes	Yes

reasonable on both the surface and wake panels. Thus, it appears from the pressure data that the adjustment of the doublet strength eliminated the problem that had adversely influenced the pressure predictions near the nozzle exit. Elimination of the obviously erroneous values of computed pressure coefficients, however, does not necessarily imply that a valid solution has been obtained. Furthermore, the discussion in Subsection 2.4 reveals that the adjustment of the doublet strength did not cause the predicted forces to reach the values that were expected.

2.3 MODEL PANELLING WITH EXACT WAKE NETWORK EDGE MATCHING

A final attempt was made to run the fighter model by dividing the wake networks into several networks in a chordwise direction. The objective was to provide exact network edge matching between the nacelle wakes and the abutting solid networks. This portion of the panelling arrangement near the nozzle exit satisfied the requirements of the PAN AIR Pilot Code. The strake and beaver tail networks were redistributed into three new networks: (1) strake leading edge to nozzle exit plane, (2) exit plane to flap trailing edge, and (3) flap trailing edge to beaver tail trailing edge. The nacelle inboard wake was panelled such that the network edges exactly matched the edges of the strake networks. This pattern was continued throughout the nacelle wakes, the wing wake, and the canard wake.

The computed pressure coefficients for this arrangement (Figure 25) include high negative values near the nozzle exit. Although the values are different from earlier evaluations, the overall data patterns are similar. It is shown in Subsection 2.4 that the computed forces on the model were substantially different for this panelling arrangement.

2.4 IMPACT OF THE ABUTMENT PROBLEM

Computed pressure coefficients near the nozzle exit have been discussed for several panelling arrangements of the fighter model. These pressure coefficients are erratic and sometimes of an unreasonable magnitude. The areas that are significantly affected are small and are located near the nozzle exit. Examination of the localized pressure field, such as those presented in the previous subsections, do not reveal the full impact of the problem on the overall aerodynamic predictions. The wing chordwise pressure distributions and the computed forces and moments can be used to quantify overall changes in the pressures on the configuration

The chordwise pressure distributions computed for the wing and canard of the fighter model with the improved panelling arrangement and with the nacelle wakes removed were compared with experimental data (Figure 26). The experimental pressure distributions correspond with the pressure data presented in Figure 20. Analysis of the experimental fighter model pressure data (Reference 3) identified an area near the leading edge of the canard that was influenced by a leading-edge vortex at an angle of attack of 4 degrees. The effects of the vortex, shaded in Figure 26, account for the discrepancy between the test and predicted pressure distributions on the canard upper surface. The test and theory match quite well at the outboard wing station and on the canard lower surface. At the inboard wing station, the correlation between predicted results and experimental data was poor. This wing station is in close proximity to the exit network, where an impermeable surface boundary condition was used in this analysis. The use of this boundary condition may have had an adverse influence on the wing pressures at this station. The solution obtained gave no indication of any problems. The chordwise pressure distributions computed for the wing and canard of the fighter model with the improved panelling arrangement and with all the wakes included in the analysis were also compared with experimental data (Figure 27). In this case the correlation between predicted results and experimental wing data was not as good as it was with the nacelle wakes off (Figure 26).

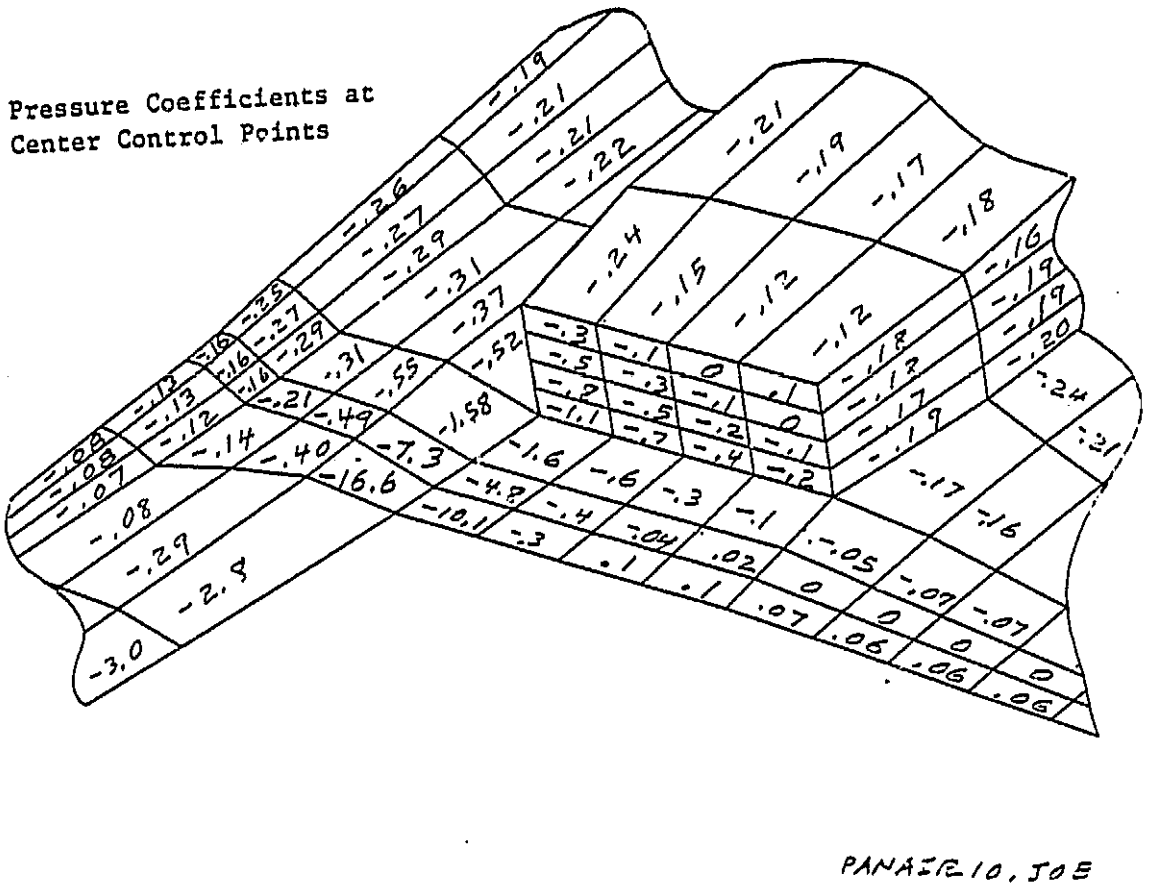

Figure 25 Pressures on Network Edge Matching Arrangment

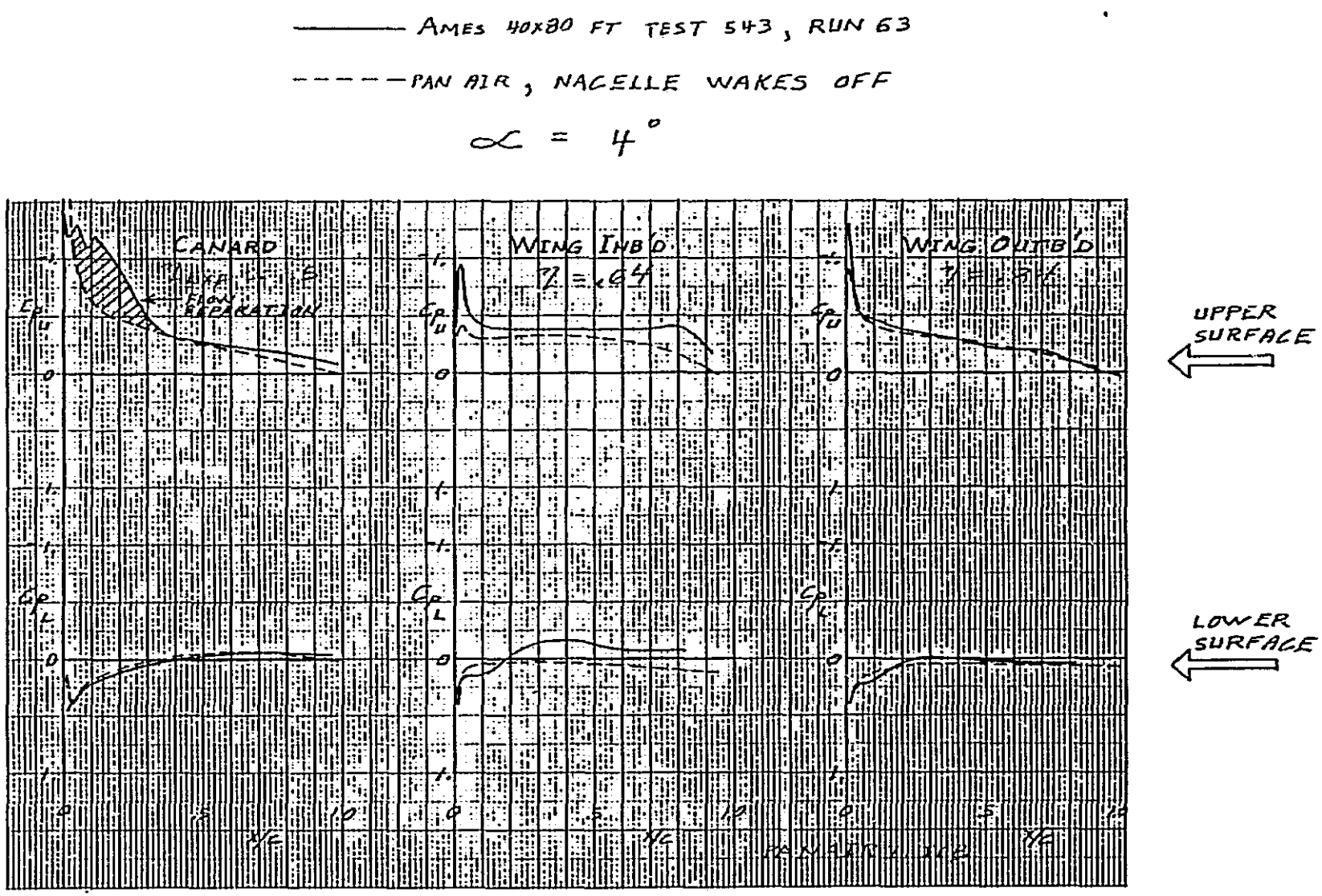

Figure 26 Chordwise Pressure Distributions, Wakes Removed

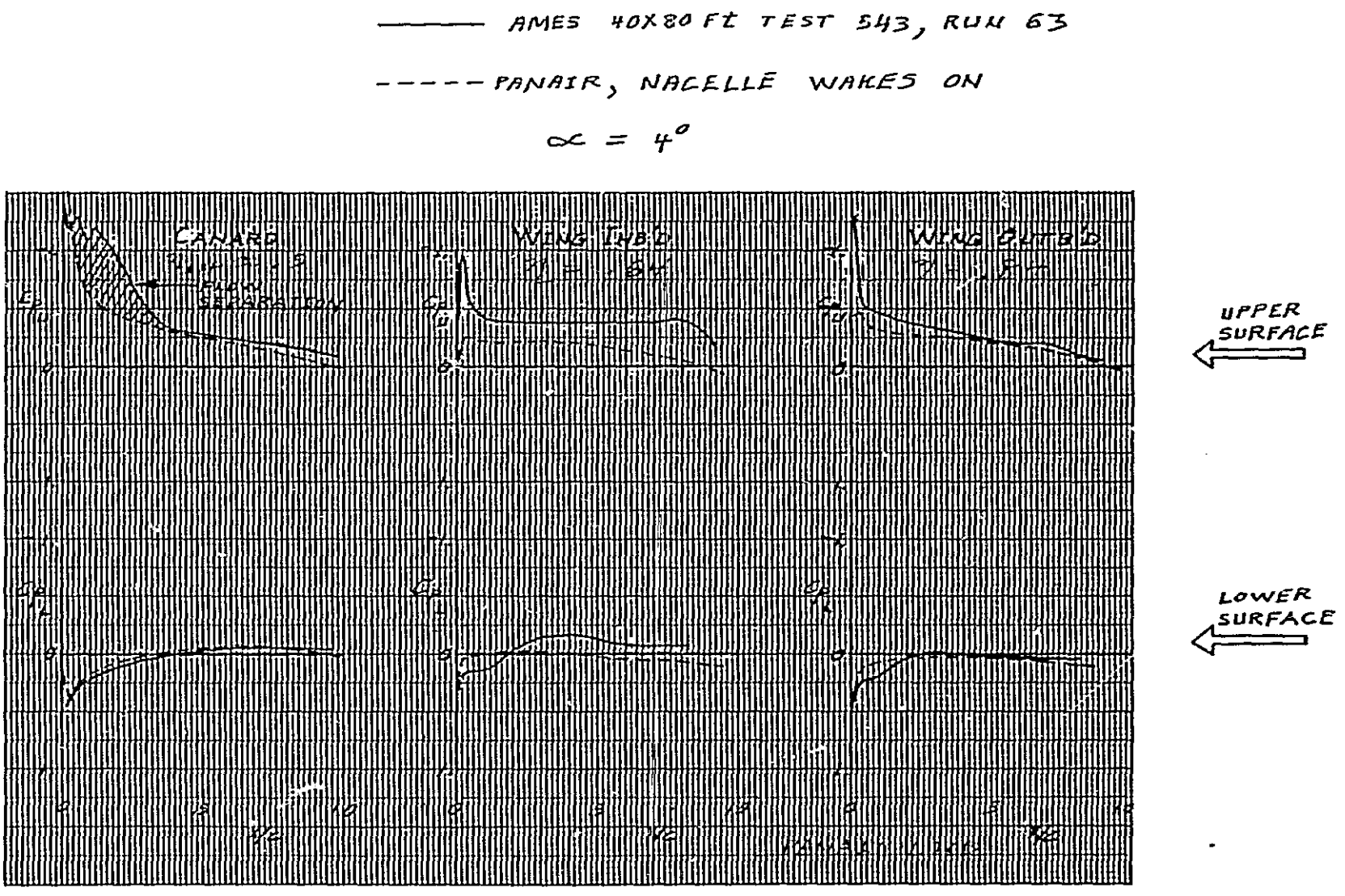

Figure 27 Chordwise Pressure Distributions, Wakes Included

The predicted lift curves for the "initial", "improved", and "matching" panelling arrangements (Figure 28) did not show good correlation with experimental data. Lift predictions for the improved panelling model are also shown in Figure 28 for (1) the nacelle wakes off and (2) for an adjusted doublet strength at the nozzle exit. The details of the input for these two runs and the resulting pressure predictions have been discussed in Subsection 2.2. The best correlation with force data was obtained when the nacelle wakes were removed.

When the boundary conditions on the improved panelling model were modified to adjust the doublet strength on the exit network to a value close to that found on adjacent networks ($\Delta\mu$=332) the following two phenomena were observed

1. The abnormally high pressure coefficient values found at certain center control points for the unadjusted case took on reasonable values as discussed in Subsection 2.2.2 (Figure 24).

2. The discrepancy between the predicted and experimental lift curves was reduced slightly, although still not in good agreement with experimental data.

From this it can be deduced that the adjustment of the doublet strength eliminated the abnormally large negative values of the pressure coefficient but did not correct the overall pressures.

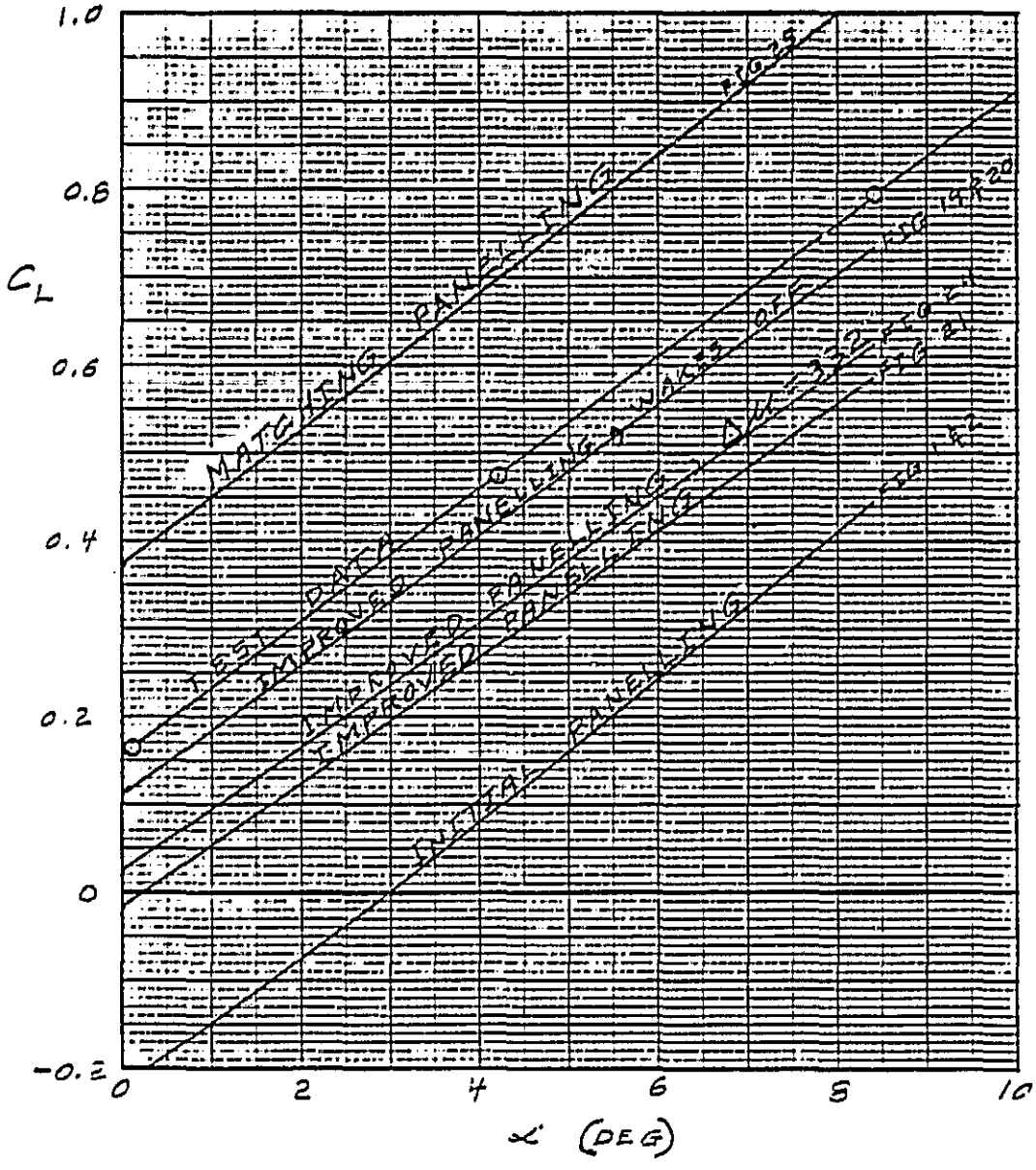

Figure 28 Test-to-Theory Lift Curve Comparisons

3 POWER EFFECTS INVESTIGATION

The investigation to find the best model to simulate power effects was accomplished with the use of the isolated nacelle model shown in Figure 29a. This model was powered by high pressure air and was tested in the 16-Ft Transonic Wind Tunnel at the NASA/Langley Research Center. Nozzle boattail pressure data were acquired for four boattail configurations at several nozzle pressure ratios and Mach numbers (Reference 3).

The effect of nozzle pressure ratio on the measured boattail pressure coefficients for two configurations are shown in Figure 29b. These data clearly indicate the significance of power effects on the boattail pressures. The nozzle configuration number 1 of Figure 29a was selected for use in this investigation, and the panelling arrangement that was devised for this configuration is shown in Figure 30. The panelling density was increased on the boattail to get the best predictions in regions of interest with a minimum expenditure of computer resources.

Two basic ideas for modeling power effects were investigated during this study that were based on simulation of the exhaust plume in the flowfield. The first approach required specification of the velocity distribution on the exit plane (Figure 31a). This was done in hope that the computed flowfield would correctly generate the required plume shape. The second approach required specification of the plume as a permeable surface with inflow velocities corresponding to known values of flow entrainment (Figure 31b). In this approach the plume shape and entrainment velocities are computed external to PAN AIR.

3.1 VELOCITY SPECIFICATION TECHNIQUES

The method illustrated in Figure 31a for simulating a jet exhaust flow is based on satisfying velocity or mass flux boundary conditions on the exit plane. Although this approach did not prove to be satisfactory, plans were to use wake networks emanating from the perimeter of the nozzle to simulate the plume. Initially, the analytical solution would allow the high-velocity flow from the exhaust to expand through the wake network. The wake network would then be adjusted in an iterative manner such that no flow would cross its boundary. At that time the wake would correctly define the boundary of the

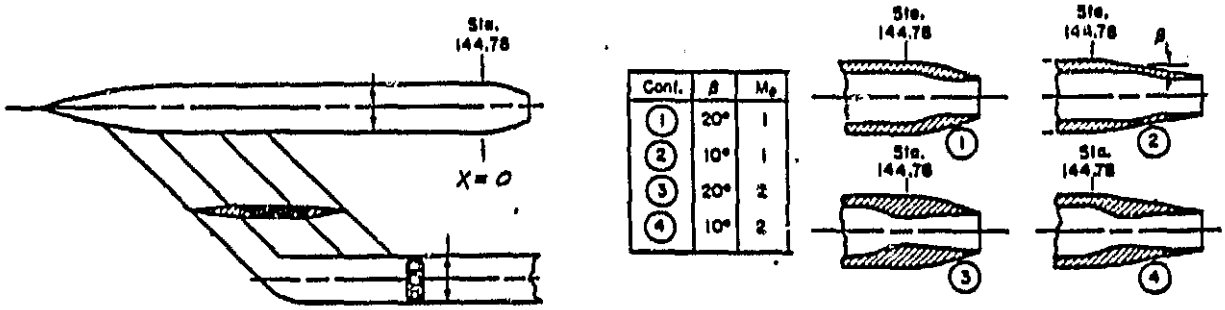

(a) NOZZLE GEOMETRY

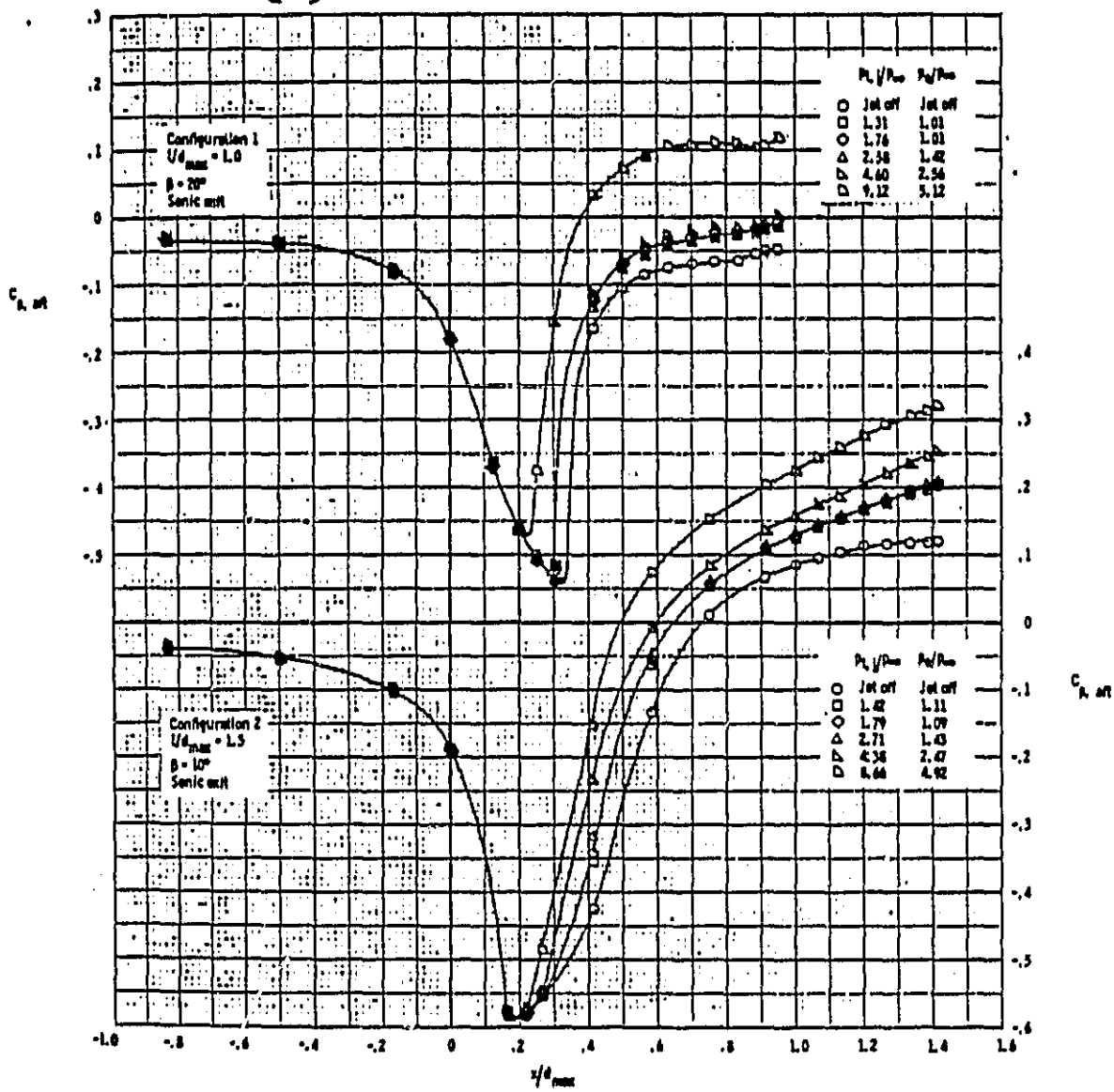

(b) EFFECTS OF POWER ON BOATTAIL PRESSURE

Figure 29 Isolated Nacelle Model

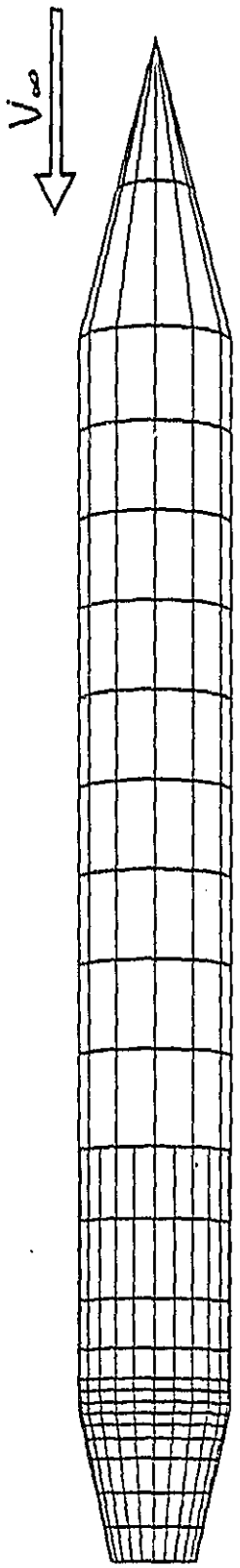

Figure 30 Panelling Arrangement For The Isolated Nacelle Model

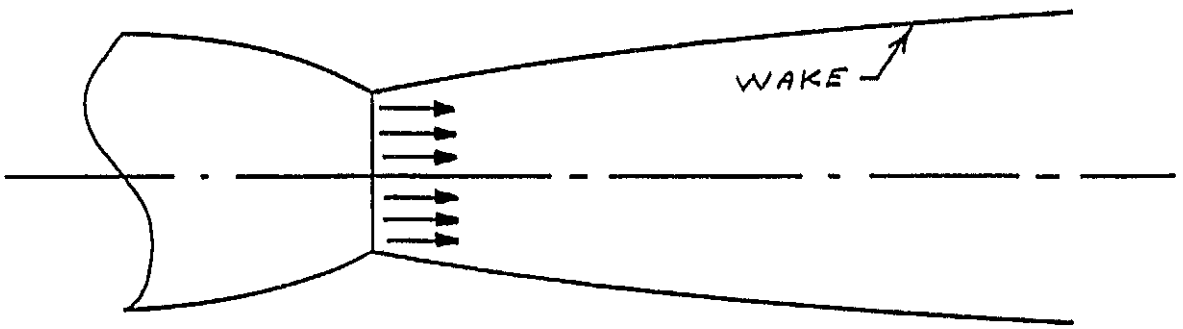

(a) VELOCITY SPECIFICATION APPROACH

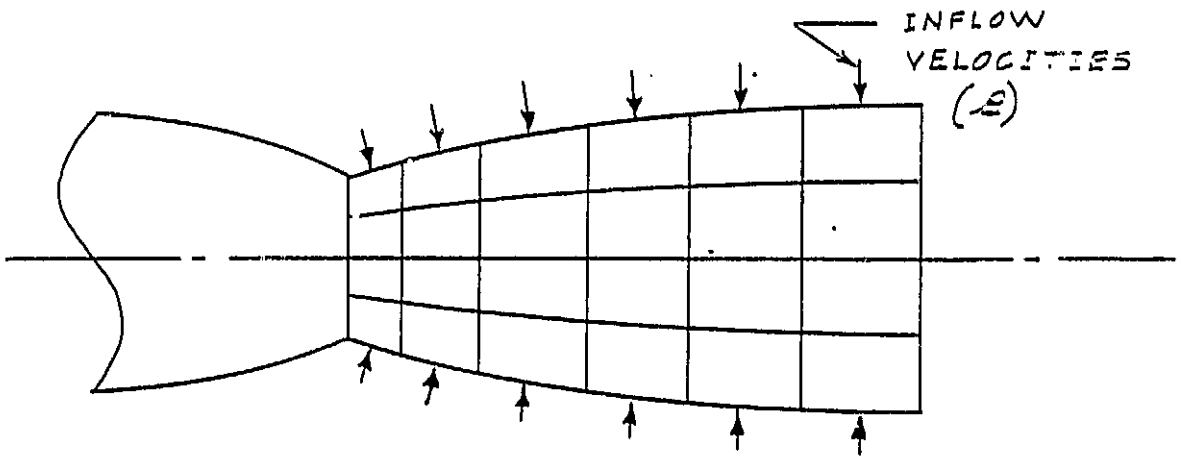

(b) PERMEABLE BODY APPROACH

Figure 31 Techniques For Modeling Exhaust Jets

inviscid plume. It was assumed that the inclusion of the wakes in the analysis model would sustain the jet velocities in the domain enclosed by the wakes.

A variety of boundary conditions were used in several computations carried out during the investigation of this modeling technique. The computed boattail pressure distributions, which are shown in the following figures, are plotted to a compressed scale. This was done so that the computed results could be shown even when they were obviously unrealistic. A pressure coefficient value of -3.96 is shown on several plots. It may be noted that this is the pressure coefficient value corresponding to an absolute vacuum at the Mach number for these runs (0.6). The code defaults to this vacuum pressure if the computed value is more negative.

The isolated nacelle was initially analyzed by PAN AIR with boundary conditions to simulate the power-off conditions. This was done to determine the influence of the wake networks on the flow field. The predictions are compared with experimental data in Figure 32. The boundary conditions of zero mass flux were used on all panels except those on the exit plane where the total potential was set to zero on the downstream side. This exit boundary condition imposed a requirement of zero tangential flow, as discussed in Subsection 2.1. In the analysis of this model, the WAKE 1 type networks were included to simulate the separated flow from the nozzle base. The pressure predictions were reasonable over the entire model. However, when an analysis was attempted with the wake networks removed, the computed pressures on the boattail region were adversely affected and reached unreasonable values near the end of the nozzle.

3.1.1 Specified Mass Flux

The power effects model analysis was initiated with the exit network boundary condition corresponding to a specified mass flux emanating from the nozzle exit network. An arbitrary value of 2.0 was selected for the total mass flux and the exit boundary conditions specified were:

$$\sigma = -\vec{U}_o \cdot \hat{n} + 2.0$$

$$\phi_L = 0$$

which are also referred to as Class 2, UPPER in the nomenclature of Reference 1.

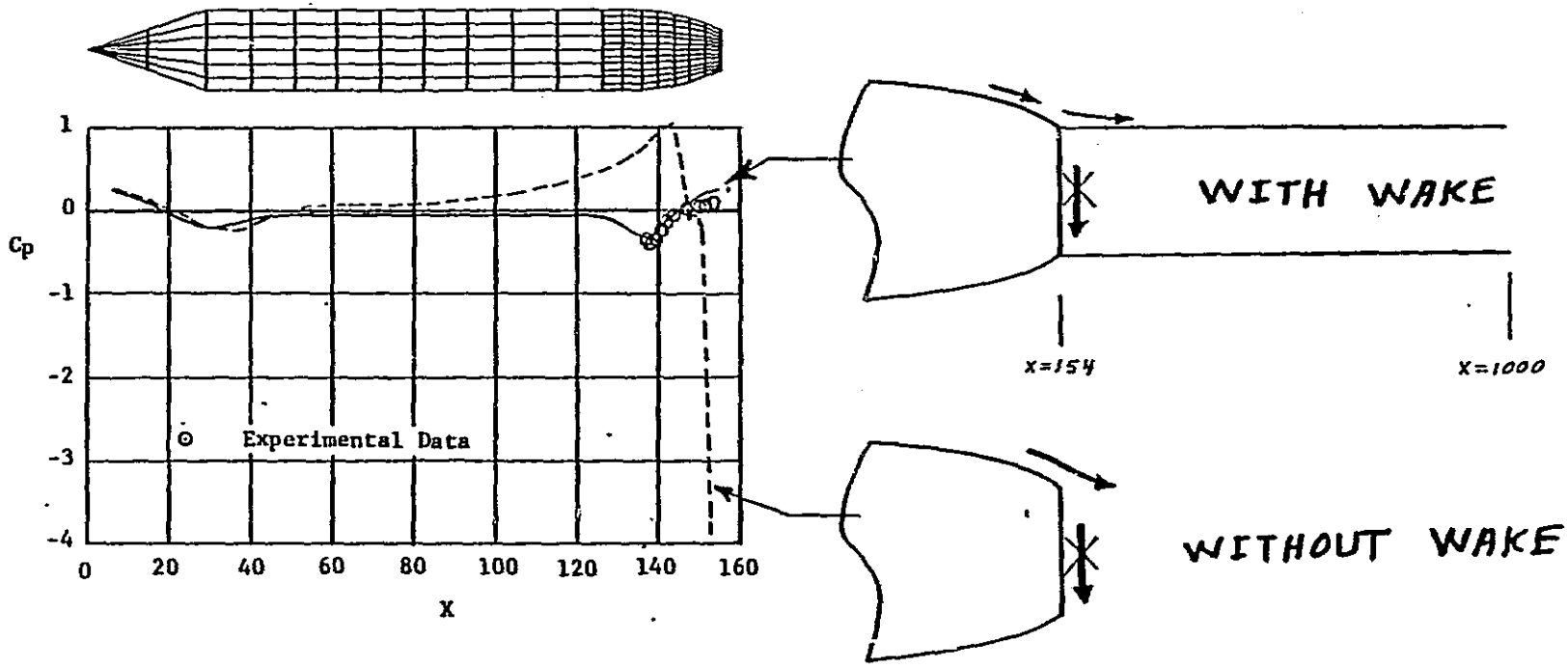

Figure 32 Isolated Nacelle Model With No Tangential Exit Flow

The constant (2.0) in the first boundary condition equation required the total mass flux normal to the exit plane to be twice the freestream velocity. With these boundary conditions and with the wakes removed, the computed pressure coefficients on the boattail of the isolated model were within an acceptable range (Figure 33). PAN AIR WAKE 1 type networks were then added. These networks force the streamwise components of the velocity to be the same on both the interior and exterior sides of the wake "tube". Thus, prescribing the interior flow emanating from the exit plane should have some effect on the exterior. However, when the wakes were included, the computed pressure coefficients were obviously wrong, with predicted pressures reaching absolute vacuum values in the boattail region. The influence of the wake was opposite that observed for the power-off case (compare Figures 32 and 33).

The model with specified mass flux and no wakes (Figure 33) appears to give the approximately correct flow field in the vicinity of the boattail. It was felt, however, that this model would not accurately predict the global effects of the plume since there is no mechanism to sustain the velocities imposed at the exit plane.

3.1.2 Specified Exit Velocity

To further explore these ideas the investigation was continued with specified exit velocity boundary conditions rather than specified mass flux. The computed pressure coefficients are shown in Figure 34. The boundary conditions used on the exit network for this analysis were

$$\vec{V}_u \cdot n = -\vec{U}_\infty \cdot \hat{n} + 2.0$$

$$\phi_- = 0$$

where the constant, 2.0, specified the magnitude of the exit flow velocity to be exactly twice the freestream velocity. When the wake was removed from the model, reasonable values of pressure coefficient were computed. However, there were the same drawbacks to this model as discussed for the model with mass flux boundary conditions. Mainly, there was no way to sustain the exhaust flow without a wake. This concept was verified by placing two survey planes behind the exit nozzle. They were located at 0.5 and 2.0 nozzle exit diameters downstream of the exit. The velocity decayed to almost freestream velocity at only 0.5 nozzle exit diameters downstream of the exit. This weakness in the model, in the opinion of the authors, makes it unusable to simulate global effects of the plume.

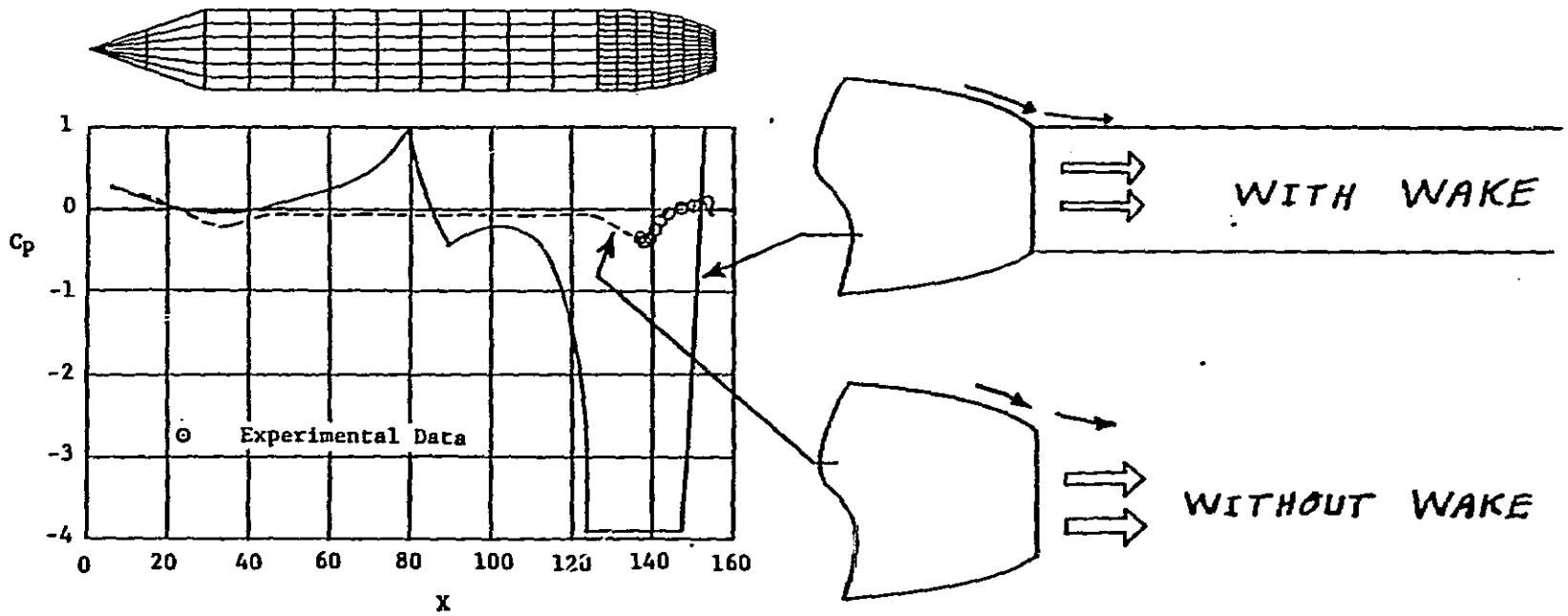

Figure 33 Isolated Nacelle Model With Specified Mass Flux

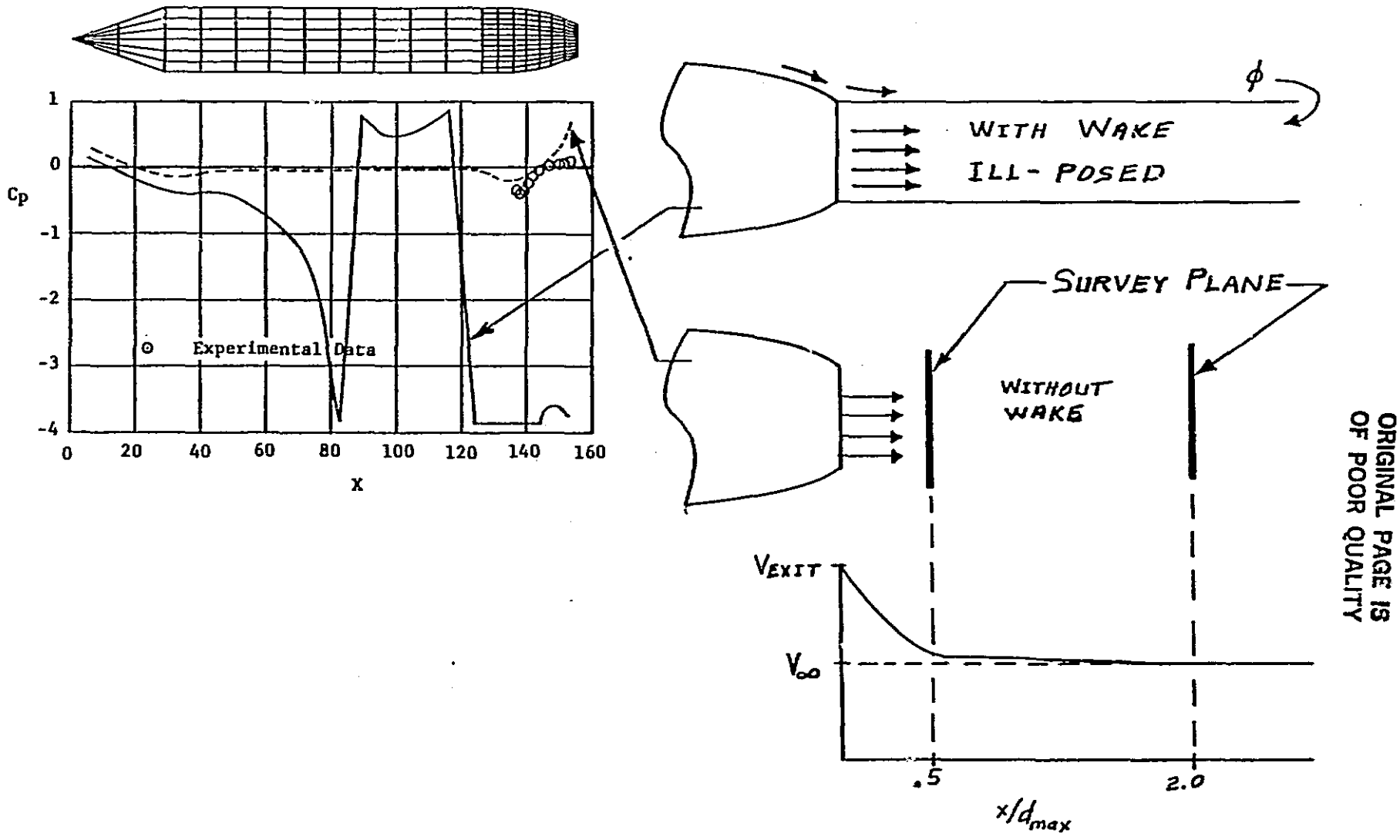

Figure 34 Isolated Nacelle Model With Specified Exit Velocity

When the wake was included, on the model with specified exit velocity, the computed flow field was obviously incorrect (Figure 34). This was the same trend that was observed for the model with the mass flux specified (Figure 32). After consultation with Dr. Erickson of NASA/Ames it was decided that these boundary conditions caused an ill-posed problem because the potential was not specified at any point within the domain enclosed by the wake. Note that the opening at the downstream end of the wake network is open and physically connects the potential on the exterior of the configuration with the potential in the domain surrounded by the wake. For tubelike networks that are sufficiently long, it is shown (Reference 2, Appendix A) that the region surrounded by the tube behaves like a closed region, even though one end is open.

Several attempts were made to remove the ambiguity in the specified exit velocity model by adding a closure network at the end of the wake. This should not have interfered with the far upstream flowfield and should have allowed the definition of the potential within the wake domain. Figure 35 illustrates this approach and the effect of the boundary conditions applied to the closure network on the computed pressure coefficients. Where the subscript L refers to the upstream side of the closure network, the three boundary conditions applied to this network were

Case 1

$$\phi_L = 0$$

$$\sigma = 0$$

Case 2

$$\phi_L = -\vec{U}_\infty \cdot \psi$$

$$\sigma = 0$$

Case 3

$$v \cdot \hat{n} = -\vec{U}_\infty \cdot \hat{n} + 2.0$$

$$\phi_L = 0$$

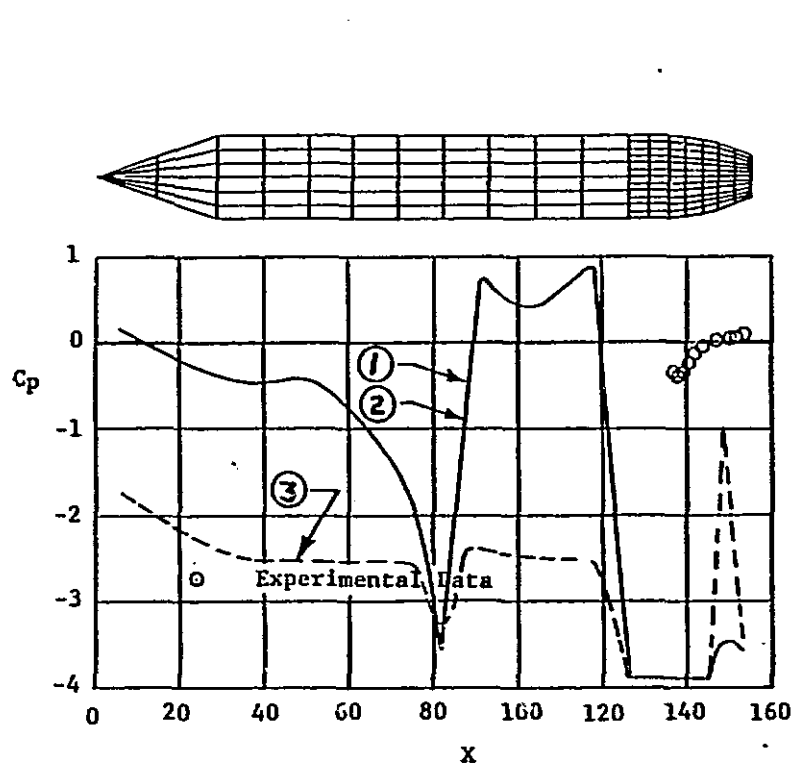

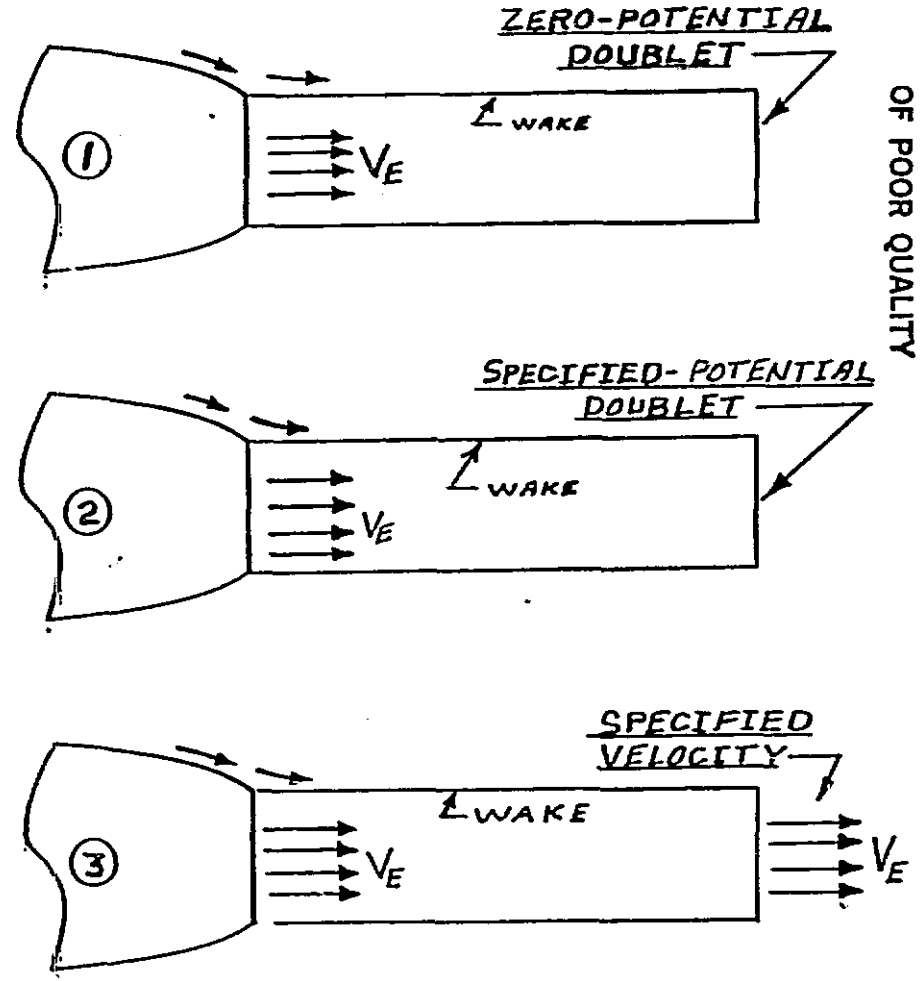

Figure 35 Isolated Nacelle Model With Specified Exit Velocity, Other Approaches

It is apparent from the computed pressure distributions that none of these three methods of specifying the potential within the wake domain improved the results. The first two methods used a doublet sheet to specify the potential in the wake domain and appeared to have negligible effect on the flowfield. The last set of boundary conditions caused the computed results to be worse by extending the abnormal pressure coefficient values upstream.

Since valid results could not be obtained for this model with the wakes included, this technique of representing the plume was abandoned in favor of the second approach which is discussed in the following subsections.

3.2 PERMEABLE PLUME MODELING TECHNIQUES

The jet simulation method illustrated in Figure 31b is based on satisfying a set of velocity conditions at a plume boundary calculated external to PAN AIR. The plume panelling is similar to the configuration panelling, except for the boundary conditions specified on the plume network, which are

$$\sigma = -\vec{U}_0 \cdot \hat{n} + \mathcal{L}$$

$$\phi_L = 0$$

and are referred to as Class 2, UPPER boundary conditions in Reference 1. Specification of the inflow mass flux to simulate entrainment is accomplished through the $\mathcal{L}$ term. This value can be prescribed in a global manner for all panels of the plume network, or it may be specified uniquely for each panel.

The initial permeable plume analysis was made with a straight plume (Figure 36) on which a global inflow velocity distribution was specified for all control points. The model was first analyzed with $\mathcal{L}$ set to zero, which corresponds to an impermeable-surface boundary condition on the plume. It was then run with $\mathcal{L}$ set to -0.2 which corresponds to an inflow mass flux of 20% of freestream velocity. The specification of this inflow induced a small reduction in pressure on the boattail of the nozzle. From the physics of the problem, it appears that the computed results show the correct trend.

To investigate the ability of this approach to induce global pertubations in the flow field, the highly divergent plume shown in Figure 37 was analyzed with a high value of

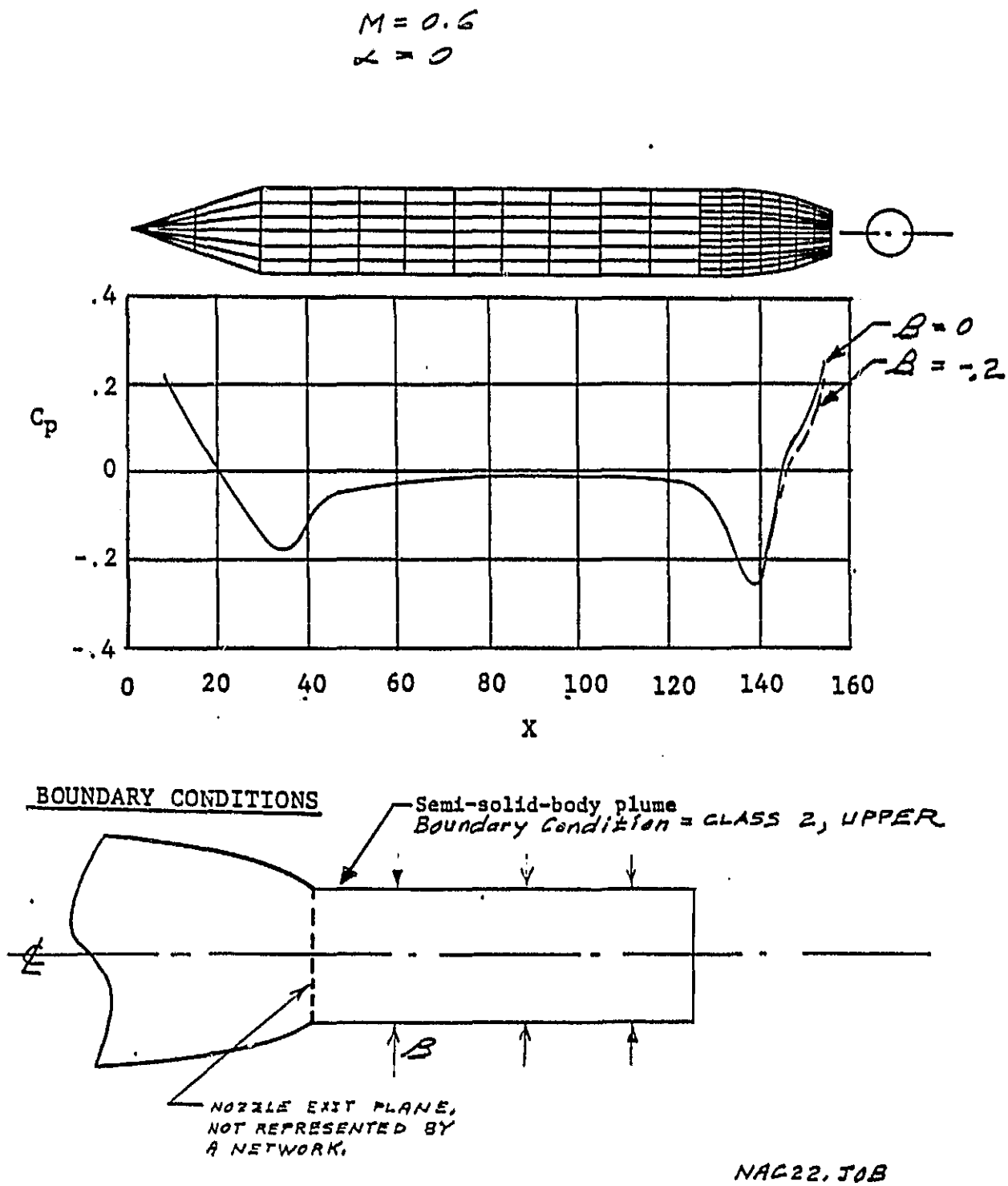

Figure 36 Isolated Nacelle Model With Cylindrical Plume

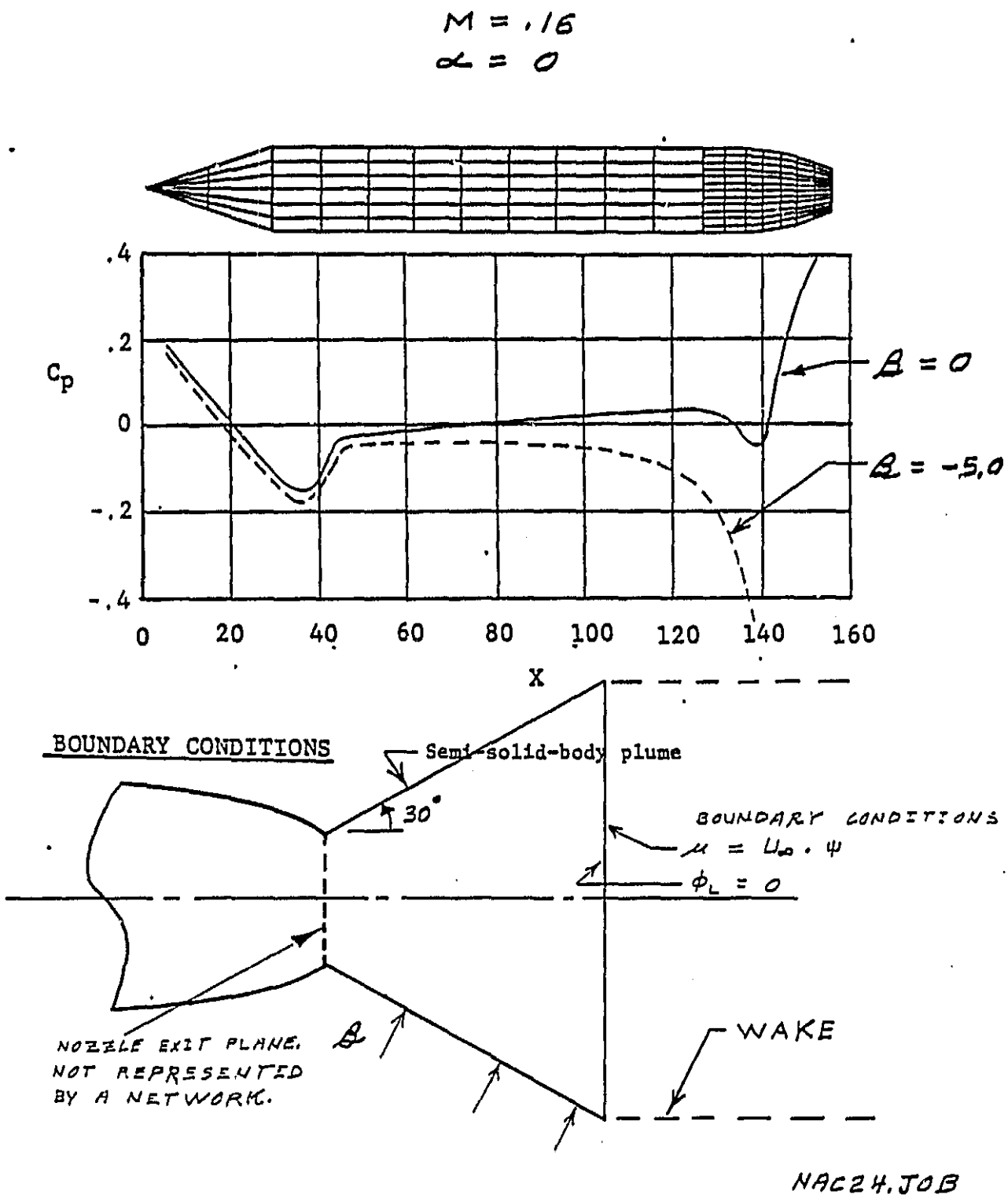

Figure 37 Isolated Nacelle Model With Conical Plume

inflow (α = -5.0). This model was selected, not based on any realistic plume shape, but to determine if the computations remained valid for extreme plume shapes and inflow velocities. Although there are no experimental data to substantiate the magnitude of the computed pressure changes, the results appeared reasonable. It was also encouraging to observe that the flowfield effects extended over the entire length of the body and were not limited to a local area near the nozzle exit.

The results of the permeable body approach were encouraging and this method was selected for further investigation.

3.3 RESULTS FOR THE ISOLATED NACELLE MODEL

Investigations of the isolated nacelle model discussed in previous subsections led to the selection of an approach by which the power-effects could be best modeled in the PAN AIR code. In this subsection, the investigation of the permeable plume approach is extended to encompass realistic input plume shapes and inflow velocity boundary conditions.

3.3.1 Prediction of Plume Characteristics

The plume characteristics required for the PAN AIR code can only be obtained through a complex analysis of the exhaust jet and the external flowfield. This analysis was accomplished through the use of the VNAP2 code, which solves the two-dimensional, time-dependent, compressible Navier-Stokes equations using the unsplit MacCormack scheme (Reference 4).

Solution of the basic equations along with the various program options allows an accurate description of the complex, highly viscous nozzle flowfield, including shock and expansion waves, to be obtained. The particular test case studied consisted of an axisymmetric converging-diverging nozzle that was designed to operate at a nozzle pressure ratio (NPR) of 4.0. The analysis of this nozzle was performed at an under expanded NPR of 6.51 in order to match existing wind tunnel data. Since the nozzle was axisymmetric, only one half plane was analyzed. A 41X23 variable spaced grid over the computational area provided approximately one thousand points at which the pressure, density, temperature, Mach number and the velocity components were determined. In

each case, the iterative solution was allowed to run well past the minimum number of iterations required to obtain a converged solution. Typically, the number of iterations required was on an order of magnitude of one thousand. Agreement between the surface pressures of the computationally derived values and experimental data for the same nozzle lead to confidence that VNAP2 accurately models the nozzle flowfield.

Although this solution of the plume provides a number of aerodynamic parameters at many points in the flowfield, it does not establish a boundary for the plume, which is needed in order to panel the plume for input to the PAN AIR code. The question then arises, "What criteria should be used to define the plume boundary?". Since the isolated nacelle model was powered by a cold jet, temperature criteria were not feasible. A velocity criteria was considered in which the boundary was defined to be the locus of points along which the local velocity was a specified ratio of freestream velocity. This criteria resulted in a plume shape that diverged rapidly, and although analytically correct, did not give the appearance of the popular conception of a plume shape.

The selected criteria for the plume boundary was based on the velocity gradient along a line perpendicular to the plume centerline. More specifically, the boundary was defined at the point of maximum velocity gradient. This boundary and the associated velocities normal to the boundary are represented in Figure 38. The axial variation in the values of these parameters is caused by the shock and expansion waves within the plume. Lines of constant Mach number are shown in Figure 39 to better illustrate the flow patterns that cause the irregular boundary. Note that the flow initially accelerates as it is exhausted from the nozzle. The flow encounters a Mach disk at the end of the first shock cell, upon which there is a rapid deceleration followed by a more gradual acceleration. The point of maximum velocity gradient is relatively close to the centerline of the plume just downstream of the Mach disk, thereby causing some irregularity in the shape of the plume boundary when the velocity gradient criteria is used.

There was some concern in using an irregular plume shape in the PAN AIR code; therefore, the plume was faired so the boundary would be smooth. This was accomplished by applying a least-squares curve fit to the points of the plume boundary and then computing the normal velocities associated with the smoothed boundary. The smoothed boundary and corresponding inflow velocities are also shown in Figure 38.

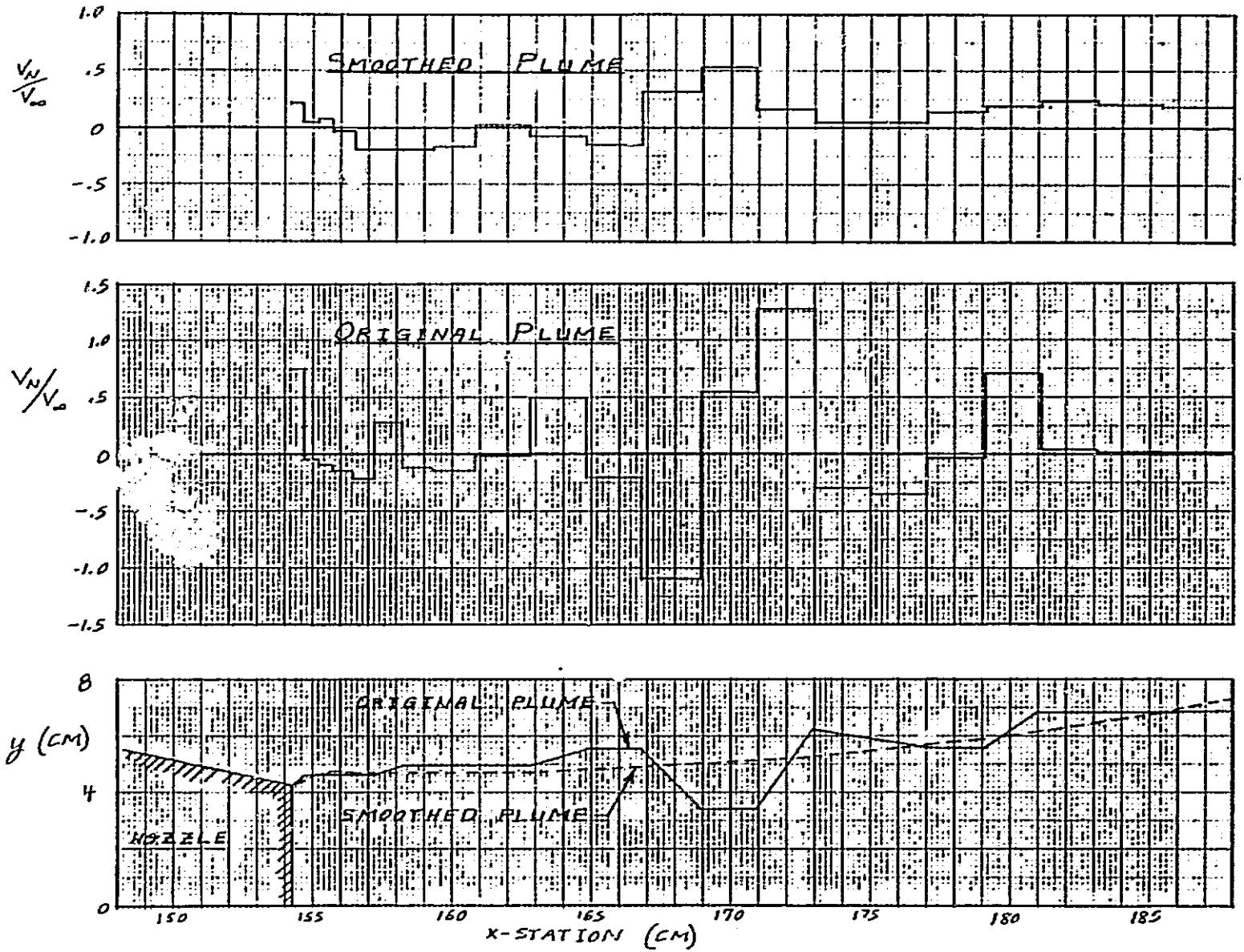

Figure 38 Navier-Stokes Solution For the Isolated Nacelle Model Plume

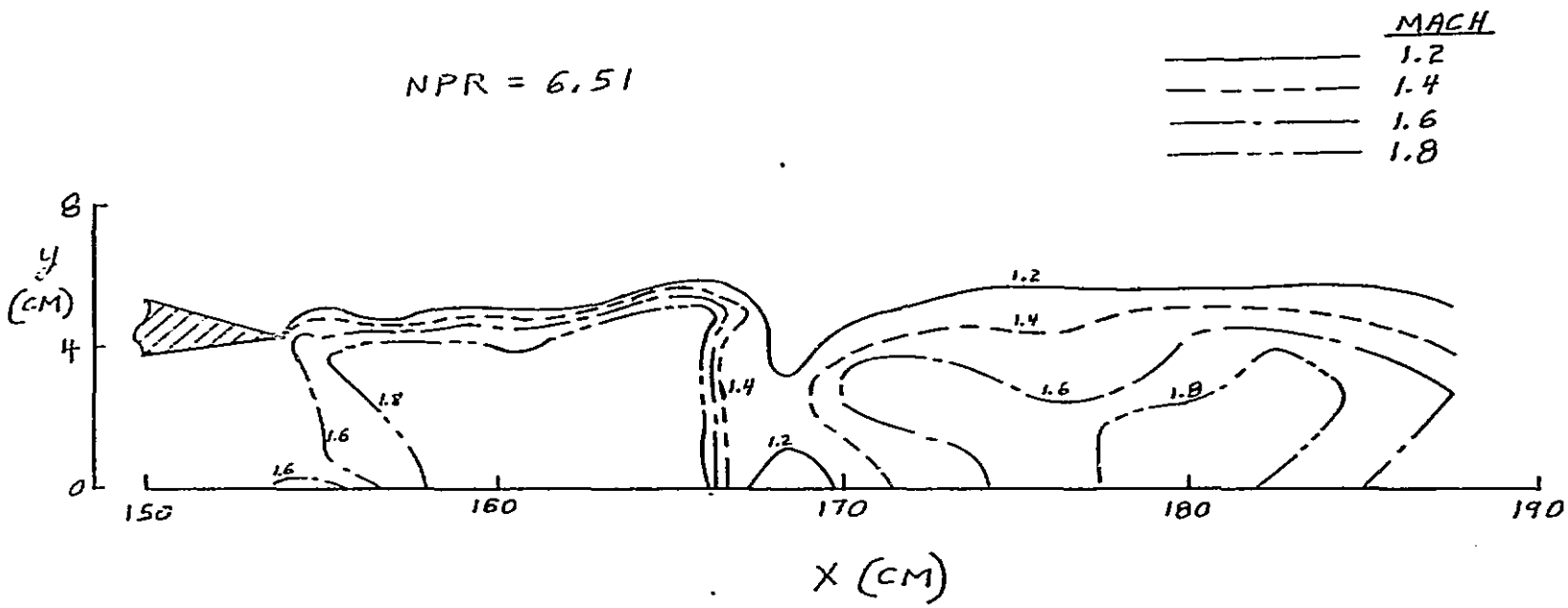

Figure 39 Mach Contours For the Isolated Nacelle Model Plume

3.3.2 Power-On Results

The isolated nacelle model was analyzed with the two plume models developed from the Navier-Stokes solution to determine if they would accurately simulate the jet exhaust effects. This was accomplished by comparing the predicted boattail pressures with the experimental data shown in Figure 29. In order to make a theoretical prediction for this pressure change, it was necessary to first be able to predict the nozzle pressures for the power-off case.

The initial run for the power-off case included a cylindrical wake and the zero total potential boundary conditions on the downstream side of the exit network as discussed in Subsection 3.1. The pressure predictions from this run, previously shown in Figure 32, were slightly higher than the experimental data near the nozzle exit. It is noted that the compressed scale in this figure makes the test-to-theory comparison appear good. When plotted to a larger scale, however, the difference is of the same order of magnitude as the power effect. In order to better model the flow separation at the end of the nozzle and improve the power-off prediction, an impermeable network was attached at the nozzle exit to continue the external slope of the nozzle boattail for a short distance downstream of the actual exit plane. The body that was used to simulate the separated flow of the nozzle is shown in Figure 40a and the resulting power-off prediction is compared with test data in Figure 41.

The panelling arrangement for the irregular-shaped plume is shown in Figure 40b and the test-to-theory comparison for an NPR of shown in Figure 41. The computed pressure increment due to removing the body that simulated the separated flow and adding the plume model accurately predicted the experimental power effects, except very near the end of the boattail where the prediction shows a slightly higher compression than test data.

The smoothed Navier-Stokes plume panelling arrangement is shown in Figure 40c and the results are compared with experimental data in Figure 42. The computed boattail pressure increment is approximately the same as for the irregular-shaped plume along most of the nozzle. Near the end of the nozzle, however, a high-pressure area occurred when the smoothed plume was used. This is felt to be the result of the smoothing process that was used on the original Navier-Stokes solution. The Navier-Stokes computed values varied widely between grid points near the exit, allowing for substantial latitude in the

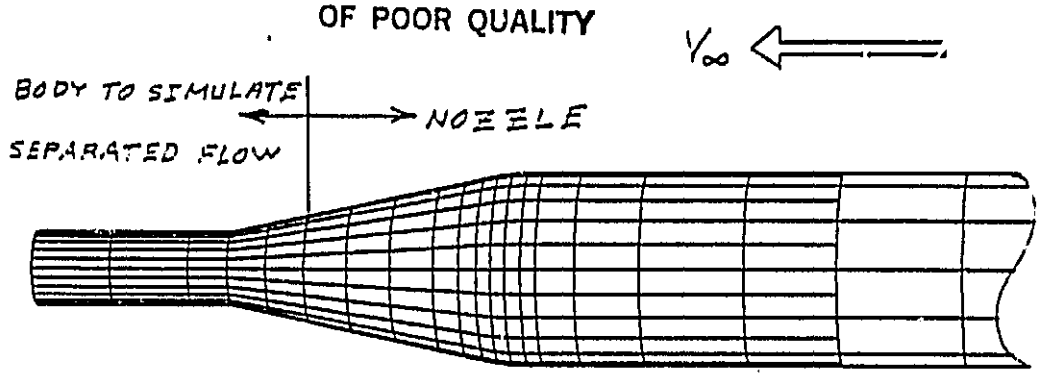

(a) Separated Flow Simulator

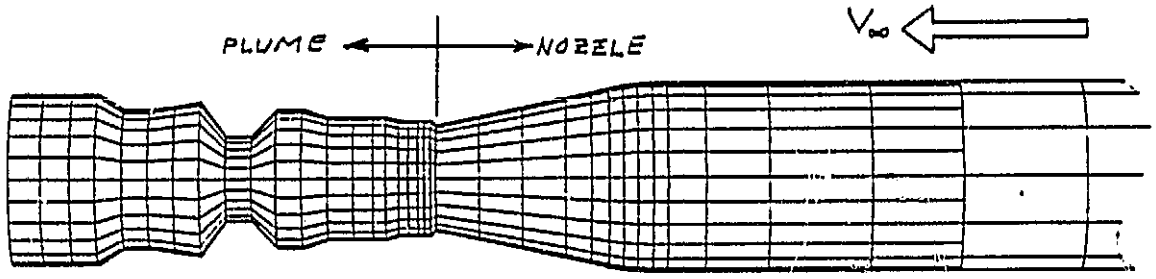

(b) Irregular-Shaped Plume

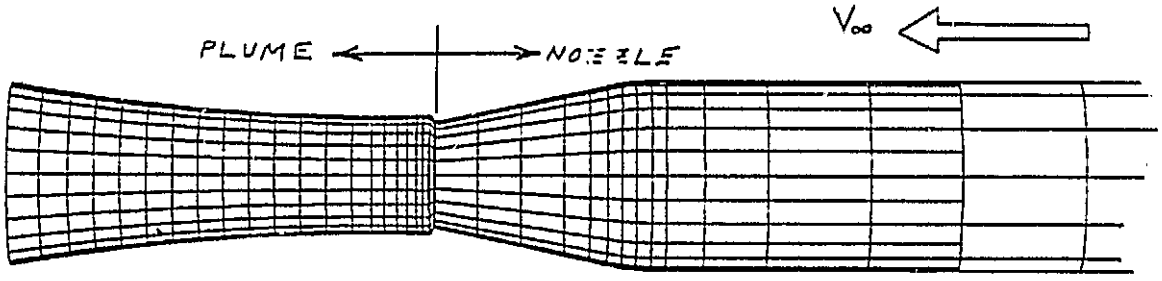

(c) Smoothed Plume

Figure 40 Panelling Arrangements For the Isolated Nacelle Model with Flow Simulator and Navier-Stokes Plumes

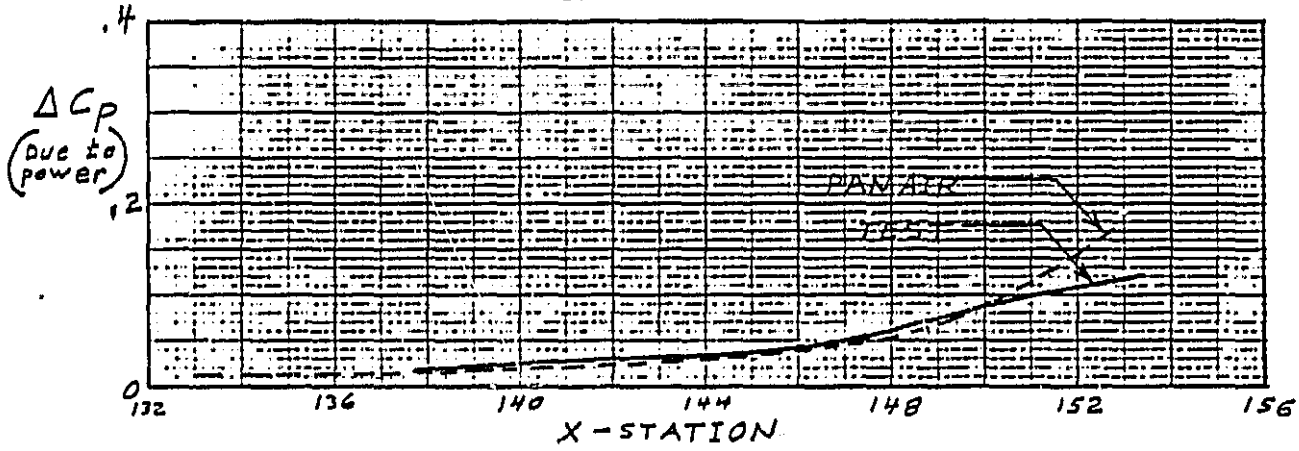

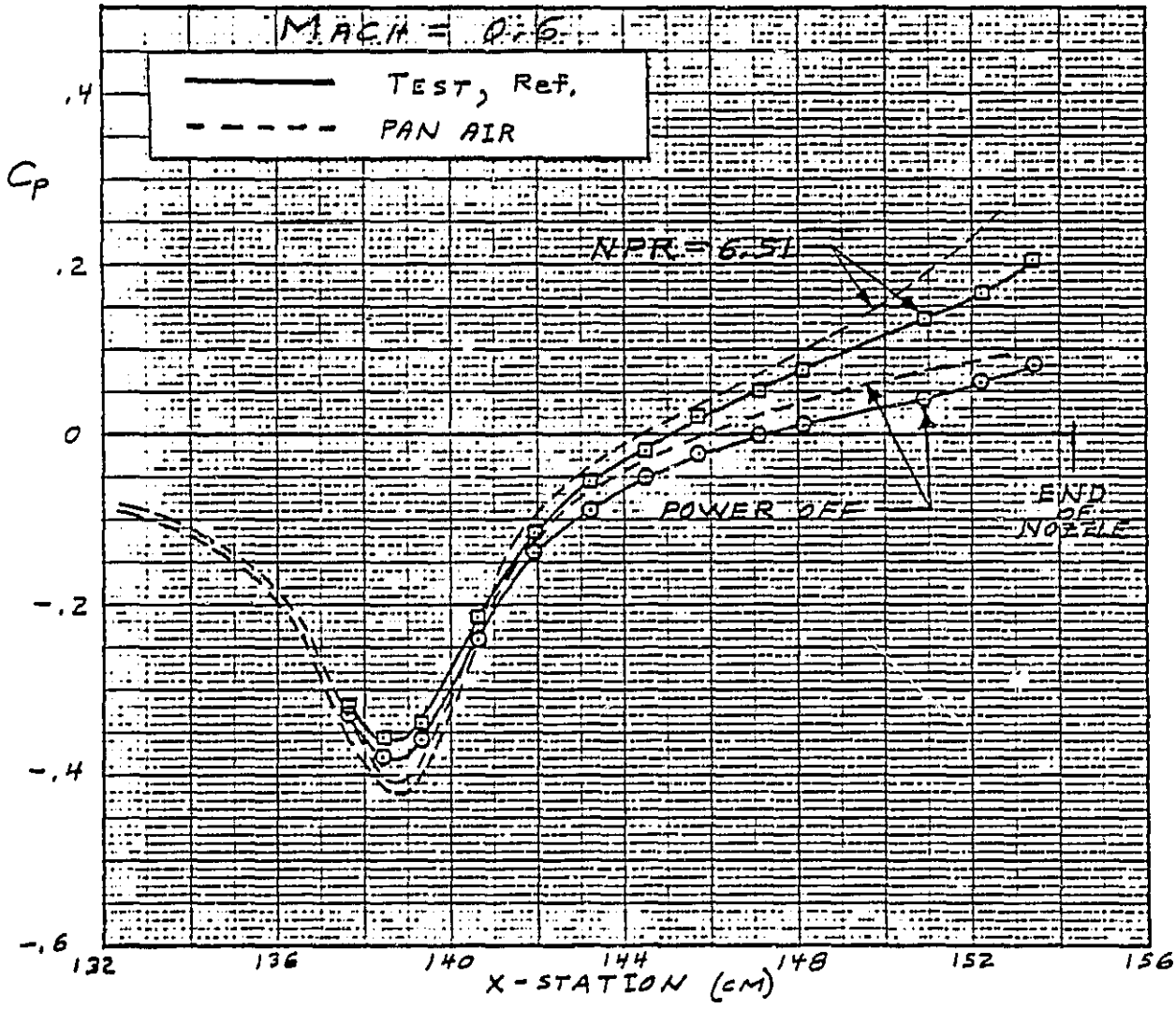

Figure 41 Boattail Pressure Predictions with Irregular-Shaped Plume

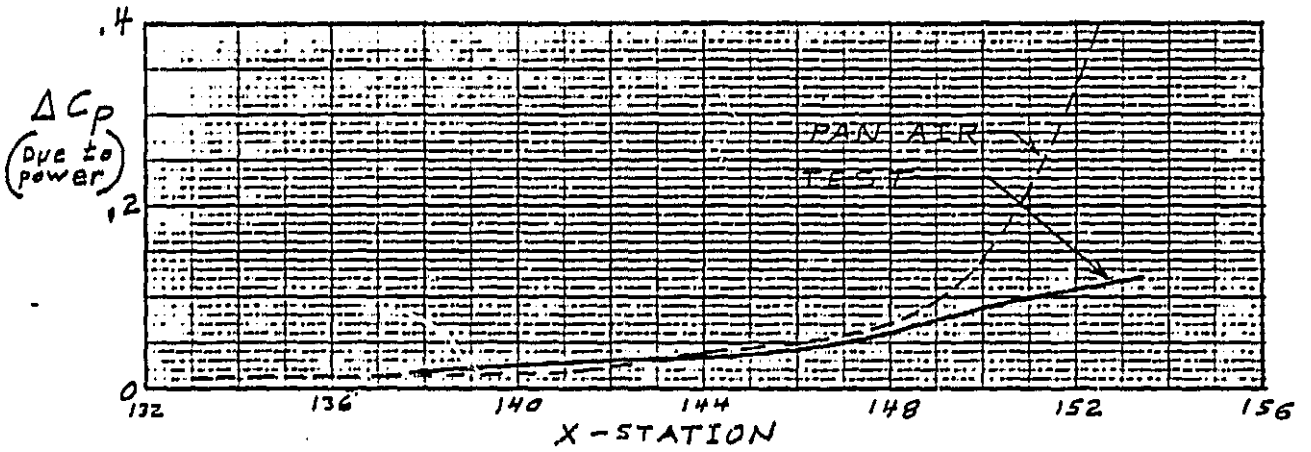

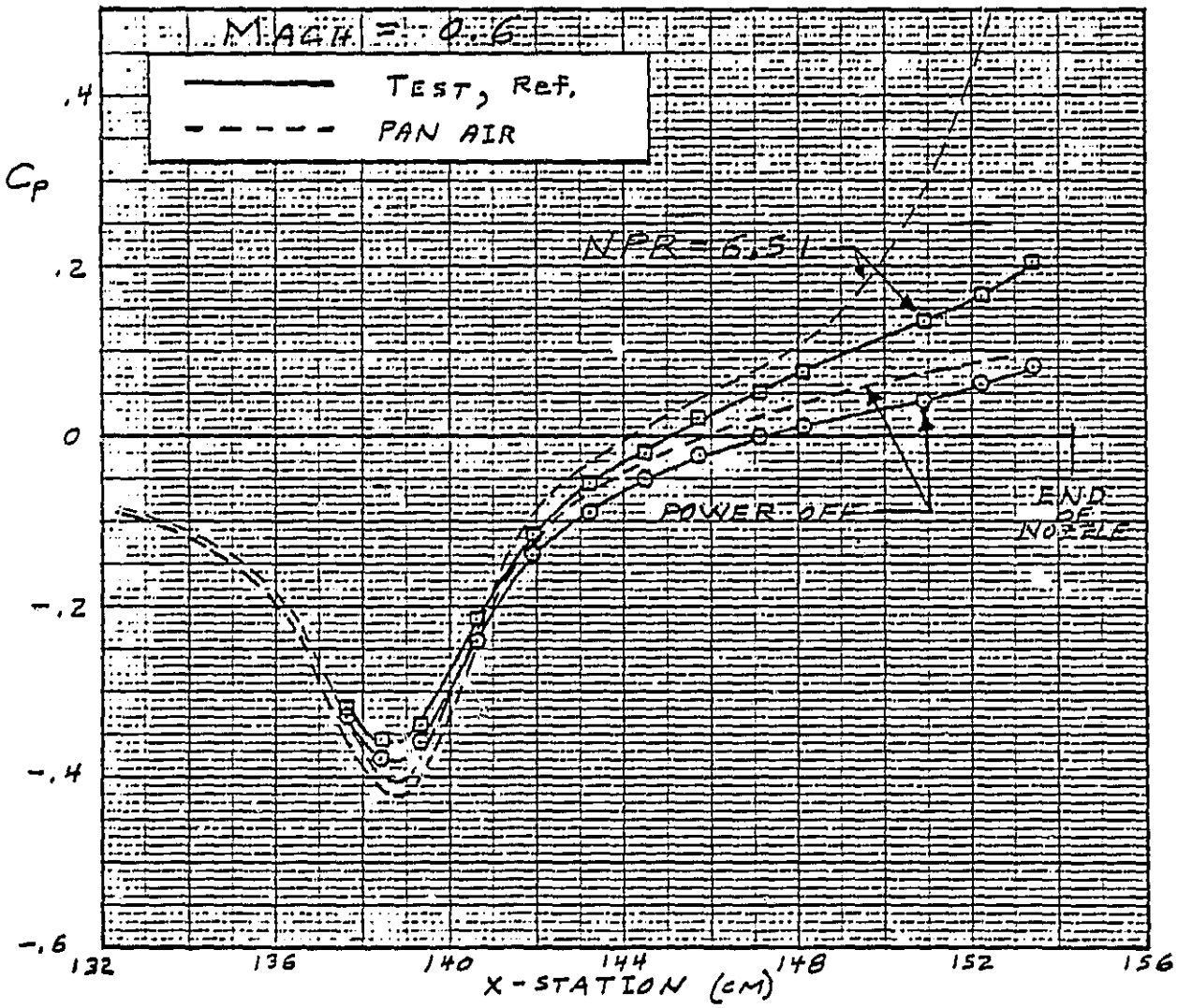

Figure 42 Boattail Pressure Prediction with Smoothed Plume

smoothing process. This situation can be avoided in future analyses by increasing the number of grid points near the nozzle exit in the Navier-Stokes solution.

The results obtained from the runs of the irregular and smoothed plumes dismissed the concerns that were previously expressed about the capability of the PAN AIR code to properly handle plumes with highly irregular shapes. The irregular-shaped plume correlated well with experimental data, and the smoothed plume produced similar results, except in a region where the smoothing process was questionable. This confirms that the permeable body approach can be effectively used to model plume effects with any reasonable combination of plume shape and inflow velocities which correspond to the flowfield.

4 CONCLUSIONS

The investigations performed in this study have made progress toward the development of methodology applicable to the analysis of the aerodynamic and propulsive flowfields associated with V/STOL configurations. Significant conclusions gleaned from this study are

(1) The results from the analysis of the fighter model correlated well with experimental data when the nozzle exit was represented as an impermeable surface and no wakes were attached to the nozzle exit.

(2) The results of the fighter model were unsatisfactory when the nacelle wakes were included and the total potential was set to zero on the downstream side of the exit network to simulate the separated flow at the aft end of the nozzle. With this representation of the flow, extreme values of pressure coefficient were computed for some panels near the nozzle exit, and the overall force predictions were adversely affected. The complex abutments around the nozzle exit included (a) the nacelle networks, which were impermeable surfaces, (b) the exit network, which was represented with a boundary condition that allowed no flow parallel to the network, and (c) the wakes, which were represented by doublet wake networks.

    Simplified models that have fewer panels and networks than the fighter model, yet include the complex abutments described above, were analyzed correctly by the code. Therefore, it seems that the logic that matches the aerodynamic parameters across these complex abutments can perform correctly under some conditions and yet go astray under other conditions.

(3) Adjustment of the doublet strength on the nacelle exit network eliminated the extreme values of pressure on the panels near the nozzle exit. It is apparent from an examination of the force predictions, however, that this only camouflaged the basic problem by eliminating the extreme values of pressure coefficient but did not correct the overall pressure distributions.

(4) The approach to exhaust jet modeling that employed the specification of mass flux or velocity boundary conditions on the exit network was found to be unsatisfactory. The use of some combinations of boundary conditions and wakes produced unreasonable pressures. Other combinations produced reasonable pressure predictions on the solid panels of the model but were judged unsuitable because the simulated jet velocity from the exit network decayed very rapidly.

(5) The technique of representing the exhaust jet with a permeable plume was found to work well. A Navier-Stokes solution to a plume was analyzed and the predicted effects of power correlated well with experimental data. It was also concluded that any reasonable definition of the plume boundary can be used provided the corresponding inflow velocities simulate the flowfield.

The PAN AIR code was found to be highly flexibile and adaptable to complex configurations. These characteristics required the use of complex methods of analysis and programming techniques and were obtained at some expense to user convenience. Furthermore, it was found that some sections of the code have not been thoroughly checked out. Although this flexibility has led to some difficulties, it is this feature that allows arbitrary boundary conditions to be specified on any selected network without having to modify the code. Thus it provides the means by which both theoretical and empirical techniques can be interfaced with the code in order to estimate the effects of various phenomena, such as separated flow and strong interactions between aerodynamic and propulsive flowfields. Since V/STOL aircraft characteristically operate in flight regimes where these flow phenomena are prevalent, these attributes make PAN AIR an excellent choice as the basis from which a useful V/STOL Methodology code can be evolved.

REFERENCES

1. Sidwell, Kenneth W., Baruah, Pranab K., and Bussoletti, John E., PAN AIR - A Computer Program for Predicting Subsonic or Supersonic Linear Potential Flows about Arbitrary Configurations Using a Higher Order Panel Method, Volume II - User's Manual, NASA Contractor Report 3252.

2. Howell, G. A., Crosthwait, E. L., and Witte, M. C., Evaluation of Pressure and Thermal Data From a Wind Tunnel Test of a Large-Scale, Powered STOL Fighter Model, NASA CR-166170, June 1981.

3. Berrier, Bobby L. and Re, Richard J., Investigation of Convergent-Divergent Nozzles Applicable to Reduced-Power Supersonic Cruise Aircraft, NASA Technical Paper 1766, December 1980.

4. Cline, M. C., VNAP2: A Computer Program for Computation of Two-Dimensional, Time-Dependent, Compressible, Turbulent Flow, Los Alamos Scientific Laboratory Report LA-8872 (August 1981).

APPENDIX A

Computer drawings of each of the networks included in the "improved" panelling arrangement of the fighter model are presented in this appendix. The results from the analysis of the arrangement are presented in Subsection 2.2.

Figures A1 through A4 show several views of the complete panel arrangement. Figures A5 through A29 show the networks individually. The abutting networks are also shown, whenever possible, so that the edge matching conditions can be seen. An attempt was made to show the individual networks from either a planform view or a profile view from the right-hand side of the configuration. However, it was sometimes necessary to roll or yaw the arrangement slightly from one of these views to clarify the network panelling. The right-hand side of the panelling arrangement is shown, and the forward portion of the networks are toward the right-hand side of the page, unless otherwise noted.

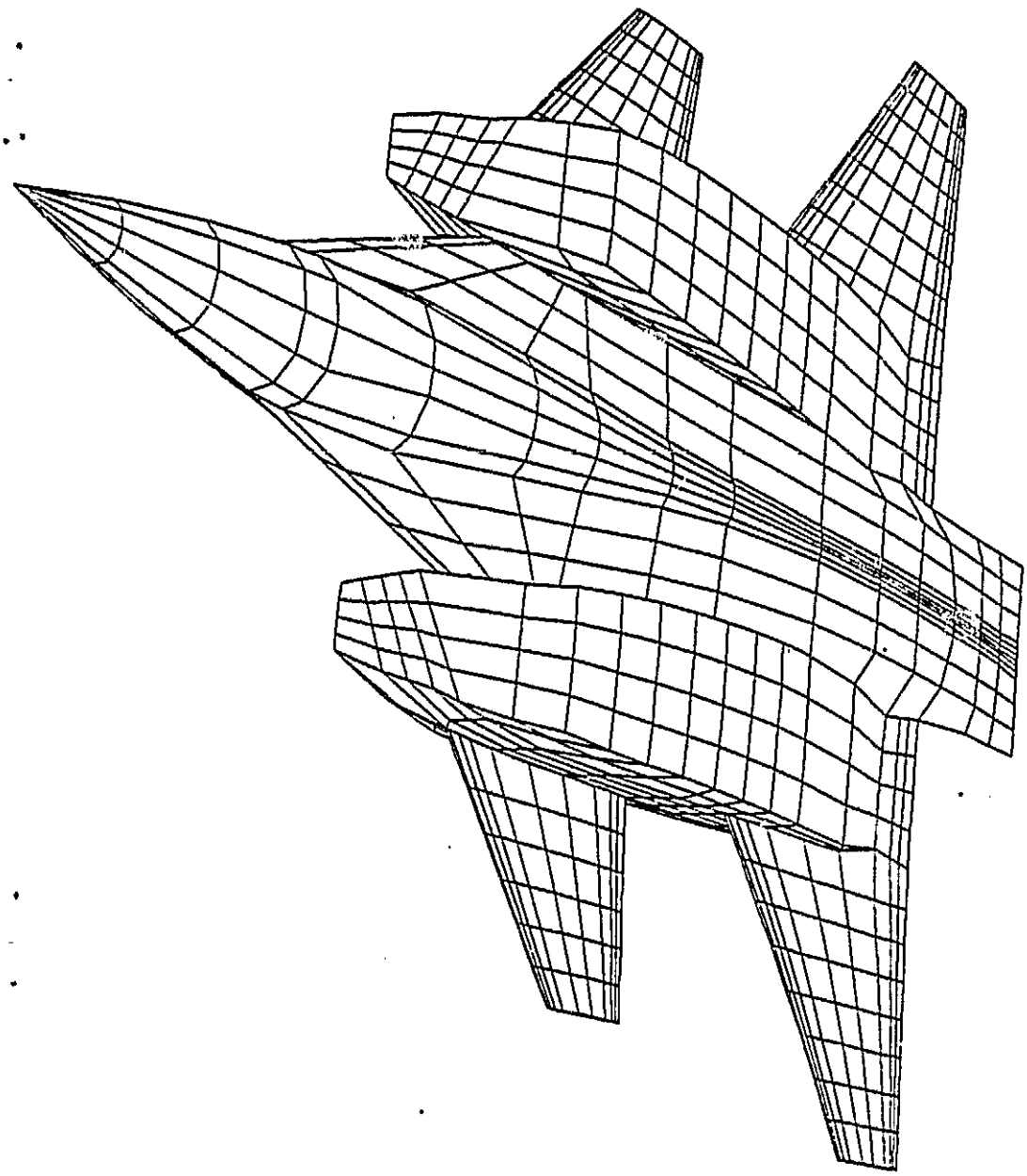

Figure A-1 View From Beneath

Figure A-2 Three-Quarter Rear View

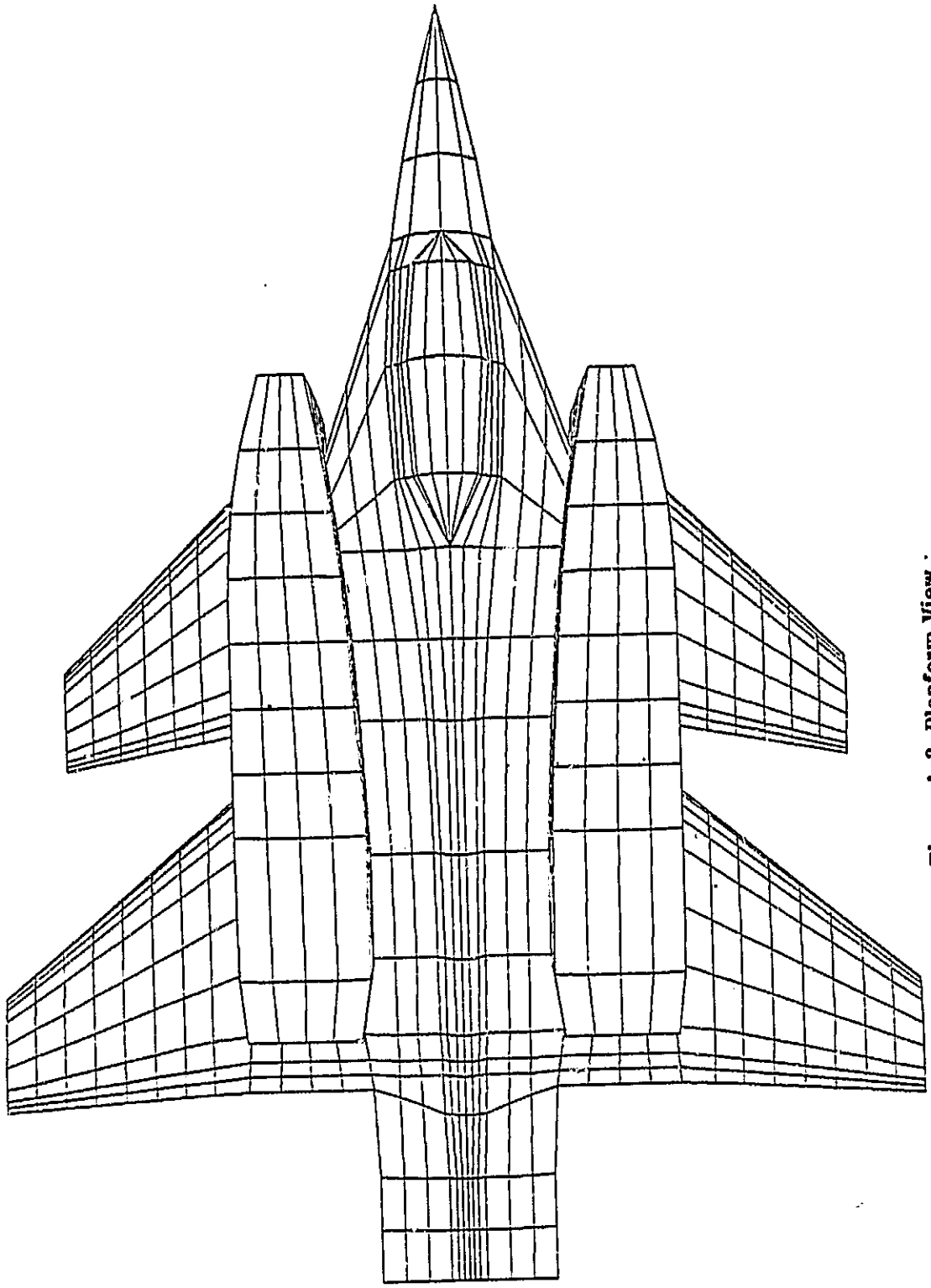

Figure A-3 Planform View

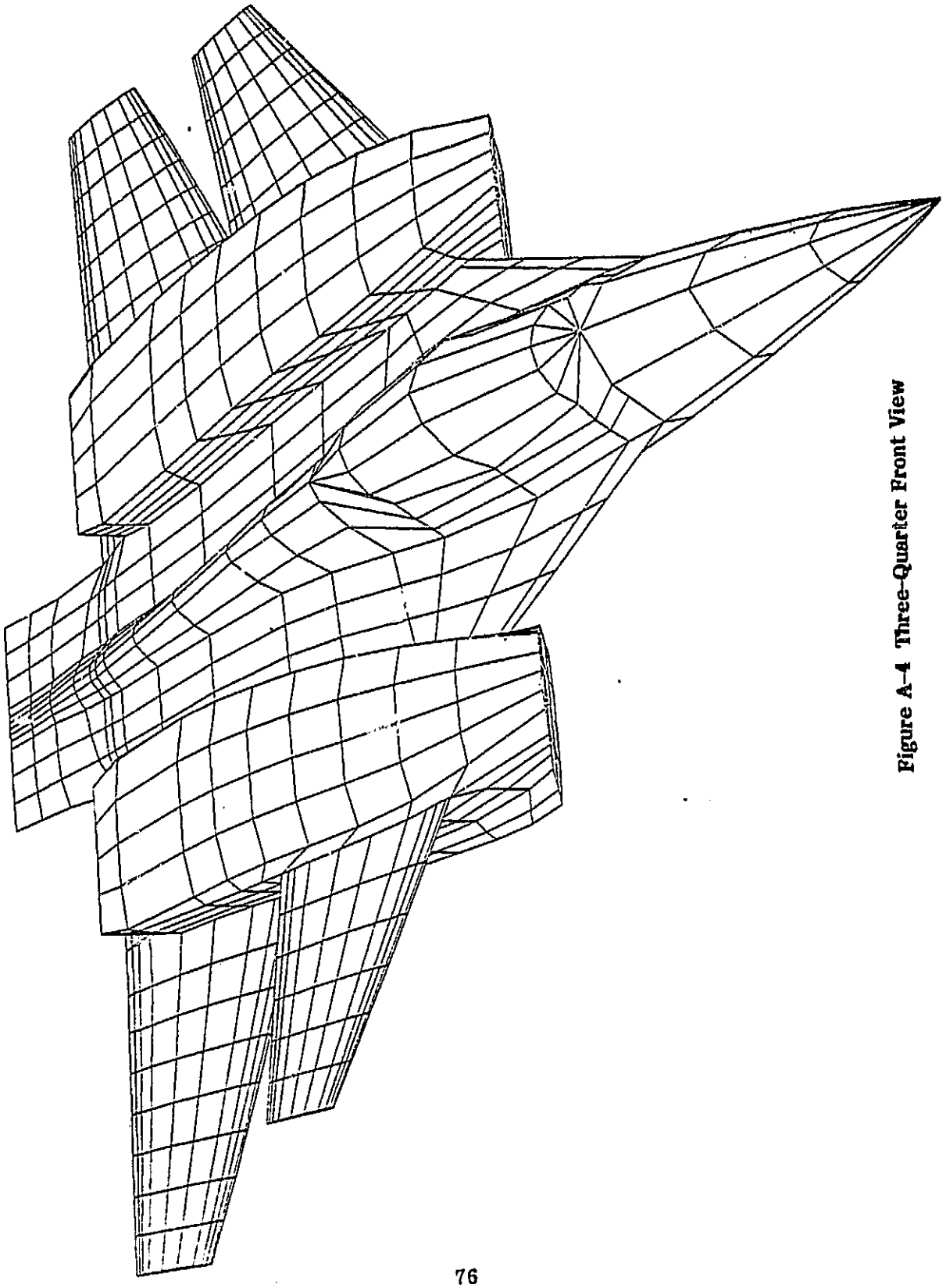

Figure A-4 Three-Quarter Front View

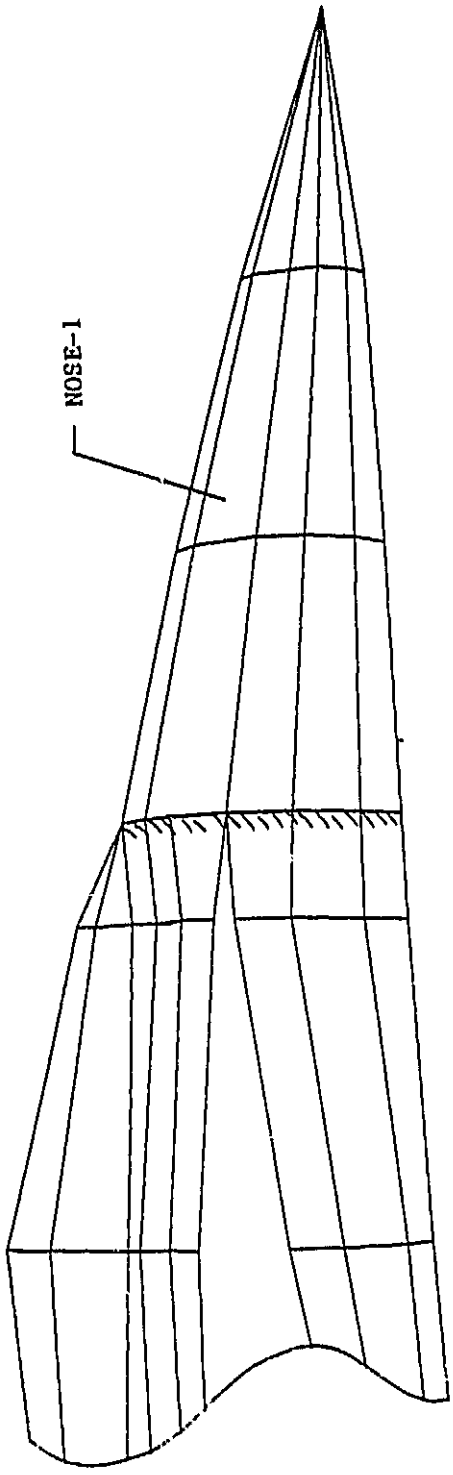

Figure A-5 Nose

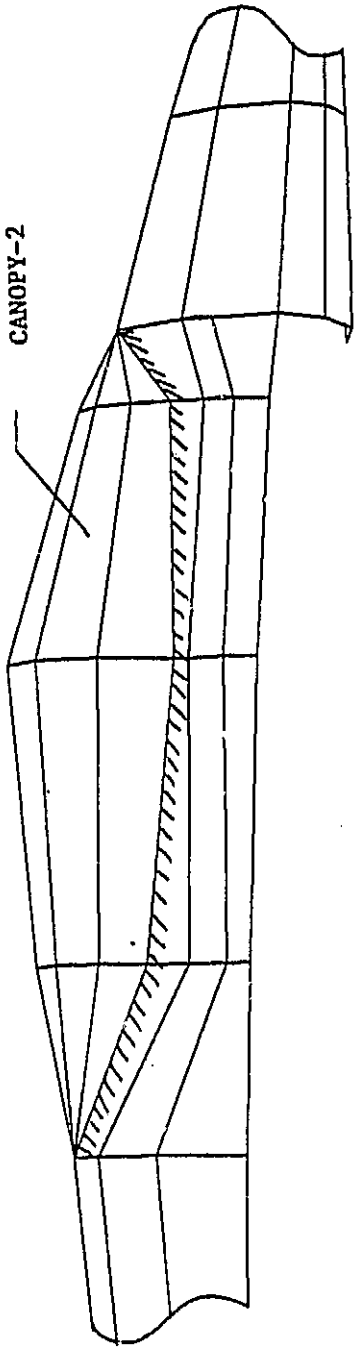

Figure A-6 Canopy

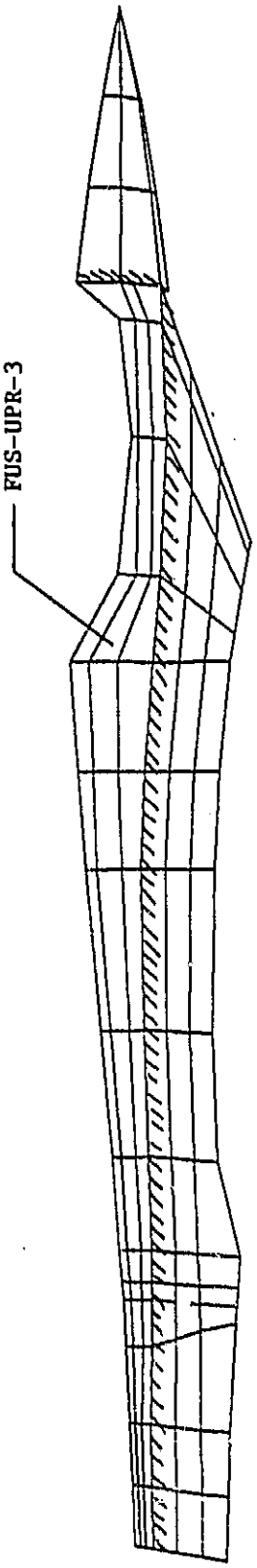

Figure A-7 Upper Fuselage

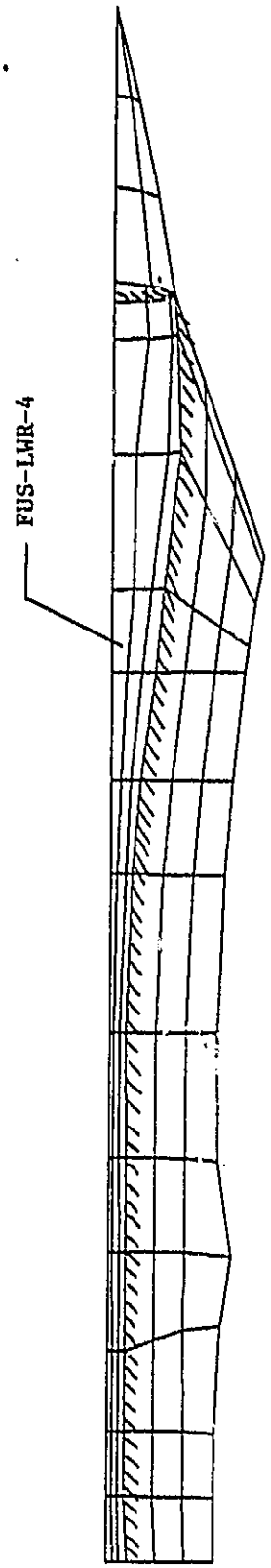

Figure A-8 Lower Fuselage

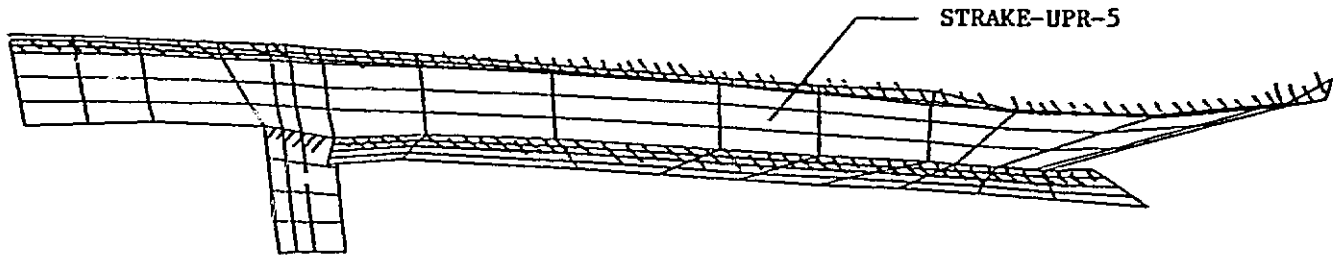

Figure A-9 Upper Strake

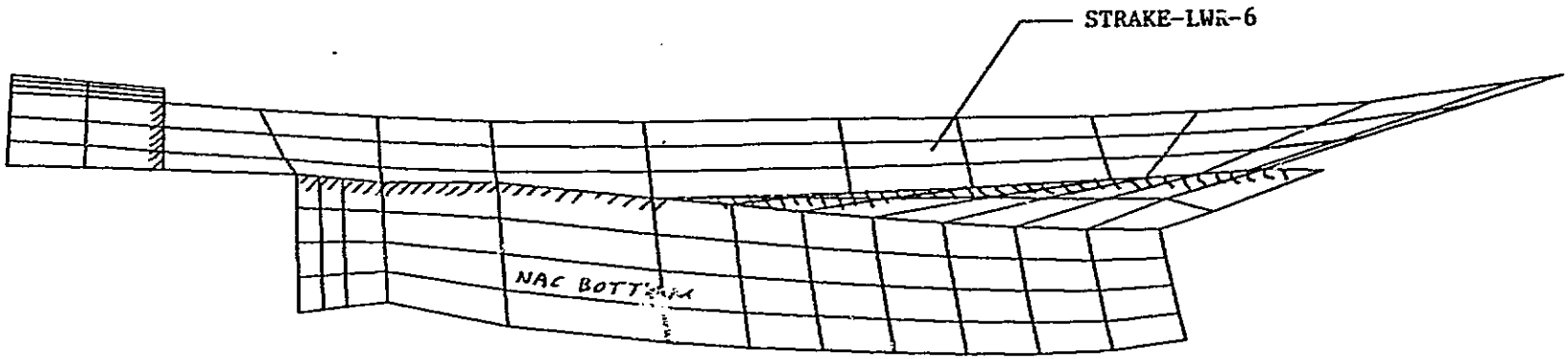

Figure A-10 Lower Strake

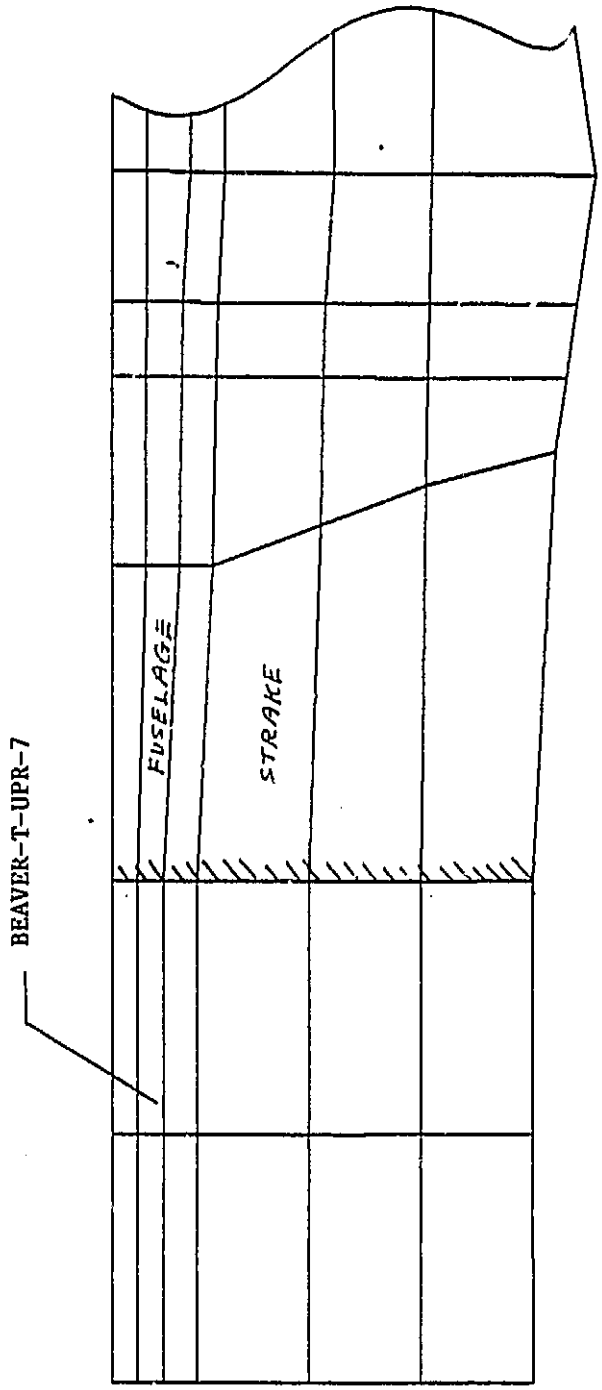

Figure A-11 Upper Beaver Tail

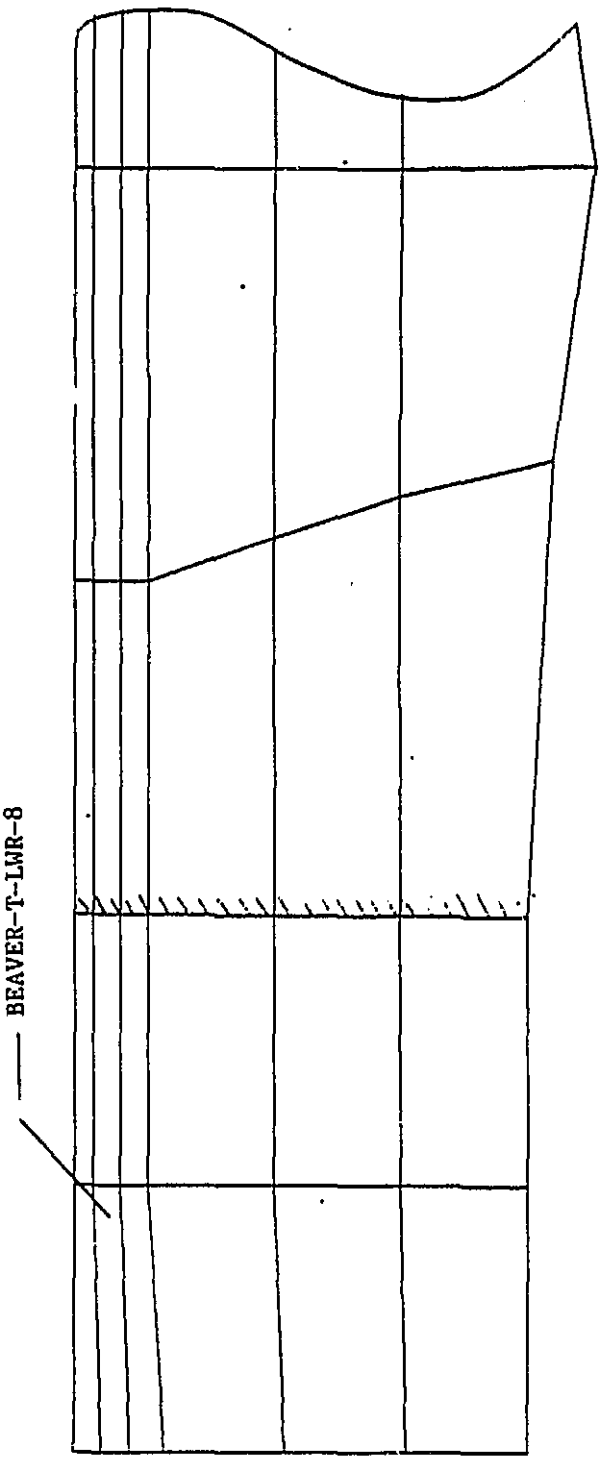

Figure A-12 Lower Beaver Tail

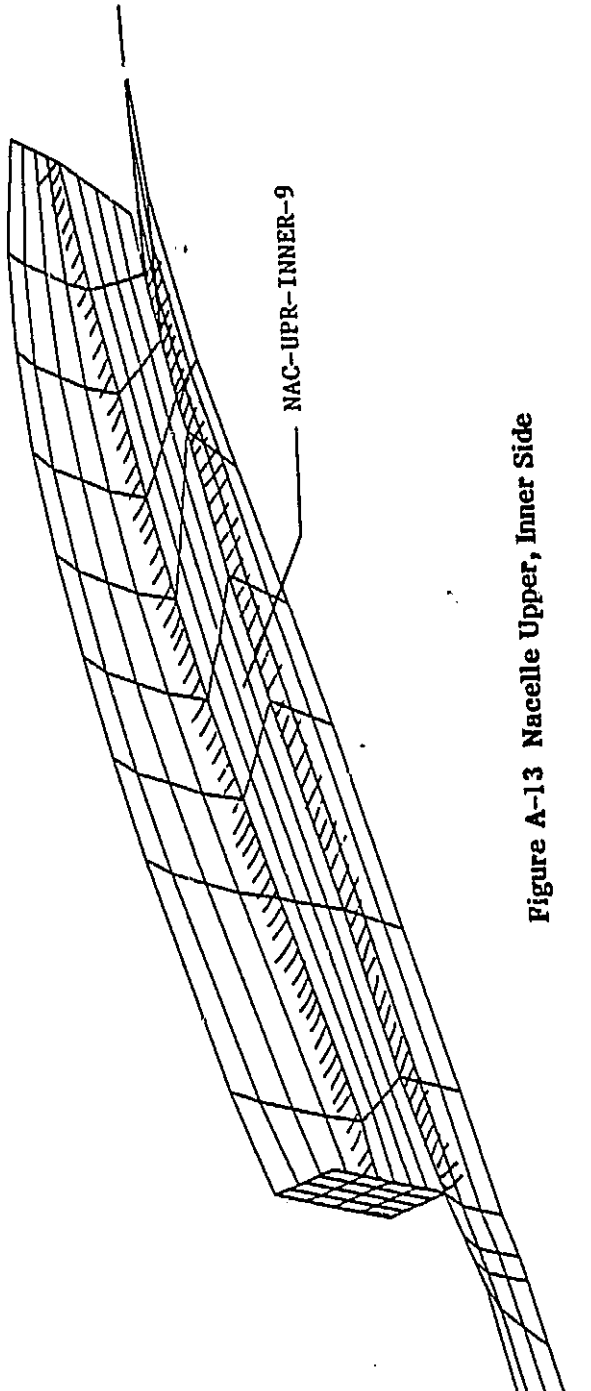

Figure A-13 Nacelle Upper, Inner Side

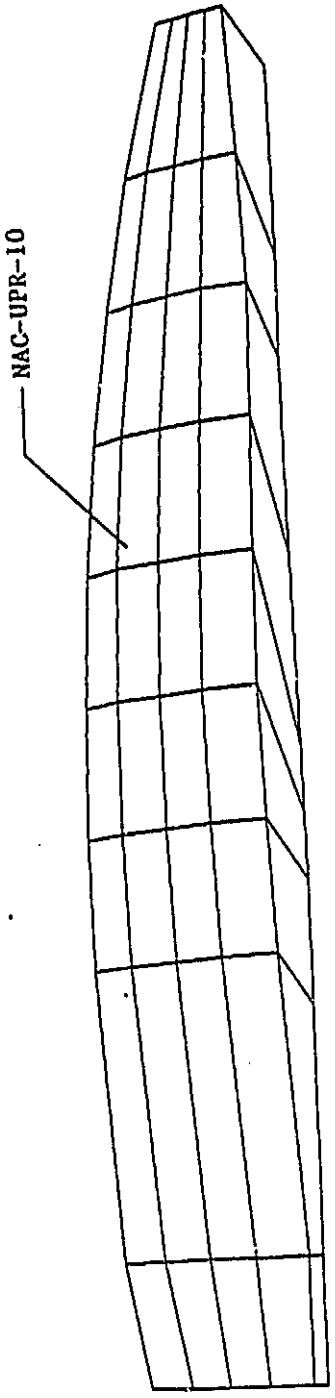

Figure A-14 Nacelle Top

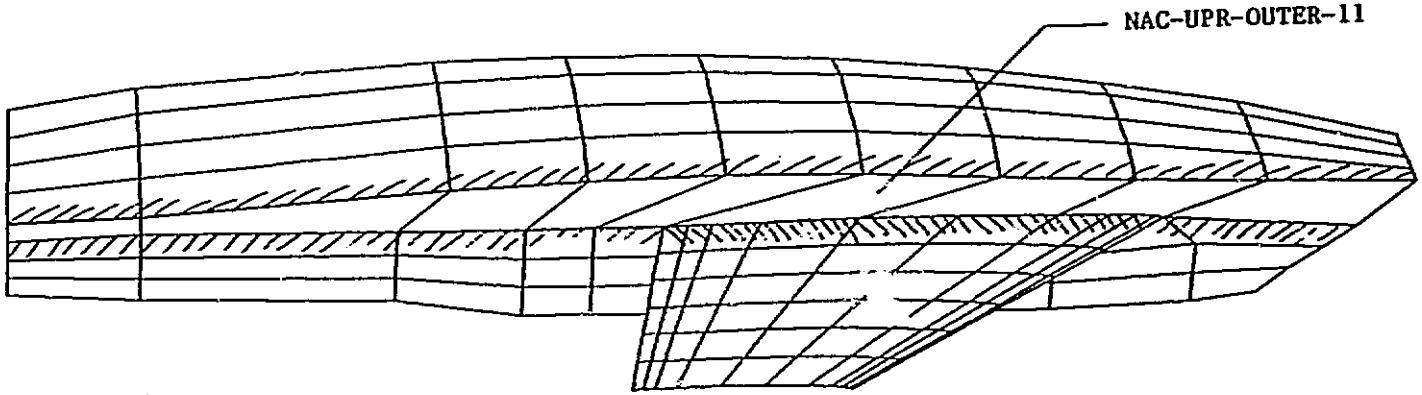

Figure A-15 Nacelle Upper, Outboard Side

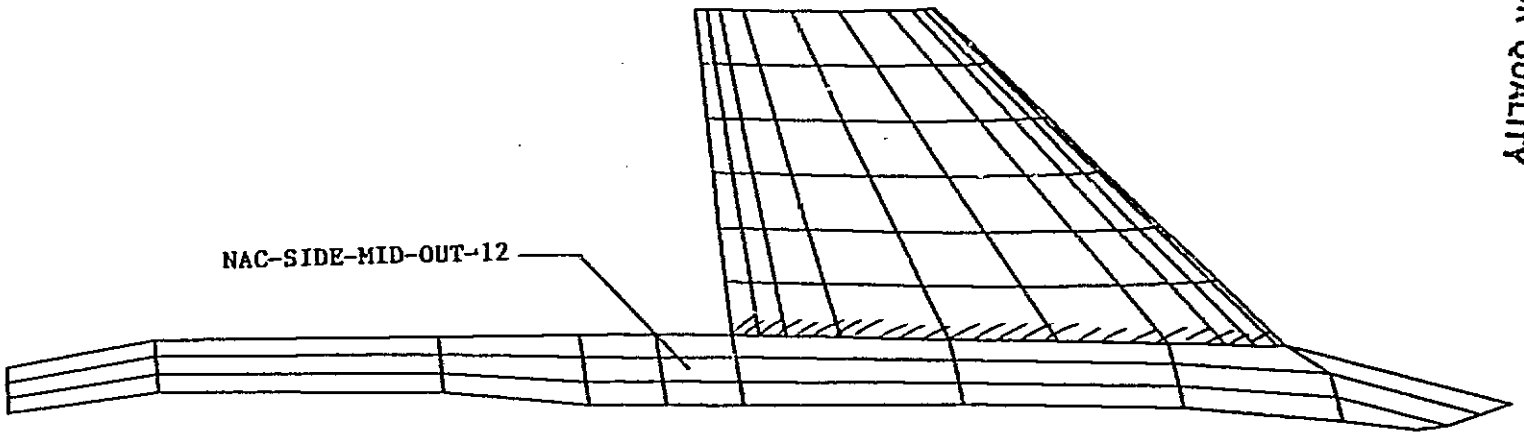

Figure A-16 Nacelle Mid, Outboard Side

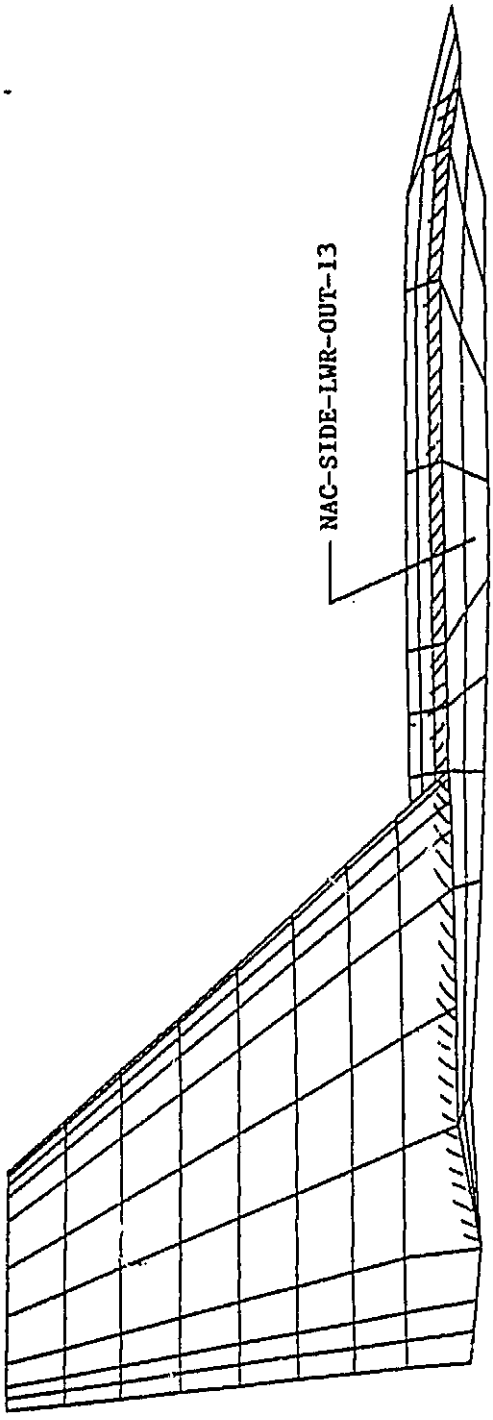

Figure A-17 Nacelle Lower, Outboard Side

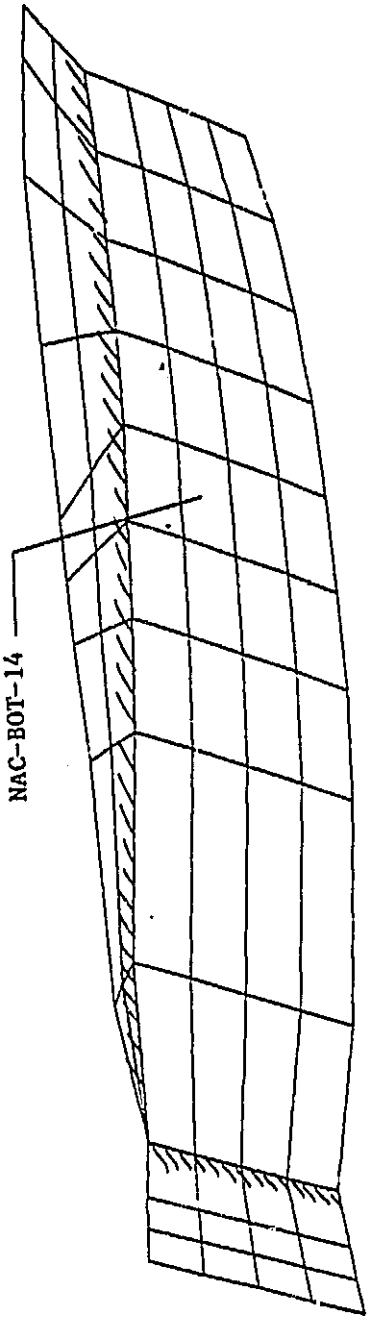

Figure A-18 Nacelle Bottom

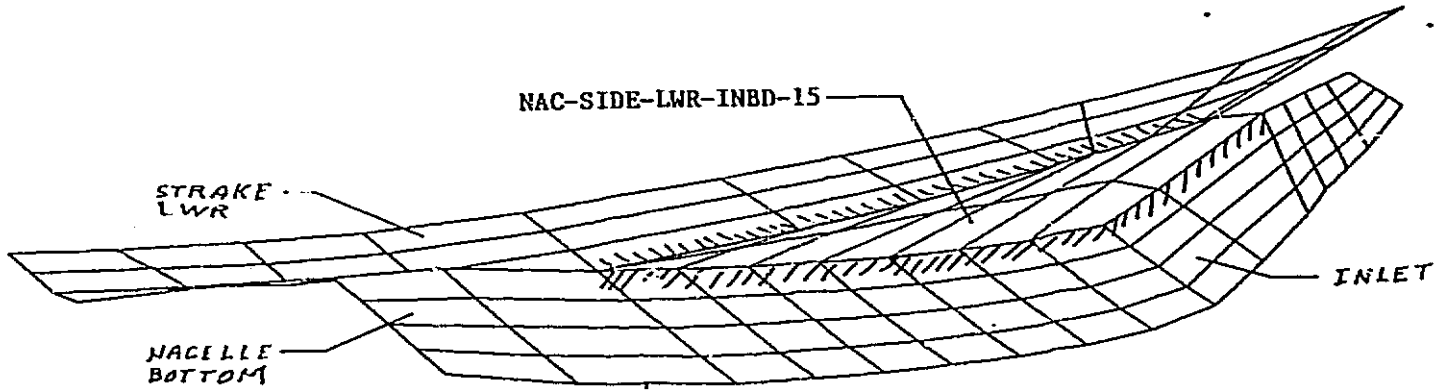

Figure A-19 Nacelle Lower, Inboard Side

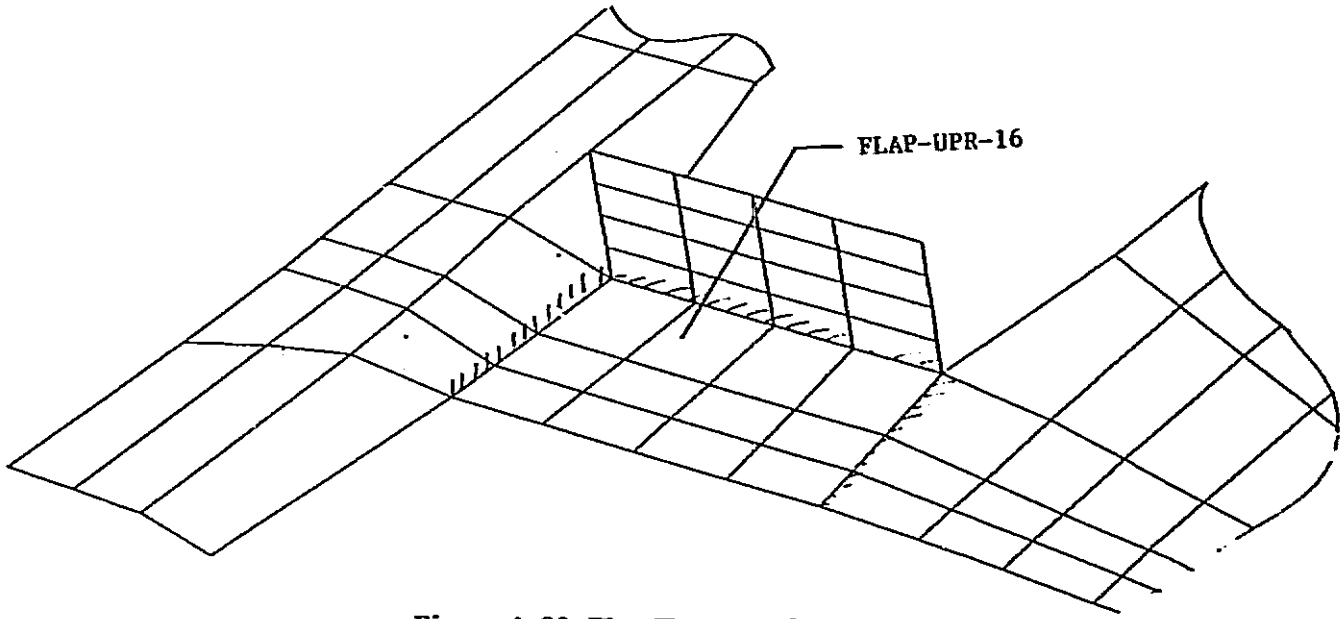

Figure A-20 Flap Upper Surface

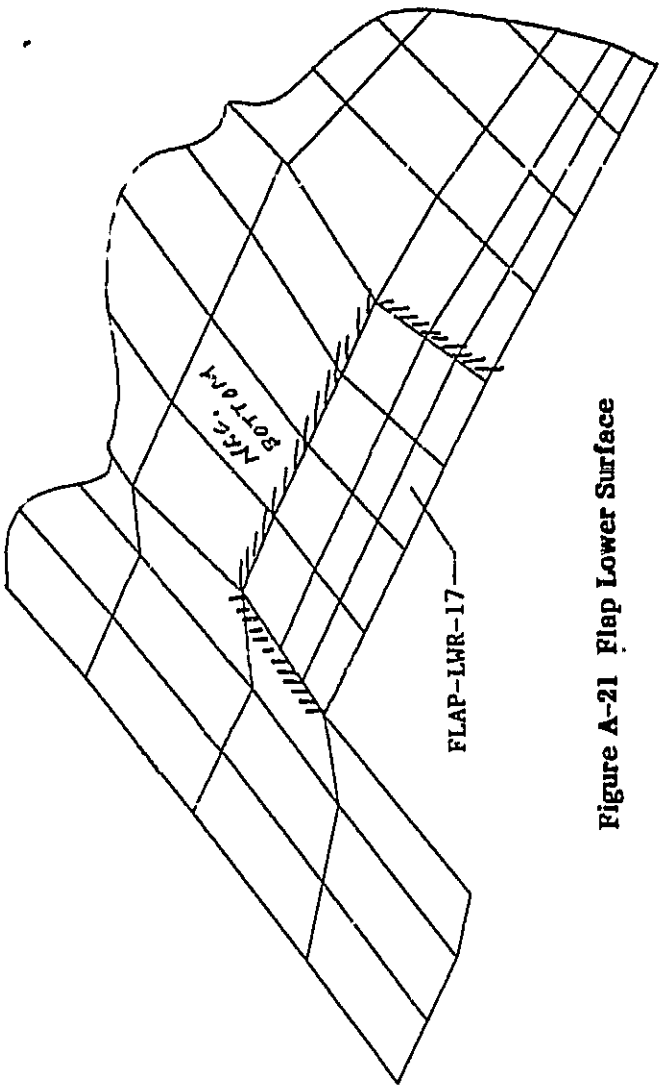

Figure A-21 Flap Lower Surface

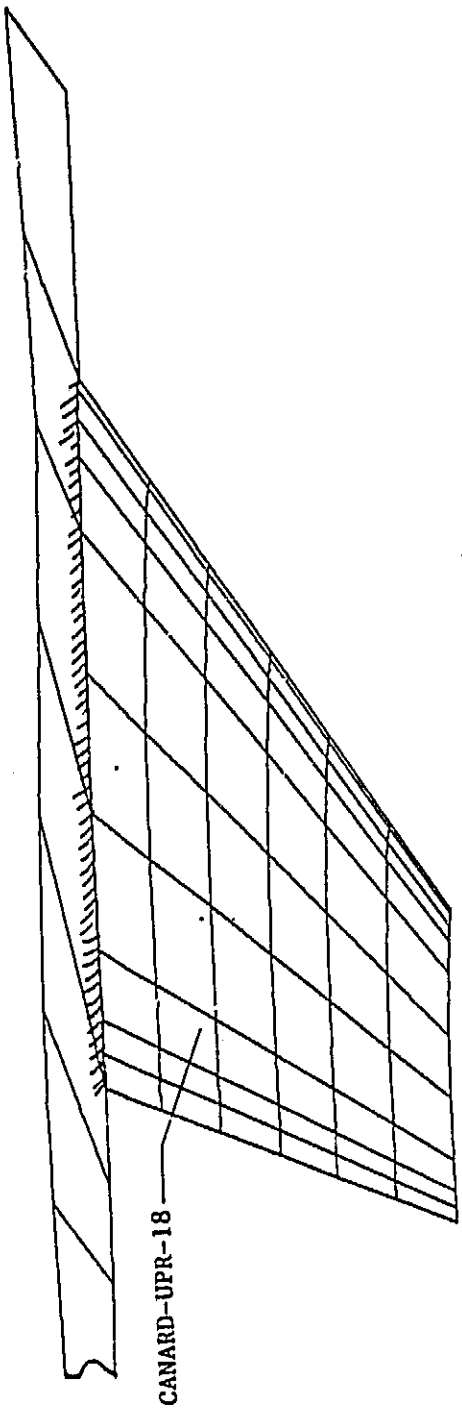

Figure A-22 Canard Upper Surface

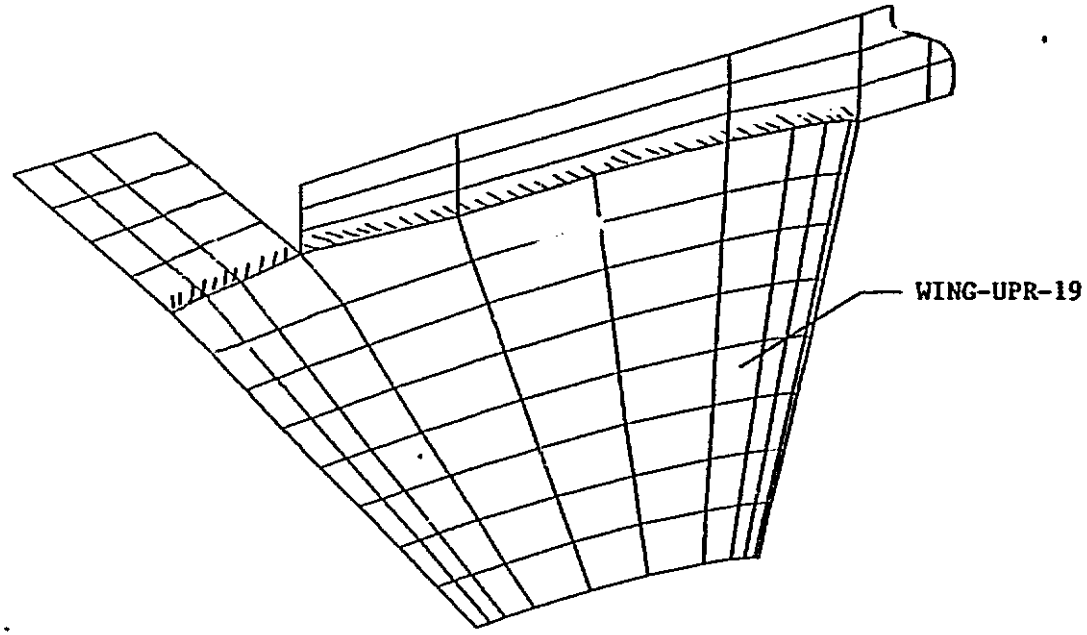

Figure A-23 Wing Upper Surface

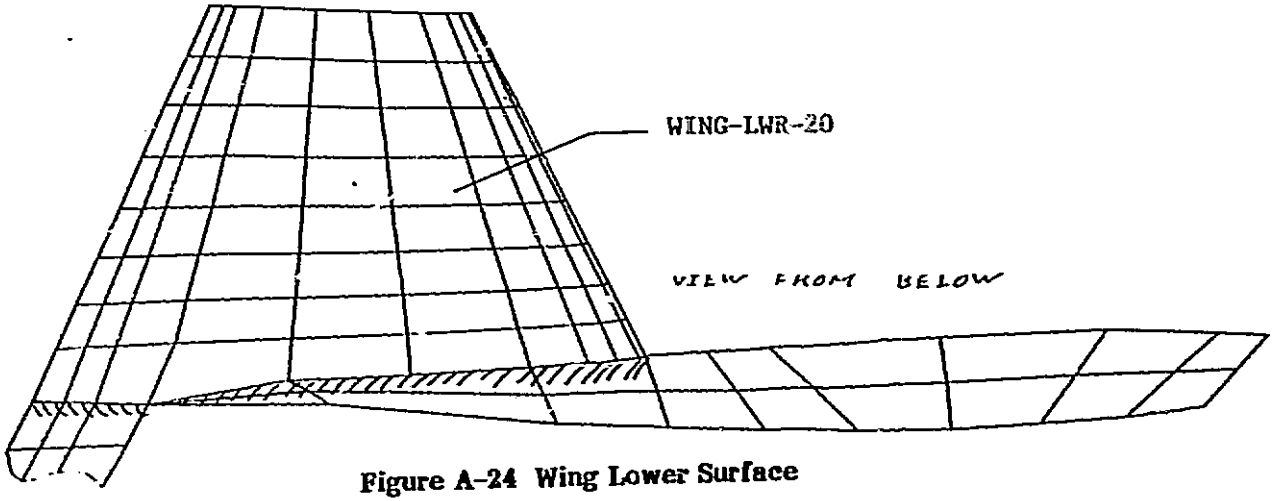

Figure A-24 Wing Lower Surface

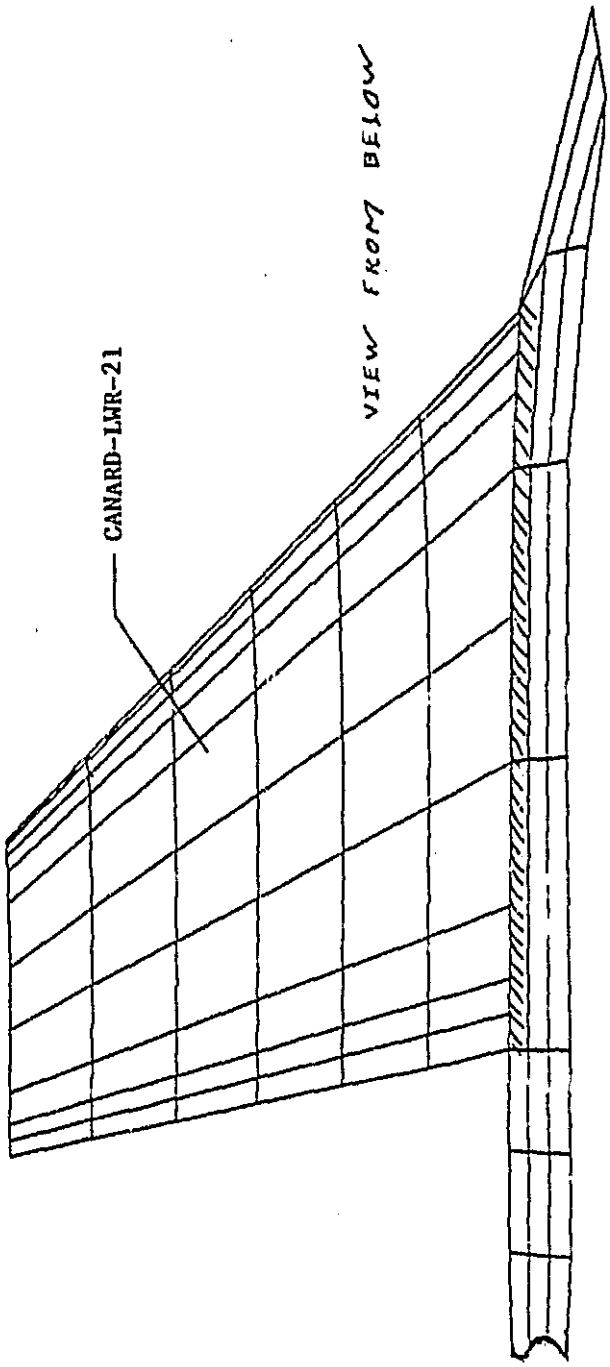

Figure A-25 Canard Lower Surface

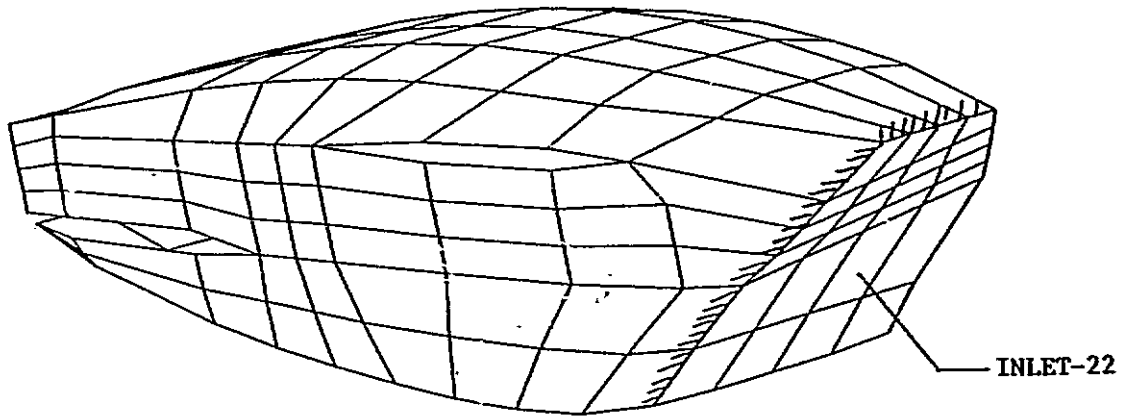

(a) View From Outboard of Nacelle

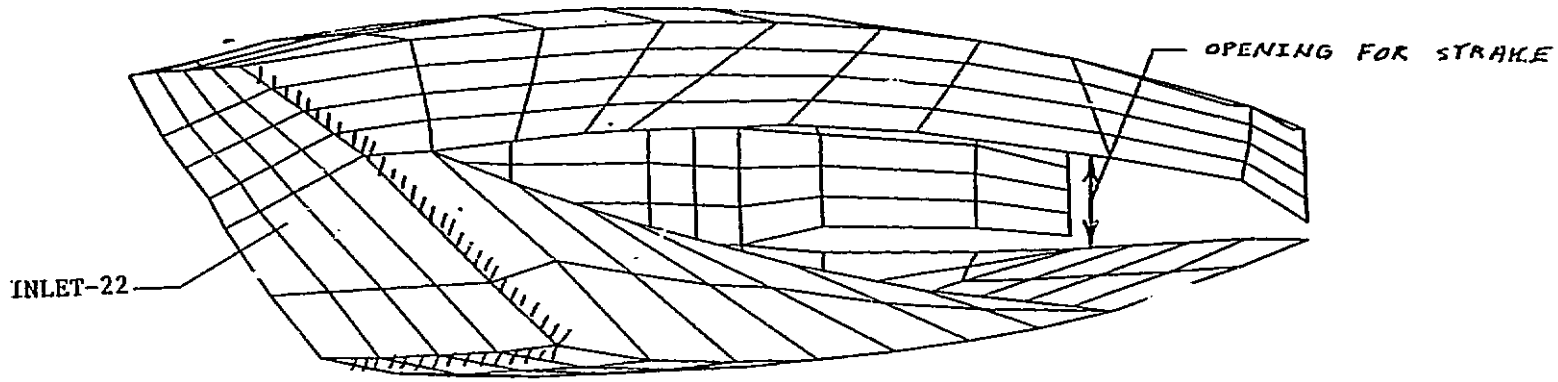

(b) View From Inboard of Nacelle

Figure A–26 Inlet

Figure A-27 Exit

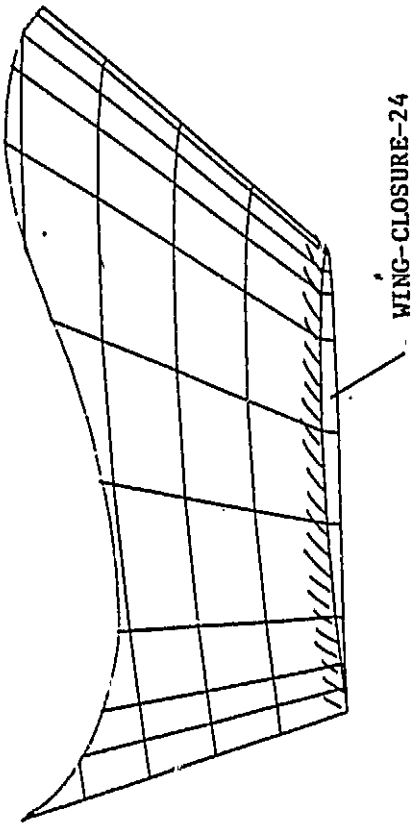

Figure A-28 Wing Tip Closure

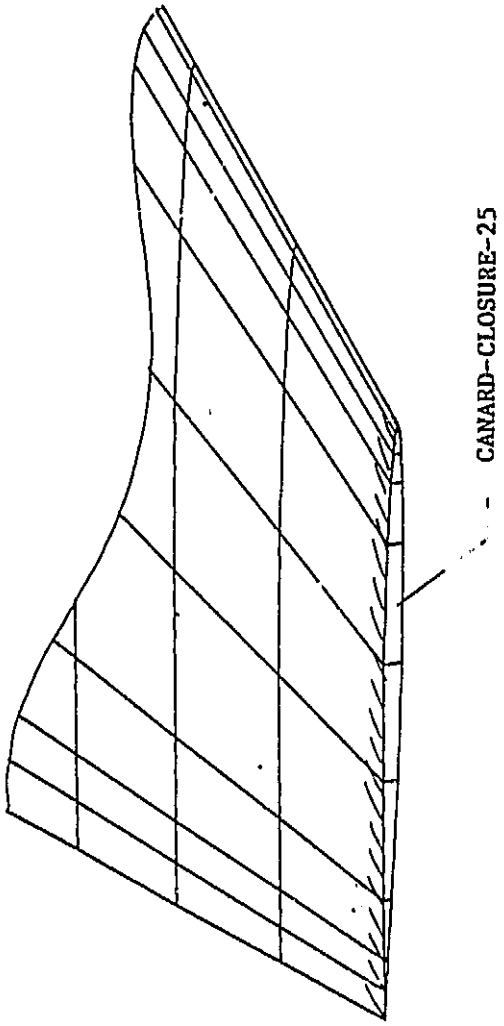

Figure A-29 Canard Tip Closure